

**Foundations and Trends[®] in Communications and
Information Theory**

Asymptotic Frame Theory for Analog Coding[®] (submitted for review July 2021)

Suggested Citation: Marina Haikin, Matan Gavish, Dustin G. Mixon and Ram Zamir (2021), “Asymptotic Frame Theory for Analog Coding[®] (submitted for review July 2021)”, Foundations and Trends[®] in Communications and Information Theory: Vol. xx, No. xx, pp 1–18. DOI: 10.1561/XXXXXXXXXX.

Marina Haikin

Amazon, Tel Aviv, Israel
mkokotov@gmail.com

Matan Gavish

Hebrew University, Jerusalem, Israel
gavish@cs.huji.ac.il

Dustin G. Mixon

The Ohio State University, Columbus, OH, USA
mixon.23@osu.edu

Ram Zamir

Tel Aviv University, Israel
zamir@eng.tau.ac.il

This article may be used only for the purpose of research, teaching, and/or private study. Commercial use or systematic downloading (by robots or other automatic processes) is prohibited without explicit Publisher approval.

now

the essence of knowledge

Boston — Delft

Contents

1	Introduction	3
1.1	Notation	10
2	An information-theoretic toy example	11
2.1	Source coding with erasures	11
2.2	Band-pass interpolation	15
2.3	Non-uniform sampling and signal amplification	19
2.4	From interpolation to frame codes	20
3	Sub-frame performance measures	21
3.1	The Welch bound	21
3.2	Noise amplification	22
3.3	Spread of eigenvalues	23
3.4	Shannon transform	25
3.5	Statistical RIP and condition number	25
3.6	Sub-frame rectangularity	26
4	Frame theory	28
4.1	Equiangular tight frames	30
4.2	Other optimal projective codes	36

4.3	Frames with well-conditioned subensembles	38
5	Random matrix theory	42
5.1	Methods of proof in RMT	44
6	Empirical ETF-MANOVA relation	46
6.1	Distance measures	47
6.2	Frames under study	48
6.3	Empirical observation method	48
6.4	Findings	50
7	Moments of an ETF subset	52
7.1	Low-order moments: exact analysis	54
7.2	General moments: asymptotic analysis	57
7.3	Concentration	62
8	Sub-frame inequalities	64
9	Applications	68
9.1	NOMA/CDMA	68
9.2	DFT codes	70
9.3	Space-time codes (STC)	72
9.4	Over-sampling and Δ - Σ modulation	73
9.5	Multiple-description (MD) source coding	73
9.6	Coded distributed computation (CDC)	75
9.7	Neural networks	77
9.8	Frames in compressed sensing: phase transition	78
10	ETF optimality conjecture	80
10.1	Erasure Welch bound	80
10.2	Minimum empirical variance and kurtosis	81
11	Conclusion and discussion	84
11.1	Summary of asymptotic results for ETF subsets	86

11.2 Open questions and conjectures	87
Acknowledgements	90
Appendices	91
A Entropy-coded dithered quantization	92
B Information theoretic proofs for sub-frame inequalities	94
C Variance of <i>1st</i> and <i>2nd</i> moments (proof of Theorem 7.2)	99
References	102

Asymptotic Frame Theory for Analog Coding[®]

(submitted for review July 2021)

Marina Haikin¹, Matan Gavish², Dustin G. Mixon³ and Ram Zamir⁴

¹*Now at Amazon. Previously at Tel Aviv University where this work was performed.*

²*Hebrew University of Jerusalem*

³*The Ohio State University*

⁴*Tel Aviv University*

ABSTRACT

Over-complete systems of vectors, or in short, frames, play the role of analog codes in many areas of communication and signal processing. To name a few, spreading sequences for code-division multiple access (CDMA), over-complete representations for multiple-description (MD) source coding, space-time codes, sensing matrices for compressed sensing (CS), and more recently, codes for unreliable distributed computation. In this survey paper we observe an information-theoretic random-like behavior of frame subsets. Such sub-frames arise in setups involving erasures (communication), random user activity (multiple access), or sparsity (signal processing), in addition to channel or quantization noise. The goodness of a frame as an analog code is a function

Marina Haikin, Matan Gavish, Dustin G. Mixon and Ram Zamir (2021), “Asymptotic Frame Theory for Analog Coding[®] (submitted for review July 2021)”, Foundations and Trends[®] in Communications and Information Theory: Vol. xx, No. xx, pp 1–18. DOI: 10.1561/XXXXXXXXXX.

of the eigenvalues of a sub-frame, averaged over all sub-frames (e.g., harmonic mean of the eigenvalues relates to least-square estimation error, while geometric mean to the Shannon transform, and condition number to the restricted isometry property).

For the highly symmetric class of Equiangular Tight Frames (ETF), as well as for other “near ETF” frames, we show that the empirical eigenvalue distribution of a randomly-selected sub-frame (*i*) is asymptotically indistinguishable from Wachter’s MANOVA distribution; and (*ii*) exhibits a universal convergence rate to this limit that is empirically indistinguishable from that of a matrix sequence drawn from MANOVA (Jacobi) ensembles of corresponding dimensions. Some of these results are shown via careful statistical analysis of empirical evidence, and some are proved analytically using random matrix theory arguments of independent interest. The goodness measures of the MANOVA limit distribution are better, in a concrete formal sense, than those of the Marchenko–Pastur distribution at the same aspect ratio, implying that deterministic analog codes are better than random (i.i.d.) analog codes. We further give evidence that the ETF (and near ETF) family is in fact superior to any other frame family in terms of its typical sub-frame goodness.

1

Introduction

A frame is an “over-complete basis”, i.e., a system of vectors that spans the space with more vectors than the space dimension (real or complex). Let us denote the space dimension by m , and the number of vectors by n , where $n > m$. The $m \times n$ frame matrix

$$F = [\mathbf{f}_1 \cdots \mathbf{f}_n] \tag{1.1}$$

is generated by stacking the frame vectors $\mathbf{f}_1, \dots, \mathbf{f}_n$ as columns, where we restrict attention to unit-norm vectors $\|\mathbf{f}_i\| = 1$.

This survey proposes an information-theoretic view on the design and analysis of frames with favorable performance. We think of a frame as an “analog code”, which can add redundancy [59], [79], [115], [131], remove redundancy [20], or multiplex information directly in the signal space [87], [108], [133]. Multiplication by the frame matrix can expand the dimension $m : n$ hence add redundancy, or reduce the dimension $n : m$ hence compress (with $\mathbf{y} = F^\dagger \mathbf{x}$ for the former and $\mathbf{x} = F \mathbf{y}$ for the latter). The aspect ratio n/m is often called the “frame redundancy”.

Although information theory tells us that reliable data transmission (adding redundancy) and compression (removing redundancy) can

be achieved by *digital* codes, real-world physical-layer communication systems combine *analog* modulation techniques that can be described in terms of frames [14], [15], [20], [60], [82], [137].¹ We are specifically interested in some old and new applications of frames that involve a combination of *random activity* and *noise*. Performance in these applications is a function of the eigenvalues of (the Gram of) a randomly selected k -subset F_S of the n frame vectors,

$$F_S = [\mathbf{f}_{i_1} \cdots \mathbf{f}_{i_k}] \quad (1.2)$$

where $S = \{i_1, \dots, i_k\} \subset [n]$, $|S| = k$. (We shall use $[n]$ to denote $\{1, \dots, n\}$.)

For example, in *non-orthogonal code-division multiple access* (NOMA-CDMA), [114], [124], [126], n users are allocated with m -length spreading sequences using the frame F , but only k out of the n users are active at any given moment, and performance is measured by the average *Shannon capacity* of the vector Gaussian channel associated with the $m \times k$ sub-matrix F_S (averaged over the subset of active users S). In transform-based *multiple-description* (MD) source coding, [60], [98], an m -dimensional vector source is expanded into n packets using the frame F ; only k packets are received, and performance is measured by the average *remote rate-distortion function* associated with F_S . In coded distributed computation (CDC), [43], [76], [78], the user (master) node expands m sub-computation tasks into n redundant tasks using the frame F , and sends them to n *noisy* computation nodes (where the noise is due to finite precision computation); only k nodes return their answers on time ($n - k$ are stragglers), and the sub-matrix F_S determines the final average precision (or noise amplification) after the user node decodes the desired computation value. Other “ (n, m, k) setups” are listed in Table 1.1.

In an ideal *noiseless* setup one could choose the frame redundancy n/m equal to the reciprocal of the activity ratio k/n , i.e., $m = k =$ the

¹Coded-modulation can be thought of as a concatenation of an outer digital code with an inner analog code or frame.

Table 1.1: (n, m, k) setups featuring analog frame codes

Application	n	m	k	$m \gtrless k$	References
Source with erasures	block-length	bandwidth	important samples	$m > k$	[64], [133]
NOMA-CDMA	users	resources (spread)	active users	$m > k$	[108], [115], [137]
Impulsive channel	block-length	bandwidth	non-erased	$m < k$	[122], [131]
Space-time coding	space \times time	diversity	non-erased	$m < k$	[117], [121]
$\Delta\Sigma$ modulation	over-sampled	original	non-erased	$m < k$	[23], [57]
Multiple descriptions	transmitted	diversity	received	$m < k$	[60], [98]
Wavelets	coefficients	source	significant coefficients	$m > k$	[73]
Compressed sensing	input	output	sparsity	$m > k$	[22], [36]
Coded computation	workers	computations	non-stragglers	$m < k$	[43], [76], [78]
Neural networks	input	output	features	$m > k$	[7]

effective number of users/packets/nodes in the examples above. This is similar to digital erasure correction using *maximum distance separable* (MDS) codes for a channel with k out of n non-erased symbols [11]. However, when *noise* is involved (channel/quantization/computation noise in the setups above), a better trade-off between noise immunity and information rate is obtained by choosing a lower/higher frame redundancy; $k < m < n$ in NOMA-CDMA, or $m < k < n$ in MD and CDC. Thus, m is a design parameter that we can optimize.

Frame design could be viewed as an attempt to find vectors $\mathbf{f}_1, \dots, \mathbf{f}_n$ in \mathbb{R}^m or \mathbb{C}^m , $n > m$, that are somehow as orthogonal to each other as possible, either in pairs ($k = 2$) or in larger k -subsets [73], [129]. As we shall see in Chapter 3, the sub-frame performance criteria mentioned above (capacity, rate-distortion function, noise amplification), denoted in general as $\Psi(F_S)$, depend on the spread of the eigenvalues of the Hessian $F_S F_S^\dagger$ or Gram $F_S^\dagger F_S$ matrices of the sub-frame F_S . More mutual orthogonality amounts to a more compact eigenvalue spectrum, and ideal performance occurs when the spectrum shrinks to a delta function, or equivalently, the sub-frame is orthogonal. The redundant nature of the frame, however, implies that most of its subsets are *not* orthogonal. Our target is therefore to find a frame whose *average* performance over all k -subsets

$$\bar{\Psi}(F, k) = \frac{1}{\binom{n}{k}} \sum_{\substack{S \subset [n] \\ |S|=k}} \Psi(F_S) \quad (1.3)$$

is good; more concretely, a frame whose *typical* subset has a *compact* eigenvalue spectrum.²

We borrow from information theory the probabilistic view of a communication channel, and the notions of typicality and typical-case (rather than worst-case) goodness [30]. The information-theoretic viewpoint leads us to look for frames with a “typically compact” subset spectrum for a given (n, m, k) triplet, and for frame *families* with the

²Spectrum compactness can be measured, e.g., by variance and kurtosis; see Section 10.2.

best attainable *asymptotic* goodness in the limit as n goes to infinity for fixed (asymptotic) redundancy ratios n/m and k/m . This fresh look on frames turns out to be fruitful, and opens many interesting questions at the intersection between signal processing, random matrix theory, geometry, harmonic analysis and information theory.

Sampling theory suggests the *low-pass frame* (LPF), the frame analog of band-limited interpolation, as a practical candidate for signal expansion. This turns out to be a far-from-optimal choice, as we shall see, due to a large noise amplification for a typical subset (which corresponds to noisy reconstruction from a non-uniform sampling pattern [86], [110]).

Information theory suggests the *random* (i.i.d.) frame as the natural candidate for a good analog code. To study these objects, *Random Matrix Theory* (RMT) offers a helpful matrix version of the law of large numbers: the eigenvalue distribution of a typical random matrix tends to *concentrate* towards a fixed distribution in the limit of large dimensions [1], [45]. Indeed, if we choose the elements of the frame matrix F as i.i.d. Gaussian variables, then the subset Gram matrix $F_S^\dagger F_S$ becomes a member from a Wishart ensemble, and its spectrum converges almost surely to the Marchenko–Pastur (MP) distribution with parameter $\beta = k/m$ [81]. We can thus compute the capacity / rate-distortion function / noise amplification associated with the Marchenko–Pastur distribution, and obtain some achievable asymptotic performance $\Psi(\text{MP}, \beta)$ for the problems described above.

Is the Marchenko–Pastur distribution (corresponding to random i.i.d. frames) the “most compact” subset spectrum we can hope for? One of the key results of our work is that better *deterministic* frames do exist. In fact, we show that a certain class of highly symmetric frames obeys a *universal concentration* law of the spectrum of a randomly-selected subset, just like in the case of a completely random (i.i.d.) matrix. Furthermore, the resulting asymptotic sub-frame spectrum is *more compact* than the MP distribution!

Equiangular tight frames (ETF), to be defined in Chapter 4, are in

a sense the most geometrically symmetric family of frames [24], [49], [129]. They have numerous applications in communications and signal analysis, and their study brings together geometry, combinatorics, probability, and harmonic analysis. In a series of papers [63], [64], [66], [67], [80], we demonstrated that ETFs, as well as other deterministic frames that we term “near ETFs”, exhibit an RMT-like behavior that is superior to random frames. Specifically, in [66] we showed empirically that for any frame within this class of frames, the eigenvalue distribution of a randomly-selected subset appears to be indistinguishable from that of a random matrix taken from the MANOVA ensemble (familiar from multivariate statistics). Furthermore, in [63], [67], [80] we (partially³) showed analytically that as $n \rightarrow \infty$, for aspect ratios $m/n \rightarrow \gamma$ and $k/m \rightarrow \beta$, this eigenvalue distribution converges almost surely to Wachter’s limiting MANOVA distribution parameterized by γ and β . The concluded asymptotic performance of the ETF family,

$$\bar{\Psi}(\text{ETF}, \gamma, \beta) = \Psi(\text{MANOVA}, \gamma, \beta), \quad (1.4)$$

is strictly better than $\Psi(\text{MP}, \beta)$, the asymptotic performance of random (i.i.d.) frames, for various performance measures Ψ . See Figure 1.1. We conjecture that in terms of these performance measures, the MANOVA distribution is, in fact, the *most compact* typical sub-frame spectrum achievable by any unit-norm deterministic frame.

In this survey paper we propose a common framework for topics at the intersection between information theory and neighboring fields. Chapter 2 addresses primarily the information theory audience, and motivates a passage from digital codes to low-pass interpolation and analog frame codes, through a side-information source coding problem. Chapter 3 formalizes the notion of a performance measure that depends

³ The proof is complete for the case $\gamma = 1/2$ [80]. For a general $0 < \gamma < 1$, we obtained a recursive formula in r for the asymptotic mean r th moment of a randomly-selected ETF subset, for $r = 1, 2, \dots$. We were able to verify symbolically that this formula coincides with the r th MANOVA moment for small r ’s, but the computation complexity explodes beyond $r = 10$, and a proof of the identity for a general $r \in \mathbb{N}$ is still missing.

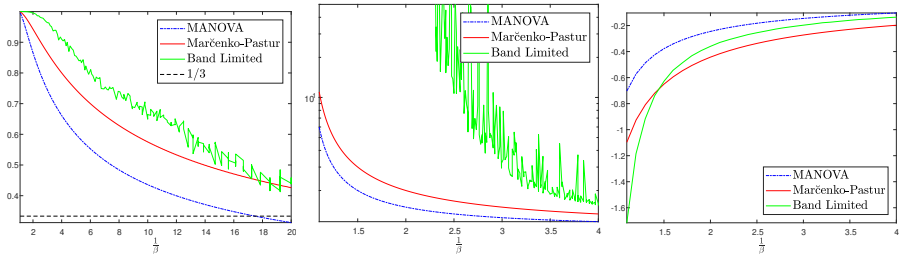


Figure 1.1: Comparison of the asymptotic performance measures $\Psi(\text{MANOVA}, \beta, \gamma)$, $\Psi(\text{Marcenko-Pastur}, \beta)$ and $\Psi(\text{Band Limited}, \beta, \gamma)$, as a function of β , for $\gamma = 1/2$ (corresponding to a sub-frame with aspect ratio β taken from a redundancy-2 frame in the families of ETF, random (i.i.d.), and LPF, respectively). Each of the three figures compares for a different sub-frame performance measure Ψ : (Left) statistical restricted isometry property (RIP) associated with compressed sensing (lower is better), where $1/3$ is the sharp RIP bound for sparse signal and low rank matrix recovery [19]; (Middle) noise amplification associated with MD and CDC (lower is better); (Right) Shannon transform associated with the capacity of NOMA-CDMA (higher is better).

on the eigenvalue spectrum of a sub-frame; e.g., noise amplification amounts to the harmonic mean of the spectrum, while capacity (Shannon transform) amounts to the geometric mean of the spectrum. Chapter 4 gives background from frame theory (in particular, earlier results on the spectral properties of sub-frames motivated by compressed sensing), while Chapter 5 gives the relevant background on random matrix theory.

The two highlights of this survey are (i) the *ETF-MANOVA relation*, connecting frame theory with random matrix theory, and (ii) the (still mostly open) possibility of *ETF superiority*. The first highlight is divided between two sections: Chapter 6 describes the empirical results of [66] regarding the universal behavior of sub-frames of ETFs and “near ETFs”; and Chapter 7 develops analytically the convergence to the MANOVA limit distribution based on the moment method (see footnote 3 above) [63], [67], [80]. To support the ETF superiority claim, we examine numerically in Chapter 9 some of the applications listed in Table 1.1; and we prove analytically in Chapter 10 the *erasure Welch bound*, which implies that tight frames have the smallest sub-frame spectral variance

among all unit-norm frames, and that ETFs have the smallest sub-frame spectral kurtosis among all unit-norm tight frames. In between these two highlights, Chapter 8 proves some sub-frame performance inequalities (in the flavor of the information-theoretic inequalities of [33]), which explain the role of the sub-frame aspect ratio k/m as a design parameter. Finally, Chapter 11 concludes and lists interesting open questions and conjectures that arise in this area.

1.1 Notation

A finite sequence of integers $\{1, \dots, n\}$ is denoted as $[n]$. Bold letters \mathbf{f}, \mathbf{x} etc. denote column vectors. The $n \times n$ identity matrix is denoted by I_n . Dagger $(\cdot)^\dagger$ denotes transpose or conjugate (Hermitian) transpose, according to the context. The set of all k -subsets of the set $[n]$ is denoted $\binom{[n]}{k}$, or $\{S \subset [n] : |S| = k\}$, or simply $\{S : |S| = k\}$ when the context is clear. Throughout we try to keep the following glossary:

m	vector space dimension
n	frame size
k	sub-frame size
p	selection probability
γ	frame aspect ratio m/n
β	sub-frame aspect ratio k/m
F	$m \times n$ frame matrix
S	k -subset of $[n]$
F_S	$m \times k$ sub-frame matrix
Ψ	performance measure

2

An information-theoretic toy example

To set the stage for the information theory audience, we begin with an “ (n, m, k) ” source coding problem that originally motivated this study [64], [83].

2.1 Source coding with erasures

Consider the setup shown in Figure 2.1, of a source with “distortion side information” at the encoder [83]. Specifically, the encoder of a (white) Gaussian source $X \sim N(0, \sigma_x^2)$ has access to a statistically independent Bernoulli(p) variable S that reveals whether the source sample X is “important” (to be reconstructed under a squared-error distortion) or not. The distortion measure is thus given by

$$d(x, \hat{x}, s) = \begin{cases} (\hat{x} - x)^2, & \text{if } s = 1 \text{ (“important”)} \\ 0, & \text{if } s = 0 \text{ (“don’t care”)}, \end{cases} \quad (2.1)$$

and the mean-squared error (MSE), i.e., the average distortion per important sample in encoding the block X_1, \dots, X_n , is given by¹

$$D = \frac{1}{np} \sum_{t=1}^n 1_{\{S_t=1\}} \cdot E\{(\hat{X}_t - X_t)^2\}. \quad (2.2)$$

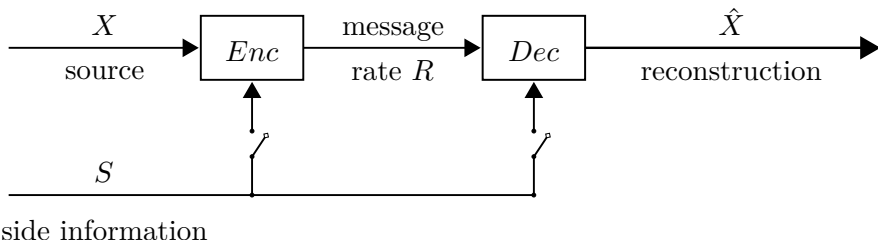


Figure 2.1: Source coding with distortion side information. Our problem of interest is when only the first switch is connected.

If also the decoder had access to the side information, then the best achievable rate-distortion trade off is given by the conditional rate-distortion function of X given S [10], [30]:

$$R_{X|S}(D) = \min_{\hat{X}} I(X; \hat{X}|S) = \frac{p}{2} \cdot \log_2 \left(\frac{\sigma_x^2}{D} \right) \quad (2.3)$$

bits per source sample, where a possible minimizing $p(\hat{x}|x, s)$ in (2.3) is the optimal quadratic-Gaussian test-channel $p^*(\hat{x}|x)$ for $s = 1$, and a degenerate channel (say, $\hat{X} \equiv 0$) for $s = 0$. This simply amounts to ignoring the non-important samples, and communicating the $k \approx np$ out of n important samples at a rate of $(1/2) \log_2(\sigma_x^2/D)$ bits per sample. Interestingly, like in some other favorite side-information problems in information theory, [29], [30], there is no loss for having access to the side information at just one end of the communication channel: the same rate-distortion trade off (2.3) can be achieved even if S is available

¹For simplicity, the normalization is by the *expected* number of important samples: $np = E\{\sum_{t=1}^n 1_{\{S_t=1\}}\}$.

only at the encoder!² A formal proof is obtained by computing the rate-distortion function of the equivalent source pair (X, S) , under the distortion measure (2.1):

$$R_{X,S}(D) = \min_{\hat{X}} I(X, S; \hat{X}) = \frac{p}{2} \cdot \log_2 \left(\frac{\sigma_x^2}{D} \right), \quad (2.4)$$

where the minimizing $p(\hat{x}|x, s)$ now has the optimum marginal $p^*(\hat{x})$ for *both* values of s ; i.e., $p(\hat{x}|x, s = 1) = p^*(\hat{x}|x)$ and $p(\hat{x}|x, s = 0) = p^*(\hat{x})$. It follows from the chain rule that the minimizing \hat{X} in (2.4) has *zero* mutual information with the side information S , i.e., $I(S; \hat{X}) = 0$, which is a necessary feature of a zero-loss solution [83].

2.1.1 Complexity of the all-digital solution

The information-theoretic promise comes however at a high price: the complexity of n -dimensional vector quantization. Specifically, to achieve the rate-distortion function (2.4) one needs to draw 2^{nR} codewords of size n at random, and to encode the source vector X_1, \dots, X_n into a jointly typical codeword: close to the important samples and arbitrary at the non-important samples [30]. Clearly, the encoding complexity is exponential in n . A simple naive solution would be first to encode the side information, i.e., describe the location of the important samples at a rate of $H_b(p) = p \log(1/p) + (1-p) \log(1/(1-p))$, e.g., 1 bit per sample for $p = 1/2$; and then to quantize only the important samples using a simple *scalar* quantizer (with just a small loss compared to optimal vector quantization)³. If however we do not want to pay the rate penalty of ~ 1 bit per sample for encoding the side information, then we cannot replace the complex n -dimensional codebook by simple scalar quantization of the important samples because their location is a

²This setup can be seen as a counterpart of the Slepian–Wolf problem, [30], [112], of “statistical side information” at the decoder.

³Entropy-coded scalar quantization exceeds the rate-distortion function by only $\approx 1/4$ bit per sample at high resolution conditions [55], [138].

priori unknown. Can we simplify the solution without sacrificing too much in rate-distortion performance?

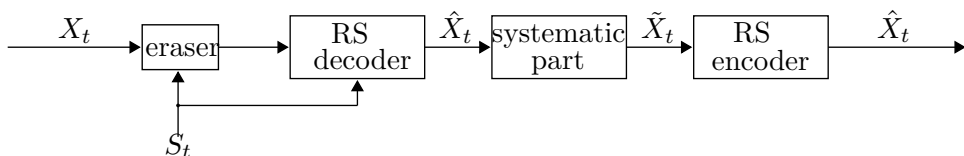


Figure 2.2: Reversed Reed–Solomon coding for a discrete source with erasures known at the encoder. Source = X_1, \dots, X_n , reconstruction = $\hat{X}_1, \dots, \hat{X}_n$, compressed version = $\tilde{X}_1, \dots, \tilde{X}_k$.

2.1.2 A simple solution in the discrete case

Martinian et al. suggested an intriguing and simple yet optimal solution based on a *reversed Reed-Solomon (RS) code* for a *lossless* variant of this problem [83]. Here, the source X is uniform over a finite alphabet \mathcal{X} , the important samples are encoded under a Hamming distortion measure:

$$d(x, \hat{x}, s) = \begin{cases} 1_{\hat{x} \neq x}, & \text{if } s = 1 \text{ (“important”)} \\ 0, & \text{if } s = 0 \text{ (“don’t care”)}, \end{cases} \quad (2.5)$$

and we target a small ($D \rightarrow 0$) average distortion. The idea of [83] was to treat the non-important samples as “erasures”, and use an erasure-correction (e.g., RS) code in *reverse*: the encoder applies RS decoding to “correct” the erasures to the codeword $\hat{\mathbf{x}}$ (that matches the source at the non-erased (important) samples $\{t : s_t = 1\}$), and then it transmits the systematic part of $\hat{\mathbf{x}}$; the decoder uses RS encoding to reconstruct $\hat{\mathbf{x}}$ from the systematic part. See Figure 2.2. Clearly, the decoder has no idea which samples are important and which are not, so $I(\mathbf{S}, \hat{\mathbf{X}}) = 0$ like in (2.4). Moreover, assuming that the number of important samples

$$k = pn \quad (2.6)$$

is (roughly) constant, the maximum-distance separable (MDS) property of RS codes implies that perfect erasure correction is possible using an (n, k) code.⁴ Thus, the size of the systematic part is k , and the coding rate is $R = (k/n) \log_2 |\mathcal{X}|$ bits per sample, as if both the encoder and decoder knew which samples are important and which not.

2.2 Band-pass interpolation

It is tempting to mimic the philosophy of the “reverse” RS-code solution above in the quadratic-Gaussian problem of Figure 2.1. We are inspired by the view of a cyclic code (in particular, an RS code) as consisting of all codewords whose Fourier transform (over the corresponding Galois field) is zero in a certain band of frequencies [11], [12]. Hence, erasure correction can be thought of as “band-limited interpolation”, while the optimum ratio k/n corresponds to the “Nyquist sampling rate” [134]. This interpretation suggests a discrete Fourier transform (DFT)-based “analog” coding scheme for real- or complex-valued vector sources, [64], as shown in Figure 2.3. Each codeword is a “low-pass” vector, i.e., an n -dimensional vector whose high DFT coefficients are zero. The encoder looks for a low-pass vector that matches the important samples, and transmits a quantized version (scalar or vector quantization) of its nonzero DFT coefficients. The decoder then reconstructs the source by inverse DFT.

2.2.1 Coding and decoding

To define the scheme precisely, assume for now that as in (2.6) the number of important samples is constant and equal to $k = pn$. Namely, the importance side-information law is “combinatorial” (n choose k) rather than Bernoulli(p). Let m , the codewords bandwidth, $k \leq m \leq n$, be a design parameter to be optimized later, and let F denote the upper

⁴Implicit in this construction is that the size of the alphabet \mathcal{X} is a prime power, and meets the Galois field requirements of the RS code.

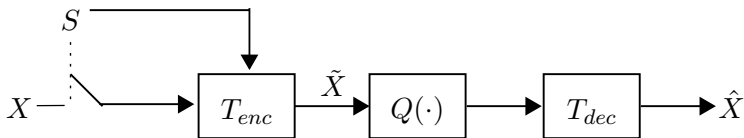


Figure 2.3: Band-limited interpolation coding scheme. Depicted are the source X_1, \dots, X_n ; important samples $\{X_t : s_t = 1\}$; encoder $m \times k$ transformation $T_{enc} = F_S(F_S^\dagger F_S)^{-1}$; quantizer input $\tilde{X}_1, \dots, \tilde{X}_m$; quantizer output $Q(\tilde{X}_1), \dots, Q(\tilde{X}_m)$; decoder $n \times m$ transformation $T_{dec} = F^\dagger$; and reconstruction $\hat{X}_1, \dots, \hat{X}_n$. This combination of DFT to handle “erasures” and quantization to introduce “noise” can be viewed as *hybrid analog–digital* coding.

$m \times n$ (lowpass) section from the $n \times n$ DFT matrix:

$$F = \frac{1}{\sqrt{m}} \begin{bmatrix} 1 & w & w^2 & \dots & w^{n-1} \\ 1 & w^2 & w^4 & \dots & w^{2(n-1)} \\ \vdots & & & & \\ 1 & w^m & w^{2m} & \dots & w^{m(n-1)} \end{bmatrix}, \quad (2.7)$$

where $w = e^{-j2\pi/n}$, $j = \sqrt{-1}$, and the $1/\sqrt{m}$ pre-factor normalizes each column to a unit norm. The vertical axis corresponds to “frequency” and the horizontal axis to “time”. The matrix F defines an “ m lowpass” codebook, i.e., vectors $\mathbf{x}' \in \mathbb{C}^n$ whose higher $n - m$ DFT coefficients are zero; these vectors live in the row space of F , so $\mathbf{x}' = F^\dagger \tilde{\mathbf{x}}$ for some “frequency vector” $\tilde{\mathbf{x}}$ in \mathbb{C}^m . The subset of the time instances of important samples, $S = \{t : s_t = 1\} \subset [n]$, defines the $m \times k$ sub-matrix F_S , (1.2), and a corresponding k sub-vector \mathbf{x}_S of the source vector $\mathbf{x} = (x_1, \dots, x_n)$. The encoder looks for a codeword \mathbf{x}' that matches the important samples sub-vector \mathbf{x}_S , and computes its corresponding frequency vector $\tilde{\mathbf{x}}$:

$$\mathbf{x}_S = (\mathbf{x}')_S = F_S^\dagger \tilde{\mathbf{x}}. \quad (2.8)$$

If $m = k$, then the solution $\tilde{\mathbf{x}} = (F_S^\dagger)^{-1} \mathbf{x}_S$ for (2.8) is unique.⁵ For $m > k$ the solution is generally not unique, and for reasons to be clear

⁵Any band of rows of the DFT matrix is “full spark”, i.e., any square sub-matrix of a DFT band is invertible [47], [113].

soon, a good estimate for $\tilde{\mathbf{x}}$ is the least-squares (LS) “pseudo inverse” solution

$$\tilde{\mathbf{x}}_{\text{LS}} = F_S \cdot (F_S^\dagger \cdot F_S)^{-1} \cdot \mathbf{x}_S, \quad (2.9)$$

i.e., the $\tilde{\mathbf{x}}$ satisfying (2.8) with the minimum squared-norm.⁶ After estimating $\tilde{\mathbf{x}}$, the encoder transmits a quantized version $Q(\tilde{\mathbf{x}})$ to the decoder, which reconstructs the source via inverse DFT:⁷

$$\hat{\mathbf{x}} = \text{IDFT}[Q(\tilde{\mathbf{x}})|0, \dots, 0] = F^\dagger \cdot Q(\tilde{\mathbf{x}}). \quad (2.10)$$

Indeed, if we neglect the quantization operation $Q(\cdot)$ in (2.10), then by (2.8) the important samples are perfectly reconstructed, i.e., $\hat{x}_t = x_t$, for all t in S .

2.2.2 Rate-distortion performance

The rate-distortion performance of this analog coding scheme depends on the characteristics of the quantization operation $Q(\cdot)$. An efficient analytical tool is the additive-noise “test channel” model of entropy-coded (subtractive) dithered quantization (ECDQ) [138], [140]. For a given pattern S of important samples, the ECDQ coding rate in bits per source sample [64] is given by

$$R_{\text{analog}}(S, D) = \frac{m}{2n} \cdot \log \left(1 + \frac{\frac{1}{m} E\{\|\tilde{\mathbf{X}}\|^2\}}{D} \right) \quad (2.11)$$

where the expectation $E\{\cdot\}$ is with respect to randomness of the source \mathbf{X} . See Appendix A. As explained earlier, LS estimation (2.9) minimizes the squared norm of $\tilde{\mathbf{X}}$, hence it minimizes the coding rate (2.11) among all possible solutions for (2.8). Using (2.9); recalling the definition of the system parameters: the non-erasure probability p , the aspect ratio

⁶Note that (2.9) is the unique solution $\tilde{\mathbf{x}}$ for (2.8) in the column space of F_S (which is a k -dimensional subspace of \mathbb{C}^m), and any other solution can be written as $\tilde{\mathbf{x}}_{\text{LS}} + \mathbf{z}$ for some \mathbf{z} in the orthogonal subspace.

⁷An equivalent solution for the case where n/m is an integer, is to *uniformly* re-sample $\mathbf{x}' = F^\dagger \tilde{\mathbf{x}}_{\text{LS}}$, transmit the m quantized uniform samples, and reconstruct by $m : n$ band-limited interpolation.

of the $m \times n$ matrix F , and the aspect ratio of the $m \times k$ sub-matrix F_S ,

$$p = \frac{k}{n}, \quad \gamma = \frac{m}{n} \quad \text{and} \quad \beta = \frac{k}{m}; \quad (2.12)$$

and assuming a white-Gaussian source $\mathbf{X} \sim N(0, \sigma_x^2 I)$, we can rewrite the ECDQ coding rate (2.11) as

$$R_{\text{analog}}(S, D) = \frac{p}{2\beta} \cdot \log \left(1 + \frac{\sigma_x^2}{D} \cdot \beta \cdot \Psi_{\text{MSE}}(F_S) \right) \quad (2.13)$$

where

$$\Psi_{\text{MSE}}(F_S) \triangleq \frac{\text{trace} \left((F_S^\dagger F_S)^{-1} \right)}{k} \quad (2.14)$$

is the *signal amplification factor* of the sub-matrix F_S .⁸ Finally, the *operational rate-distortion function* of the system is the average of the ECDQ coding rate over all k -subsets $S \subset [n]$:

$$\bar{R}_{\text{analog}}(D) = \frac{1}{\binom{n}{k}} \sum_{S:|S|=k} R_{\text{analog}}(S, D) \quad (2.15)$$

as in (1.3).

In view of (2.11)-(2.15), the system performance differs from the information-theoretic bound (2.4) in three aspects, which contribute to the loss of the analog coding scheme with respect to the optimum performance (2.3): (i) the “+1” term inside the log; (ii) the design parameter $\beta \leq 1$ that appears both as a pre-log factor and inside the log; and (iii) the signal-amplification factor (2.14). The “+1” term is negligible for high signal-to-distortion ratio $\sigma_x^2 \gg D$, and it can be eliminated (for $\beta = \Psi_{\text{MSE}} = 1$) if we replace LS estimation by minimum mean-squared error (MMSE) estimation [64]. As for the role of β , since the function $x \log(1 + a/x)$ is monotonically *increasing* in x , choosing $\beta < 1$ can only be justified if the effect on reducing the signal amplification factor $\Psi_{\text{MSE}}(F_S)$ is stronger for sufficiently many subsets S .

⁸The notation uses “MSE” because (2.14) plays the role of mean-square error (MSE) amplification in other problems; see Chapter 9.

2.3 Non-uniform sampling and signal amplification

The signal amplification factor (2.14) plays a key role in understanding frame goodness. As we shall see, it is greater than or equal to 1 for every subset S , and it tends to increase with the subset size k , i.e., with β (see Chapter 8). The equality $\Psi_{MSE}(F_S) = 1$ holds if and only if the column vectors of F_S are orthogonal. Indeed, if $l = n/k$ is an integer and the pattern S happens to fall on a uniform grid (i.e., $t_i = t_1 + (i - 1)l$ modulo n , for $i = 1, \dots, k$), then for $\beta = 1$, the sub-matrix F_S becomes a $k \times k$ DFT matrix, up to a constant phase shift. Thus, F_S is unitary and $F_S^\dagger F_S$ is an identity matrix, $\Psi_{MSE} = 1$, and the coding rate $R_{\text{analog}}(S = \text{uniform}, D)$ coincides with the information-theoretic bound (2.4) at high signal-to-distortion ratio. (If we multiply the reconstruction by the Wiener estimation coefficient, then for a uniform pattern the scheme is optimal for any signal-to-distortion ratio [64]).

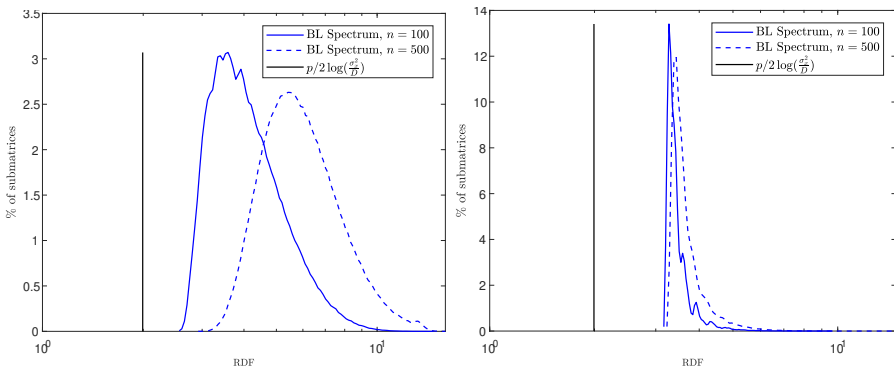


Figure 2.4: Histogram of the operational RDF $R_{\text{analog}}(S, D)$ for random subsets S from a low-pass (BL) frame with two frame sizes ($n = 100$ and 500), for $\sigma_x^2/D = 1000$, $p = 0.4$, and: (left) $\gamma = 1/2$ and $\beta = 0.8$; (right) $\gamma = 2/3$ and $\beta = 0.6$. The vertical line shows Shannon's RDF (2.3).

A typical pattern S of a Bernoulli process is, however, far from being uniform, and so the signal amplification factor (2.14) is typically

strictly greater than one. This phenomena is known in the literature as *noise amplification* in signal recovery from noisy non-uniform samples [86], [110]. It implies that the operational rate-distortion function (2.15) of the analog “bandlimited interpolation” scheme fails to achieve the information-theoretic bound (2.4), as was already observed (for $\beta = 1$) in [83] and [84]. Figure 2.4 shows a histogram of $R_{\text{analog}}(S = \text{random}, D)$ for two values of β . We see that the overall effect of decreasing β below one is to reduce the rate. We also see that in this case, a larger frame size ($n = 500$) is worse than a smaller one ($n = 100$). In any case, the average loss compared to (2.4) is still much higher than the ~ 1 bit penalty of the naive side information coding scheme.

2.4 From interpolation to frame codes

Fortunately, the analog “band-limited interpolation” coding approach can be saved by replacing the low-pass DFT matrix (2.7) by frames which are more robust to the erasure pattern. Analog codes follow a long line of works in the communications literature, that used linear transform-based codes for noise and erasures, under names like “DFT codes” [106], [131], “coding over the reals” [82], “analog BCH/RS codes” [107], [119], and in a broad sense also in *sigma-delta modulation* [25], *code-division multiple access* [108], *multiple-description coding* [60], [98], *space-time coding* [117], and *coded distributed computation* [76]. In the context of the current work, the low-pass DFT matrix F is a special case of a *harmonic frame*, i.e., a subset of the rows of the DFT matrix [118], [129]. This viewpoint opens our discussion to general frames in the form of (1.1), and the rich frame theory. Interestingly, in a sharp contrast to the consecutive band of frequencies in the low-pass frame (2.7), the performance of analog coding is optimized by an “irregular” (random-like) selection of the DFT rows, which leads us to *equiangular tight frames* [133].

3

Sub-frame performance measures

The previous chapter provided an information-theoretic motivation to assess a frame by averaging a specific performance measure (noise amplification) over sub-frames of a fixed size. In this section we show that this, as well as other relevant frame performance measures, are functions of the *eigenvalue spectrum* of sub-frames. The sub-frame-average viewpoint will motivate our search for “good” frames. We start yet with another well known frame performance measure, the mean-squared *pairwise cross correlation*, and the notions of the Welch bound and a *tight frame*.

3.1 The Welch bound

The development of code-division multiple access (CDMA) triggered the introduction of the Welch bound (WB) [130] on the average squared-correlation between all distinct pairs of an over-complete set of unit-norm vectors $\{\mathbf{f}_1, \dots, \mathbf{f}_n\}$ in \mathbb{R}^m or \mathbb{C}^m :

$$\frac{1}{(n-1)n} \sum_{i \neq j} |\langle \mathbf{f}_i, \mathbf{f}_j \rangle|^2 \geq \frac{n-m}{(n-1)m}. \quad (3.1)$$

The Welch bound is achieved with equality if and only if the frame $F = [\mathbf{f}_1 \cdots \mathbf{f}_n]$ is *tight*, i.e., $F \cdot F^\dagger = (n/m) \cdot I_m$ [73], [108], [133]. For example, the low-pass frame (2.7) and the repetition frame $F = [I_m \cdots I_m]$ (or any union of orthonormal bases) are tight. The weakness of the Welch bound (3.1), however, is that it measures the frame as a *whole*. While “the whole is greater than the sum of its parts”, in our problems of interest every (or almost every) individual part must be good, so tightness is not sufficient.

3.2 Noise amplification

Let us return to the erasure source coding problem of Section 2.1. At high signal-to-distortion ratio, each term in the operational rate-distortion function (2.15) becomes $(m/2n) \cdot \log(\Psi_{\text{MSE}}(F_S))$, plus some constant independent of the frame matrix F , where $\Psi_{\text{MSE}}(F_S)$ is defined in (2.14). This gives rise to a subset-average performance measure of the form (1.3), to which we refer as “MSE goodness”:

$$L_{\text{MSE}}(F, k) = \frac{1}{\binom{n}{k}} \sum_{S:|S|=k} \log(\Psi_{\text{MSE}}(F_S)), \quad (3.2)$$

where the sum is over all k -subsets S of $[n]$, i.e., over all $m \times k$ submatrices F_S of F . The MSE goodness measure (3.2) implies a frame optimization criterion for any triplet $n \geq m \geq k$:

$$L_{\text{MSE}}^*(n, m, k) = \min_F L_{\text{MSE}}(F, k), \quad (3.3)$$

where the minimization is taken over all $m \times n$ unit-norm frames (1.1).¹ Once the minimal loss function (3.3) is known, we can go back and optimize the free bandwidth parameter m (or equivalently $\beta = k/m$) in the operational rate distortion function (2.15) as a function of the number of non-erased samples k (or equivalently the erasure probability p) and the signal-to-distortion ratio σ_x^2/D . We note that other problems of interest give rise to the complementary case where $n \geq k \geq m$ (i.e.,

¹The spark of F must be larger than k , otherwise the sum in (3.2) is infinite [47].

β is now greater than 1), in which case the MSE performance measure (2.14) is computed with respect to the sub-frame Hessian $F_S F_S^\dagger$ rather than the Gram matrix $F_S^\dagger F_S$:

$$\Psi_{\text{MSE}}(F_S) = \frac{\text{trace}\left((F_S F_S^\dagger)^{-1}\right)}{k}.$$

3.2.1 Asymptotic goodness

Information theory tends to look on the asymptotic performance of large block codes, at some fixed redundancy. It is therefore tempting to explore the large dimensional behavior of (3.3), when the aspect ratios $\beta = k/m$ and $\gamma = m/n$ in (2.12) are held fixed:

$$L_{\text{MSE}}^*(\gamma, \beta) \triangleq \liminf_{n \rightarrow \infty} L_{\text{MSE}}^*(n, m = \lfloor n\gamma \rfloor, k = \lfloor n\gamma\beta \rfloor), \quad (3.4)$$

and to find a frame family with aspect ratio going to γ that asymptotically achieves it. Alternatively, we can use Bernoulli(p) (rather than combinatorial) selection of the pattern S (as in the original source coding problem of Section 2.1), where the subset size k becomes a random variable with expectation pn . We expect that rare events where k significantly deviates from pn are asymptotically negligible, so

$$L_{\text{MSE}}^*(\gamma, p) = L_{\text{MSE}}^*(\gamma, \beta = p/\gamma). \quad (3.5)$$

Assuming this asymptotic MSE goodness measure is not zero, it reflects a fundamental loss of analog coding with respect to the information theoretic bound (2.3).

3.3 Spread of eigenvalues

The performance measures (2.14) and (3.2) are functions of the $k \times k$ sub-frame Gram matrix $F_S^\dagger F_S$. It is useful and insightful to express them in terms of the eigenvalues $\lambda_1, \dots, \lambda_k$ of $F_S^\dagger F_S$ (i.e., the squared nonzero singular values of the sub-matrix F_S). Recall that the trace of a matrix is equal to the sum of its eigenvalues, so $\lambda_1 + \dots + \lambda_k = \text{trace}\left((F_S^\dagger F_S)\right) = k$,

where the last equality follows because F_S is composed of k unit-norm vectors. Also, the eigenvalues of an inverse matrix are the inverse eigenvalues. Thus, the signal amplification factor (2.14) of a specific sub-matrix can be written as

$$\Psi_{\text{MSE}}(F_S) = (1/k) \left[\lambda_1^{-1} + \dots + \lambda_k^{-1} \right] = \frac{\left[\frac{\lambda_1 + \dots + \lambda_k}{k} \right]}{\left[\frac{1/\lambda_1 + \dots + 1/\lambda_k}{k} \right]^{-1}}, \quad (3.6)$$

i.e., as the *arithmetic-to-harmonic means ratio* (AHMR) of the eigenvalues of the Gram sub-matrix $F_S^\dagger F_S$. By the *means inequality*, the AHMR is greater than or equal to one, with equality if and only if all the eigenvalues are equal (and in our case, if all the eigenvalues are equal to one). Thus, $\Psi_{\text{MSE}}(F_S)$ is greater than or equal to one, with equality if and only if $F_S^\dagger F_S$ is an identity matrix, i.e., the column vectors of F_S are orthogonal.

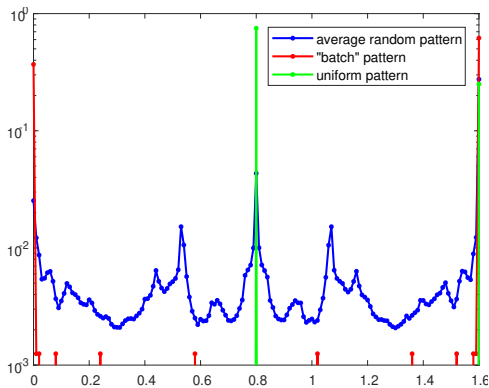


Figure 3.1: Eigenvalues of subsets of the LPF frame (2.7), with $p = 1/2$, $\gamma = 0.625$, $\beta = 0.8$ ($n = 1600$, $m = 1000$, $k = 800$), for several possible patterns S : uniform, random, batch.

Clearly, since $n > m$, not all subsets of $\{\mathbf{f}_1, \dots, \mathbf{f}_n\}$ can be orthogonal, so $\Psi_{\text{MSE}}(F_S)$ must be greater than one for some patterns S . Figure 3.1 illustrates the spread of the eigenvalues $\lambda_1, \dots, \lambda_k$ of $F_S F_S^\dagger$ around their mean (i.e., 1) for the low-pass frame (2.7), for three possible patterns: uniform sampling, random-like sampling, and consecutive

samples (batch). We observe that for this frame the eigenvalue spread is very sensitive to the pattern S . Thus, a “good” frame should be robust in the sense that the eigenvalue spread of (most of) its subsets is small.

3.4 Shannon transform

The Shannon transform of the sub-matrix F_S is the capacity of a multiple-input multiple-output (MIMO) AWGN channel characterized by F_S [121], [124], [126], [136]. At high signal-to-noise ratio, and assuming $n \geq k \geq m$, the Shannon transform gives rise to a “log-det” *geometric-to-arithmetic means ratio* goodness measure of the $m \times k$ sub-frame F_S :

$$\Psi_{\text{Shannon}}(F_S) = \frac{1}{m} \cdot \log \left(\det[\beta^{-1} \cdot F_S F_S^\dagger] \right) \quad (3.7a)$$

$$= \log \left(\frac{\sqrt[m]{\lambda_1 \cdots \lambda_m}}{\frac{\lambda_1 + \cdots + \lambda_m}{m}} \right). \quad (3.7b)$$

Similarly to (3.6), the argument of the logarithm is smaller than or equal to one, with equality if and only if the eigenvalues of $F_S F_S^\dagger$ are identical. Thus, Ψ_{Shannon} is another measure for the spread of the eigenvalues of F_S . The corresponding average sub-frame performance measure (1.3) is the “Shannon goodness”:

$$L_{\text{Shannon}}(F, k) = \frac{1}{\binom{n}{k}} \sum_{S: |S|=k} \Psi_{\text{Shannon}}(F_S) \quad (3.8)$$

where the sum is over all k -subsets of $[n]$. As above, we define the associated frame optimization criterion

$$L_{\text{Shannon}}^*(n, m, k) = \max_F L_{\text{Shannon}}(F, k), \quad (3.9)$$

as well as the asymptotic counterparts $L_{\text{Shannon}}^*(\gamma, \beta)$ and $L_{\text{Shannon}}^*(\gamma, p)$ (for Bernoulli(p) selection) as in (3.3)-(3.5).

3.5 Statistical RIP and condition number

We now turn to performance measures which look only on the *edges* of the sub-frame spectrum. In compressed sensing, the Restricted Isometry

Property (RIP) is a well-known sufficient condition for sparse recovery [22]. A “sensing” frame F satisfies a δ -RIP of order k if the spectral radius of $F_S^\dagger F_S - I_k$, i.e.,

$$\Psi_{RIP}(F_S) = \max\{\lambda_{max}(F_S) - 1, 1 - \lambda_{min}(F_S)\}, \quad (3.10)$$

is uniformly bounded by δ for all k -subsets S of $[n]$, where λ_{max} and λ_{min} are the maximum and minimum eigenvalues of the Gram matrix $F_S^\dagger F_S$. For $\delta < 1/2$, this condition guarantees perfect recovery, via ℓ_1 -minimization, in sensing any $k/2$ -sparse vector, while $\delta < 1/3$ allows one to sense any k -sparse vector [19], [21], [22], [51].²

The RIP is, however, dominated by the worst subset, which is too restrictive in view of the “typical” approach of information theory. The *statistical RIP* allows some fraction of the subsets to exceed the uniform bound [20]. The fraction of “good” subsets can be written as an average of the indicator of the event $\{\Psi_{RIP}(F_S) \leq \delta\}$ over the subset S , and we may wish to maximize it over all $m \times n$ frames F :

$$L_{StRIP}^*(n, m, k, \delta) = \max_F \frac{1}{\binom{n}{k}} \sum_{S: |S|=k} 1_{\{\Psi_{RIP}(F_S) \leq \delta\}}. \quad (3.11)$$

To complete the picture, we shall also define the closely related notion of sub-frame condition number

$$\Psi_{\text{cond}}(F_S) = \frac{\lambda_{\max}(F_S)}{\lambda_{\min}(F_S)} \quad (3.12)$$

and the associated sub-frame average (1.3) (or statistical δ -average as in (3.11)), as well as the corresponding optimum “ (n, m, k) frame” as in (3.3) and (3.9).

3.6 Sub-frame rectangularity

In Chapter 8 we show that the sub-frame performance measures above (in particular, $L_{\text{MSE}}(n, m, k)$ and $L_{\text{Shannon}}(n, m, k)$) exhibit a natural

²(1) Doesn't the vector dimension m play any role in the recovery threshold?
(2) The source of uncertainty here is the location of the sparse components of the input vector (unlike in the previous two performance measures, where the source of uncertainty is additive noise).

monotonic behavior as a function of the sub-frame aspect ratio k/m . The more rectangular is the sub-frame, the better is the average goodness of the frame. See also Figure [2.4](#).

4

Frame theory

In this section we formalize the discussion of frames and introduce a few important examples. Frame theory is the study of overcomplete systems in a Hilbert space. In particular, a sequence $\{\mathbf{f}_i\}_{i \in I}$ of vectors in a Hilbert space H is said to be a *frame* if there exist constants $a, b > 0$ such that

$$a\|\mathbf{x}\|^2 \leq \sum_{i \in I} |\langle \mathbf{x}, \mathbf{f}_i \rangle|^2 \leq b\|\mathbf{x}\|^2 \quad (4.1)$$

for every $\mathbf{x} \in H$. If $a = b$, then $\{\mathbf{f}_i\}_{i \in I}$ is known as a *tight frame*, in which case the frame enjoys a painless reconstruction formula [32]:

$$\mathbf{x} = \frac{1}{a} \sum_{i \in I} \langle \mathbf{x}, \mathbf{f}_i \rangle \mathbf{f}_i.$$

As an example, one may verify that the *low-pass frame* (2.7) obtained from the first m rows of the $n \times n$ discrete Fourier transform matrix is a tight frame for \mathbb{C}^m . In general, one may select any m rows from any $n \times n$ unitary matrix to produce a tight frame of n vectors in \mathbb{C}^m . As another example, one may combine r orthonormal bases for \mathbb{C}^m to produce a tight frame consisting of $n = rm$ vectors. For instance, the *repetition frame* consists of r copies of the same basis, while the

spike-and-sine frame combines the identity basis with the Fourier basis. Note that for *unit-norm tight* frames, the constants in (4.1) satisfy $a = b = n/m$.

Frames were introduced in 1952 by Duffin and Schaeffer [38] in the context of nonharmonic Fourier series. More recently, frames have been used as models for data processing, as information about $\mathbf{x} \in H$ can be recovered from the frame coefficients $\{\langle \mathbf{x}, \mathbf{f}_i \rangle\}_{i \in I}$. Most of the work in this direction has focused on the case in which H has finite dimension, in which case we put $I = [n]$, and we abuse notation by letting F denote both the sequence $\{\mathbf{f}_i\}_{i \in [n]}$ and the matrix whose i th column is \mathbf{f}_i . Some frames are particularly well suited for information recovery after corruption in the coefficient domain. For example, of all frames with unit-norm elements, tight frames are the most robust to a single erasure under additive white gaussian noise [59].

Intuitively, a frame is more robust to data corruption when no two frame elements capture similar information. Suppose each frame element has unit norm, and for the sake of illustration, consider \mathbf{x} drawn from a gaussian distribution with identity covariance. Then each frame coefficient $\langle \mathbf{x}, \mathbf{f}_i \rangle$ has standard gaussian distribution, and the covariance between $\langle \mathbf{x}, \mathbf{f}_i \rangle$ and $\langle \mathbf{x}, \mathbf{f}_j \rangle$ is $\langle \mathbf{f}_i, \mathbf{f}_j \rangle$. As such, if we want to minimize the common information between all pairs of frame elements, we are inclined to minimize the *coherence* of F , defined as

$$\nu(F) \triangleq \max_{\substack{i, j \in [n] \\ i \neq j}} |\langle \mathbf{f}_i, \mathbf{f}_j \rangle|.$$

In fact, of all unit norm tight frames, the ones that minimize coherence are most robust to two erasures under additive white gaussian noise [69].

An alternative interpretation is available in the context of coding theory. Recall that given a compact metric space X with metric d , an *optimal code* in (X, d) of size n is a subset $C \subseteq X$ for which the minimum distance

$$\delta(C) \triangleq \min_{\substack{x, y \in C \\ x \neq y}} d(x, y)$$

is maximized. (Here, we ask X to be compact so that an optimal code necessarily exists.) There has been extraordinary success in studying optimal codes in Hamming space and the sphere. In this survey paper, we are concerned with another metric space. Specifically, for each $\mathbb{F} \in \{\mathbb{R}, \mathbb{C}\}$, let $\mathbb{F}\mathbb{P}^{m-1}$ denote *projective space*, i.e., the set of 1-dimensional subspaces of \mathbb{F}^m . One may define the *chordal distance* over projective space by

$$d(S, T) \triangleq \|P_S - P_T\|_F, \quad S, T \in \mathbb{F}\mathbb{P}^{m-1}.$$

Here, P_S denotes the $m \times m$ orthogonal projection matrix onto S , while $\|\cdot\|_F$ denotes the Frobenius matrix norm. For unit vectors \mathbf{x} and \mathbf{y} , it is straightforward to verify that

$$d(\text{span}\{\mathbf{x}\}, \text{span}\{\mathbf{y}\}) = \sqrt{2(1 - |\langle \mathbf{x}, \mathbf{y} \rangle|^2)}.$$

It follows that optimal codes in projective space correspond to ensembles of vectors that minimize coherence.

In the following subsection, we discuss a particularly nice family of optimal projective codes known as *equiangular tight frames*. Later, we briefly survey other known optimal projective codes before discussing frames with well-conditioned subensembles.

4.1 Equiangular tight frames

This subsection is concerned with a particularly special type of frame. We start with a definition:

Definition 4.1. We say $\{\mathbf{f}_i\}_{i \in [n]}$ in \mathbb{C}^m is an *equiangular tight frame (ETF)* if there exist constants $\nu, r \geq 0$ such that

$$|\langle \mathbf{f}_i, \mathbf{f}_j \rangle| = \begin{cases} 1 & \text{if } i = j \\ \nu & \text{if } i \neq j, \end{cases} \quad (4.2a)$$

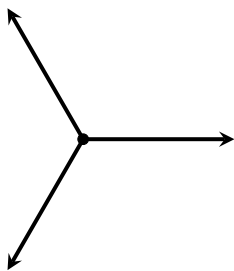
and

$$\sum_{i \in [n]} \mathbf{f}_i \mathbf{f}_i^* = r I_m. \quad (4.2b)$$

Notice that if F is an $m \times n$ ETF, then ν and r are equal to its coherence $\nu(F)$ and redundancy n/m , respectively. As an example, one may verify that

$$F := \begin{bmatrix} 1 & -\frac{1}{2} & -\frac{1}{2} \\ 0 & \frac{\sqrt{3}}{2} & -\frac{\sqrt{3}}{2} \end{bmatrix}$$

is an ETF with $\nu = \frac{1}{2}$ and $r = \frac{3}{2}$. This example is affectionately known as the *Mercedes-Benz frame* due to its resemblance to the luxury vehicle logo:



Equiangular tight frames are important in part because they correspond to a certain type of optimal projective code. The following result (a strengthened form of (3.1)) makes this explicit:

Proposition 1 (The “maximum” Welch bound [115], [130]). Suppose $F = \{\mathbf{f}_i\}_{i \in [n]}$ with $\mathbf{f}_i \in \mathbb{C}^m$ satisfying $\|\mathbf{f}_i\| = 1$ for each $i \in [n]$. Then

$$\nu(F) \geq \sqrt{\frac{n-m}{m(n-1)}}, \quad (4.3)$$

with equality if and only if F is an equiangular tight frame. In particular, the constant ν in (4.2a) is equal to the lower bound in (4.3).

Not only are ETFs optimal projective codes, they simultaneously minimize an infinite family of potential energies, specifically, those of the form

$$\sum_{\substack{i, j \in [n] \\ i \neq j}} g(1 - |\langle \mathbf{f}_i, \mathbf{f}_j \rangle|^2),$$

where $g: (0, 1] \rightarrow \mathbb{R}$ is any function satisfying $(-1)^k g^{(k)}(x) \geq 0$ for every $x \in (0, 1]$ and $k \in \mathbb{N}$; see [26] for details. For example, one may take

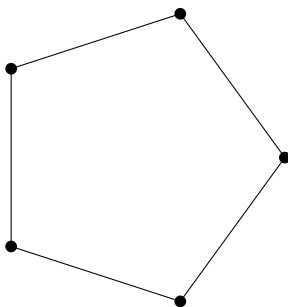
$g(x) = x^{-c}$ or $g(x) = e^{-cx}$ for any $c > 0$. For this reason, we should think of ETFs as extremely special objects, and indeed, they appear to be quite rare. ETFs do not exist for most pairs (m, n) , and most of the known ETFs arise from combinatorial designs. In what follows, we briefly describe the most fundamental examples; see [27] for surveys on the relevant combinatorial designs, and see [48] for a survey on ETFs.

4.1.1 Strongly regular graphs

Suppose $F = \{\mathbf{f}_i\}_{i \in [n]}$ is an ETF with $\mathbf{f}_i \in \mathbb{R}^m$ for every $i \in [n]$. Then the Gram matrix of F takes the form

$$F^\dagger F = I_n + \nu(F) \cdot S, \quad (4.4)$$

where S is the so-called *Seidel adjacency matrix* of a regular 2-graph [109]; these correspond to a certain class of *strongly regular graphs* [128]. To illustrate, we consider the cyclic graph on 5 vertices:



This graph is strongly regular since every vertex has the same degree (i.e., 2), adjacent vertices all have the same number of common neighbors (i.e., 0), and non-adjacent vertices have the same number of common neighbors (i.e., 1). Let V denote the vertex set of this graph, and consider the 6×6 Seidel adjacency matrix S with rows and columns indexed by $V \cup \{\infty\}$, where $S_{ii} = 0$, $S_{ij} = -1$ if $i, j \in V$ and $i \leftrightarrow j$,

and otherwise $S_{ij} = 1$:

$$S = \left[\begin{array}{c|ccccc} 0 & + & + & + & + & + \\ \hline + & 0 & - & + & + & - \\ + & - & 0 & - & + & + \\ + & + & - & 0 & - & + \\ + & + & + & - & 0 & - \\ + & - & + & + & - & 0 \end{array} \right]. \quad (4.5)$$

One may verify that $G := I_6 + \frac{1}{\sqrt{5}}S$ has eigenvalues 0 and 2, both with multiplicity 3, meaning G is the Gram matrix of an ETF of 6 vectors in \mathbb{R}^3 . In fact, the vectors in this ETF can be obtained by grouping the 12 vertices of the icosahedron into 6 antipodal pairs and selecting a representative point from each pair. In other words, the 6 lines spanned by the icosahedron's vertices form an optimal projective code.

4.1.2 Difference sets

Next, we consider *harmonic frames*, which are constructed by sampling rows of the character table of a finite abelian group G . Specifically, we take $n = |G|$ and select a subset of characters $D \subseteq \hat{G}$ so that for each $g \in G$, we have $\mathbf{f}_g \in \mathbb{C}^D$ defined by $\mathbf{f}_g(\chi) = \chi(g)$ for every $\chi \in D$. Such frames $\{\mathbf{f}_g\}_{g \in G}$ are necessarily tight, and they form ETFs (after scaling by $|D|^{-1/2}$) precisely when D is a *difference set*, meaning there exists $\lambda \in \mathbb{N}$ such that every non-identity member of \hat{G} can be expressed as a difference of two members of D in exactly λ ways [34], [115], [133].

For an illustrative example, take G to be the abelian group $\mathbb{Z}/7\mathbb{Z}$. We claim that $\{1, 2, 4\}$ is a difference set in G . This can be easily seen from the difference table:

–	1	2	4
1	0	6	4
2	1	0	5
4	3	2	0

For example, $1 - 2 = -1 \equiv 6 \pmod{7}$, and so 6 appears in the difference

table at entry (1, 2). Since the off-diagonal entries of the difference table evenly cover the nonzero members of $\mathbb{Z}/7\mathbb{Z}$ (specifically, with $\lambda = 1$), it follows that $\{1, 2, 4\}$ is a difference set. Next, we consider the characters of G . Let $\chi \in \hat{G}$ denote the function $\chi: G \rightarrow \mathbb{C} \setminus \{0\}$ defined by $\chi(g) := e^{2\pi jg/7}$, where $j = \sqrt{-1}$. Then χ is a homomorphism of G and its entrywise powers $\{\chi^k\}_{k=0}^6$ form the character group $\hat{G} \cong G$. It follows that $D \triangleq \{\chi^1, \chi^2, \chi^4\}$ is a difference set for \hat{G} . Denoting $\omega \triangleq e^{2\pi j/7}$, then the above procedure gives

$$F \triangleq \frac{1}{\sqrt{3}} \begin{bmatrix} \omega^0 & \omega^1 & \omega^2 & \omega^3 & \omega^4 & \omega^5 & \omega^6 \\ \omega^0 & \omega^2 & \omega^4 & \omega^6 & \omega^1 & \omega^3 & \omega^5 \\ \omega^0 & \omega^4 & \omega^1 & \omega^5 & \omega^2 & \omega^6 & \omega^3 \end{bmatrix}.$$

Equivalently, we select the rows of the 7×7 discrete Fourier transform matrix that are indexed by $\{1, 2, 4\}$. This approach allows one to design ETFs by selecting rows from other character tables such as the appropriate $2^k \times 2^k$ Hadamard matrix.

4.1.3 Block designs

A third combinatorial construction of ETFs arises from block designs. Let B denote any $(v, b, r, k, \lambda = 1)$ -balanced incomplete block design (BIBD), i.e., B is a collection of b size- k subsets of $[v]$ (called *blocks*) such that every point resides in exactly r blocks and every pair of points resides in exactly $\lambda = 1$ block. For each $x \in [v]$, let B_x denote the size- r set of blocks that contain x , let H_x denote any complex Hadamard matrix of order $r + 1$ with rows indexed by $B_x \cup \{\infty\}$, and for each $z \in [r + 1]$, consider the vector $\mathbf{f}_{(x,z)} \in \mathbb{C}^B$ defined by

$$\mathbf{f}_{(x,z)}(y) \triangleq \begin{cases} H_x(y, z) & \text{if } y \in B_x \\ 0 & \text{otherwise.} \end{cases}$$

Then $\{\mathbf{f}_{(x,z)}\}_{x \in [v], z \in [r+1]}$ forms an ETF (after scaling by $r^{-1/2}$) [50]. This construction is known as the *Steiner equiangular tight frame*.

As an example, take $v := 3$ and $B := \{\{1, 2\}, \{1, 3\}, \{2, 3\}\}$. Then B is a BIBD with $b = 3$, $k = 2$, $r = 2$, and $\lambda = 1$. Notice that

$B_1 = \{\{1, 2\}, \{1, 3\}\}$, $B_2 = \{\{1, 2\}, \{2, 3\}\}$, and $B_3 = \{\{1, 3\}, \{2, 3\}\}$. Put $\omega \triangleq e^{2\pi j/3}$ and take

$$H \triangleq \begin{bmatrix} 1 & 1 & 1 \\ 1 & \omega & \omega^2 \\ 1 & \omega^2 & \omega \end{bmatrix}.$$

For each $x \in \{1, 2, 3\}$, we take H_x to be a copy of H in which the first row is indexed by ∞ and the other two rows are indexed by B_x . Then the above procedure gives

$$F \triangleq \frac{1}{\sqrt{2}} \begin{bmatrix} 1 & \omega & \omega^2 & 1 & \omega^2 & \omega & 0 & 0 & 0 \\ 1 & \omega^2 & \omega & 0 & 0 & 0 & 1 & \omega & \omega^2 \\ 0 & 0 & 0 & 1 & \omega & \omega^2 & 1 & \omega^2 & \omega \end{bmatrix}. \quad (4.6)$$

One may verify that (v, k, λ) determines the full list of parameters (v, b, r, k, λ) of a BIBD by virtue of the following identities:

$$bk = vr, \quad \lambda(v - 1) = r(k - 1),$$

which in turn determines the size of the corresponding Steiner ETF; specifically, there are $n = (r + 1)v$ vectors in $m = b$ dimensions. For every fixed $k_0 \geq 2$, there is an infinite family of BIBDs with $k = k_0$ and $\lambda = 1$. This produces an infinite sequence of Steiner ETFs with $m \rightarrow \infty$ and $\gamma \rightarrow \frac{1}{k_0}$.

4.1.4 Zauner's conjecture

The longest standing open problem concerning ETFs was posed in 1999 by Zauner in his PhD thesis [142]. This conjecture predicts the existence of ETFs of m^2 vectors in \mathbb{C}^m for every dimension m ; notably, $\gamma \rightarrow 0$ as $m \rightarrow \infty$. Furthermore, these ETFs appear to be constructed from orbits of the Heisenberg–Weyl group. To be explicit, let $\{\mathbf{e}_k\}_{k=0}^{m-1}$ denote the identity basis of \mathbb{C}^m with zero-based indices, and consider the translation and modulation operators defined by

$$T\mathbf{e}_k = \mathbf{e}_{(k+1) \bmod m}, \quad M\mathbf{e}_k = e^{2\pi i k/m} \cdot \mathbf{e}_k,$$

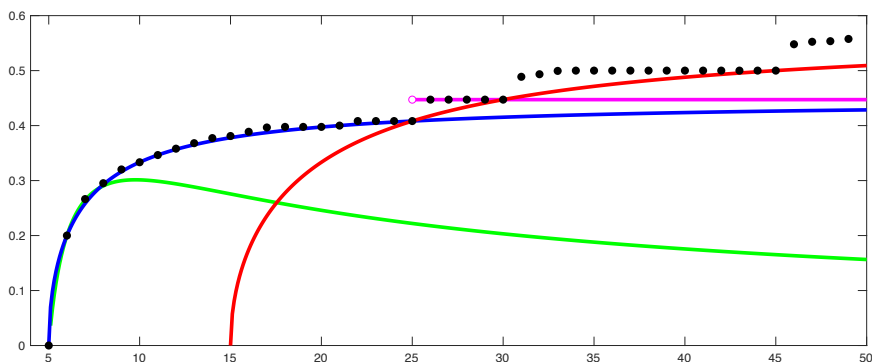


Figure 4.1: From [70]. Various bounds on coherence of $n \in \{5, \dots, 49\}$ unit vectors in \mathbb{C}^5 . The Bukh–Cox bound is in green, the “maximum” Welch bound in blue, the orthoplex bound in pink, and the Levenshtein bound in red. Points in black denote the coherence of the best known code of n points in $\mathbb{C}\mathbb{P}^4$, maintained in [70].

and extended linearly. Zauner predicts that for each dimension $m \in \mathbb{N}$, there exists a vector $\mathbf{f} \in \mathbb{C}^m$ such that the time–frequency shifts $\{T^a M^b \mathbf{f}\}_{a,b=0}^{m-1}$ form an ETF. Such ETFs play a significant role in the quantum information theory literature, where they are known as symmetric, informationally complete, positive operator–valued measures (SIC-POVMs). Accordingly, there has been a flurry of work to prove Zauner’s conjecture. Today, we know that for every $m \leq 151$, there exists $\mathbf{f} \in \mathbb{C}^m$ such that $\{T^a M^b \mathbf{f}\}_{a,b=0}^{m-1}$ is within machine precision of satisfying the ETF conditions [53]. Furthermore, for a fraction of these dimensions, an exact construction is known [3]. It appears that a general construction will depend on a strengthened version of the Stark conjectures from algebraic number theory [72], which explains why it has been so difficult to prove Zauner’s conjecture.

4.2 Other optimal projective codes

While most work on projective codes has focused on ETFs, other types of optimal projective codes have been discovered by achieving equality in

alternative bounds; see Figure 4.1 for an illustration. The most successful construction of this sort arises from mutually unbiased bases. Here, we say that $m \times m$ unitary matrices U_1, \dots, U_k are mutually unbiased if for every $i, j \in [k]$ with $i \neq j$, it holds that every entry of $U_i^\dagger U_j$ has modulus $m^{-1/2}$. Given $k = m + 1$ mutually unbiased bases, it holds that the $m(m + 1)$ columns of $[U_1 \cdots U_{m+1}]$ form an optimal projective code. In fact, they achieve equality in both the orthoplex bound [28] and the Levenshtein bound [62], [77]. Such projective codes are known to exist whenever m is a power of a prime [132]. Beyond mutually unbiased bases, there are few known constructions that achieve equality in the Levenshtein bound [62], [89]. By comparison, the orthoplex bound is much easier to work with: Given a projective code of size at least $m^2 + 2$ that achieves equality in the orthoplex bound, removing any vector produces another code that achieves equality in the orthoplex bound. Going the other direction, one may achieve equality in the orthoplex bound by appending the identity basis to an appropriately incoherent harmonic frame with at least $m^2 - m + 1$ frame elements [13]. Recently, Bukh and Cox [18] introduced a new bound on projective codes of size $m + O(\sqrt{m})$. Notably, equality in this bound occurs precisely when there exists $k \in \mathbb{N}$ such that n is a multiple of k^2 , $m = n - k$, and there exists an ETF of k^2 vectors in \mathbb{C}^k . (Mind the relationship to Zauner’s conjecture.)

For (m, n) such that $2 \leq m \leq 7$ and $m + 2 \leq n \leq 49$, the best known codes of n points in $\mathbb{C}\mathbb{P}^{m-1}$ are maintained in [70]. For most choices of (m, n) , it appears to be impossible to achieve equality in the above general bounds, and so other techniques are required to perform the optimization. In the special case where $m = 2$, we note that $\mathbb{C}\mathbb{P}^1$ is isometrically isomorphic to the sphere S^2 , and so our problem reduces to the famous Tammes problem. Here, optimal codes are known for $n \leq 14$ and $n = 24$ [95]. In the absence of a tight lower bound, the techniques here are rather different: one enumerates a large number of candidate solutions (think “critical points”) before pruning the list until

identifying the complete set of solutions. The most recent results of this form have relied on computer assistance. To date, this accounts for all known optimal codes for $\mathbb{C}\mathbb{P}^{m-1}$. In the case of $\mathbb{R}\mathbb{P}^{m-1}$, additional codes have been proved optimal using a Tammes-inspired approach [9], [91] as well as techniques from computational algebraic geometry [46], [92], but the latter techniques do not transfer easily to the complex case.

4.3 Frames with well-conditioned subensembles

Compressed sensing spurred substantial interest in a particular matrix design problem: Given integers $k < n$ and $\delta \in (0, 1/2)$, find the smallest $m \in \mathbb{N}$ for which there exists $F = \{\mathbf{f}_i\}_{i \in [n]}$ with $\mathbf{f}_i \in \mathbb{C}^m$ such that for every k -subset $S \in \binom{[n]}{k}$, the Gram matrix G_S of $\{\mathbf{f}_i\}_{i \in S}$ satisfies the matrix inequality

$$(1 - \delta)I \preceq G_S \preceq (1 + \delta)I.$$

(Note that this is slightly stronger than asking every G_S to be well conditioned, since the eigenvalues must reside in the fixed interval $[1 - \delta, 1 + \delta]$.) This is the *restricted isometry property* (compare with (3.10) with $G_S = F_S^\dagger F_S$), and any ensemble with the property can be used as columns of a sensing matrix in compressed sensing. Of course, we must have $m \geq k$, since otherwise G_S would be rank deficient. Also, the interesting regime is $m \leq n$ since one may otherwise design F to consist of orthonormal vectors. If the entries of each vector in F are independent with distribution $N(0, 1/m)$, then F exhibits the restricted isometry property with high probability in the regime $m \asymp (k/\delta^2) \log(n/k)$ [52].

Different applications of compressed sensing lead to different design constraints, and this has led researchers to develop restricted isometries with additional structural properties, such as partial Fourier, partial circulant, or Gabor structure [68], [74]. All of these constructions exhibit the restricted isometry property in the regime $m \asymp k \text{ poly}(1/\delta, \log n)$, and they do so with the help of the probabilistic method; note that for a fixed δ , this is identical to the scaling of the gaussian construction up

to log factors in n . Every known restricted isometry with this scaling is a random matrix that exhibits some small failure probability. This motivated Terry Tao to pose the derandomization problem of finding explicit restricted isometries.

This derandomization problem is an instance of what Avi Wigderson calls a *hay in a haystack problem*, in which random objects satisfy a given property with high probability, while explicit constructions consistently produce objects that do not exhibit that property; other examples include Ramsey graphs and the Gilbert–Varshamov bound for linear codes. To make our derandomization problem well defined, one might leverage ideas from computational complexity, which in turn forces us to pose things asymptotically. Given an infinite $\mathcal{M} \subseteq \mathbb{N}$, we say a sequence $\{F_m\}_{m \in \mathcal{M}}$ with each F_m being a tuple of $n(m)$ vectors in \mathbb{C}^m is *explicit* if there exists an algorithm that on input $m \in \mathcal{M}$ takes $\text{poly}(m, n(m))$ time to output F_m . This model of explicitness precludes certain unwanted solutions to the derandomization problem. As an example of an unwanted solution, one could consider all 2^{mn} possible n -tuples of vectors in \mathbb{C}^m with entries in $\{\pm 1/\sqrt{m}\}$, and for each of these, one could further compute the spectrum of the Gram matrix of the vectors indexed by S for each $S \in \binom{[n]}{k}$. This deterministic process allows one to identify a restricted isometry with $m \asymp (k/\delta^2) \log(m/k)$, but the algorithm is too slow to be considered explicit.

Having made precise the notion of explicitness, we may now enunciate the explicit restricted isometry problem: Find the largest $k = k(m)$ for which there exists an explicit (k, δ) -restricted isometry of $n = (1 + \Omega(1)) \cdot m$ vectors in \mathbb{C}^m for some fixed $\delta \in (0, 1/2)$, and an infinite sequence m in \mathbb{N} . For $k = 1$, we may simply select F to consist of unit-norm vectors, since each $S \in \binom{[n]}{1}$ takes the form $S = \{i\}$, in which case $G_S = \|\mathbf{f}_i\|^2 = 1$. Next, for $k = 2$, we have $S = \{i, j\}$ with $i \neq j$. If we assume that F consists of unit-norm vectors, then we have

$$G_S = \begin{bmatrix} 1 & \langle \mathbf{f}_i, \mathbf{f}_j \rangle \\ \langle \mathbf{f}_j, \mathbf{f}_i \rangle & 1 \end{bmatrix}.$$

Considering $\text{trace}(G_S) = 2$ and $\det(G_S) = 1 - |\langle \mathbf{f}_i, \mathbf{f}_j \rangle|^2$, it follows that the eigenvalues of G_S are $1 \pm |\langle \mathbf{f}_i, \mathbf{f}_j \rangle|$. As such, finding a $(2, \delta)$ -restricted isometry with unit-norm vectors and minimal δ is equivalent to minimizing coherence $\nu(F)$, i.e., finding an optimal projective code. Intuitively, optimal projective codes are good candidates for restricted isometries for even larger values of k .

This is made rigorous with the Gershgorin circle theorem, which implies that the eigenvalues of G_K must reside between $1 - (k - 1)\nu(F)$ and $1 + (k - 1)\nu(F)$. Pleasingly, a smaller coherence implies that the spectrum resides in a smaller interval. In particular, F is necessarily a (k, δ) -restricted isometry whenever $\nu(F) \leq \delta/(k - 1)$. However, combining the “maximum” Welch bound and the constraint $n = (1 + \Omega(1)) \cdot m$ gives

$$\frac{\delta}{k-1} \geq \nu(F) \geq \sqrt{\frac{n-m}{m(n-1)}} \geq \Omega\left(\frac{1}{\sqrt{m}}\right),$$

and so $k \lesssim \delta\sqrt{m}$. This is a far cry from the linear scaling of k that is obtained from probabilistic constructions. Interestingly, certain optimal projective codes reveal that Gershgorin isn’t to blame for this performance gap, as it sometimes gives the correct scaling. For example, equation (4.6) determines 9 vectors in \mathbb{C}^3 that achieve equality in the Welch bound, meaning $\nu(F) = 1/2$. According to Gershgorin, every subensemble of size $k < 1/\nu(F) + 1 = 3$ is linearly independent, and conversely, the first 3 columns vectors are linearly dependent. In general, Steiner ETFs all have the property that the Gershgorin analysis is sharp, and so one must consider higher-order statistics in order to break the square-root bottleneck $k \lesssim \delta\sqrt{m}$.

To this end, Bourgain et al. [16] introduced the (k, θ) -flat restricted isometry property, which states that

$$\left| \sum_{i \in I} \sum_{j \in J} \langle \mathbf{f}_i, \mathbf{f}_j \rangle \right| \leq \theta \sqrt{|I||J|}$$

for every disjoint $I, J \subseteq [n]$ with $|I| \leq k$ and $|J| \leq k$. A technical argument involving convexity and dyadic decomposition [16], [17], [90] gives that every (k, θ) -flat restricted isometry of unit-norm vectors is also

a $(2k, 150\theta \log k)$ -restricted isometry. With this higher-order statistic, Bourgain et al. leverage ideas from additive combinatorics to show that a certain ensemble with $n \asymp m^{1+\epsilon}$ is a $(k, 1/3)$ -restricted isometry with $k \asymp m^{1/2+\epsilon}$ for $\epsilon \approx 3.6 \cdot 10^{-15}$. Alternatively, this higher-order statistic can be used to show that the Paley equiangular tight frame of $2m$ vectors in \mathbb{C}^m is a $(k, 1/3)$ -restricted isometry with $k \asymp m^{1/2+\epsilon}$ for larger choices of $\epsilon > 0$, conditioned on a conjecture in number theory concerning cancellations in the Legendre symbol [5]. Despite a decade of work in this area, these are the only results that break the square-root bottleneck in the explicit restricted isometry problem, leaving a substantial gap compared to random constructions.

Interestingly, given an equiangular tight frame F for \mathbb{C}^m and $k \gg m^{1/2}$, the proportion of $S \in \binom{[n]}{k}$ for which either $G_S \prec (1 - \delta)I$ or $G_S \succ (1 + \delta)I$ is quite small. That is, if there are any subsets precluding an equiangular tight frame from being a restricted isometry, they are relatively few. This was first observed by Tropp [120], who demonstrated that equiangular tight frames (and similar ensembles) satisfy $(1 - \delta)I \preceq G_S \preceq (1 + \delta)I$ for all but a fraction $1/\text{poly}(k)$ of $S \in \binom{[n]}{k}$ whenever $k \leq cm/\log m$ for an appropriately small choice of $c > 0$. In fact, this phenomenon allows one to obtain strong compressed sensing guarantees for random sparse signals. This behavior motivated Calderbank et al. [20] to introduce a notion of *statistical restricted isometry* and construct several examples. (See (3.11).) In pursuit of a more detailed description of this phenomenon, Gurevich and Hadani [61] demonstrated that for appropriately incoherent ensembles, the spectrum of G_S satisfies Wigner’s semicircle law when $S \sim \text{Unif}(\binom{[n]}{k})$ with $k = o(m)$. This can be viewed as an edge case of the “ETF-MANOVA relation”, [66], [67], that the spectrum of G_S empirically satisfies a MANOVA law when $k \sim cm$ for some $c \in (0, 1)$. This observation also enjoys precursors in the context of random Parseval frames with various distributions [2], [44], [123]. More on that in Sections 6 and 7.

5

Random matrix theory

The main focus of this survey paper is a relation between subsets of deterministic frames and random matrix ensembles [66], [67]. Random matrix theory (RMT) studies properties, and in particular spectral properties, of matrix-valued random variables. The empirical spectral distribution (ESD) of a symmetric (or Hermitian in the complex case) $n \times n$ matrix G_n , with eigenvalues $\lambda_1 \leq \dots \leq \lambda_n$ (which are real-valued due to symmetry), is defined as

$$\mu_n(x) = \mu_{G_n}(x) = \frac{1}{n} \sum_{i=1}^n \mathbf{1}_{\{\lambda_i \leq x\}} \quad (5.1)$$

where $\mathbf{1}_E$ is the indicator of the event E . The cumulative distribution (5.1) can be thought of as the integral of the “empirical spectral density function”,

$$f_n(x) = \frac{d\mu_n(x)}{dx} = \frac{1}{n} \sum_{i=1}^n \delta(x - \lambda_i) \quad (5.2)$$

where $\delta(x)$ is Dirac’s delta function.

Early results in RMT typically looked at a sequence of random matrices, say X_n , and asserted that the ESD of (a normalized version

and/or the Gram matrix of) X_n converges in distribution to some specified limiting spectral distribution μ . The theory came to the world in the 1950's with Wigner's *semi-circle law*, for the limiting ESD of a symmetric matrix whose diagonal and upper triangular entries are i.i.d. random variables [45].

Another famous example, closer to the topic of our survey paper, is the Marchenko–Pastur law that states the following. Let X_n be a sequence of random matrices, such that X_n is m_n -by- n , and such that the entries of X_n are all i.i.d of zero mean and unit variance. Assume that $m_n/n \rightarrow \beta$ as $n \rightarrow \infty$, with $\beta \geq 1$. In 1967, Marchenko and Pastur proved that the empirical distribution $\mu_n(x)$ of the eigenvalues of the “Wishart” random matrix $X_n^\dagger X_n/m_n$ converges in distribution to the distribution $\mu_\beta(x)$ with density

$$f_\beta(x) = \frac{\sqrt{(\lambda_+ - x)(x - \lambda_-)}}{2\pi\beta x} \cdot \mathbf{1}_{[\lambda_- \leq x \leq \lambda_+]}(x) \quad (5.3)$$

where the support edge points are $\lambda_\pm = (1 \pm \sqrt{\beta})^2$.

A similar yet slightly less known result arises in multivariate statistics. Let A and B be k -by- $(n - m)$ and k -by- m matrices, respectively, whose entries are Gaussian i.i.d. Consider the random matrix

$$\frac{n}{m} (AA^\dagger + BB^\dagger)^{-\frac{1}{2}} BB^\dagger (AA^\dagger + BB^\dagger)^{-\frac{1}{2}} \quad (5.4)$$

and denote its distribution by MANOVA(n, m, k) [94]. Wachter [127] discovered that, as $k/m \rightarrow \beta \leq 1$ and $m/n \rightarrow \gamma$, the empirical distribution of the eigenvalues of a random matrix drawn from MANOVA(n, m, k) converges in distribution to the distribution with density

$$f_{\beta,\gamma}(x) = \frac{\sqrt{(\lambda_+ - x)(x - \lambda_-)}}{2\beta\pi x(1 - \gamma x)} \cdot \mathbf{1}_{[\lambda_- \leq x \leq \lambda_+]}(x) + \left(1 + \frac{1}{\beta} - \frac{1}{\beta\gamma}\right)^+ \cdot \delta\left(x - \frac{1}{\gamma}\right) \quad (5.5)$$

where $\lambda_\pm = [\sqrt{\beta(1 - \gamma)} \pm \sqrt{1 - \beta\gamma}]^2$, which is known as *Wachter's asymptotic MANOVA distribution*.¹ Recently, [42] proved convergence

¹The x -axis in (5.5) is scaled by γ compared to [37], due to the factor n/m in (5.4) which does not exist in the ensemble definition in [37].

to this limiting spectral distribution even when the Gaussian assumption is removed, namely, when the entries of the matrices above are simply i.i.d, in analogy with the Wigner and the Marchenko–Pastur laws.

The MANOVA distribution (5.5) reduces to the Marchenko–Pastur distribution (5.3) in the limit as $\gamma \rightarrow 0$. A second interesting case is $\gamma = 1/2$, where the MANOVA density (5.5) is symmetric around its center $(\lambda_+ + \lambda_-)/2$, and its centralized version is known as the Kesten–McKay distribution [37], [88].

More recent results in RMT established connections between the MANOVA distribution and the spectrum of matrices with a reduced (non-i.i.d.) randomness. One example is a fixed sub-rectangle of a random matrix, taken from a Haar distribution over all orthogonal/unitary matrices [39]. Another example is a random sub-rectangle (a random set of rows and columns) of the discrete Fourier transform matrix [44].² The MANOVA (β, γ) parameters are determined by the fraction of rows/columns in the sub-rectangle. We shall return to these examples, which are close in spirit to the ETF-MANOVA relation, in Chapter 6.

5.1 Methods of proof in RMT

In his original work, Wigner proved convergence of the moments of the ESD [1], [45]. The r -th moment of a (cumulative) distribution $\mu(x)$ (with a density $f(x) = d\mu(x)/dx$) is defined as

$$M_r(\mu) = \int x^r d\mu(x) = \int x^r f(x) dx \quad (5.6)$$

for $r = 1, 2, \dots$. The r -th moment of a symmetric/Hermitian matrix G_n with an ESD μ_n (5.1) is defined similarly as

$$M_r(\mu_n) = \int x^r d\mu_n(x) = \frac{1}{n} \sum_{i=1}^n \lambda_i^r = \frac{1}{n} \text{trace}(G_n^r) \quad (5.7)$$

where the second equality follows from (5.1)–(5.2), and the last equality follows because (i) the eigenvalues of the power of a matrix are powers

²Though the author of [44] did not identify the limiting law as the Wachter distribution.

of the eigenvalues; and (ii) the trace of a matrix is equal to the sum of its eigenvalues.

The *moments method* aims to show that there exists some law μ , such that $M_r(\mu_n)$ (which is a random variable for a random G_n) converges almost surely as n goes to infinity to the moment $M_r(\mu)$ for all r , and to conclude that μ_n converges in distribution to μ . Typically, the analysis is split into two steps: (i) convergence of the *mean* moment to the limiting moment, i.e.,

$$E\{M_r(\mu_n)\} \rightarrow M_r(\mu) \quad (5.8)$$

and (ii) concentration, i.e., that the *variance* of $M_r(\mu_n)$ vanishes sufficiently fast in n , say, that

$$\sum_{n=1}^{\infty} \text{var}\{M_r(\mu_n)\} < \infty. \quad (5.9)$$

The two conditions (5.8) and (5.9) imply the almost sure convergence of $M_r(\mu_n)$ to $M_r(\mu)$; which, if held for all moments r , implies the desired convergence in distribution of the ESD to the limiting law μ [116, exercise 2.4.6].

In Chapter 7 we use the moment method to prove the asymptotic ETF-MANOVA relation. Other general analytical tools in RMT, namely, the *Stieltjes transform* (which can be thought of as the moment generating function of the ESD), and the method of *free probability*, can be found in [1], [45].

6

Empirical ETF-MANOVA relation

In this and the next chapter, we shall see evidence for an intriguing RMT phenomenon that arises in a class of deterministic frames. Equiangular tight frames (ETFs) are highly symmetric objects constructed to minimize a *local* condition, namely, the pairwise absolute correlation (4.2). It stands to reason that such a highly symmetric structure will exhibit emergent *global* structure, namely, that some form of emergent structure can be found in the group correlations between subsets of vectors from an ETF. A natural place to look for such structure is the spectrum of the covariance matrix. Indeed, the spectral decomposition of the pairwise distance (or angle) matrix determines, up to rotation, the global point arrangement in Euclidean space.

At a first glance, the ETF-MANOVA relation [66] may seem surprising; why should a MANOVA distribution appear in the spectral decomposition of the empirical covariance of ETF subsets? However, hints that this might be the case, in the case of tight frames of random design, have appeared in the literature since 1980's. Wachter's original paper [127] has noted that his limiting law arises as the limiting empirical spectral distribution of covariance matrix of Haar frames, namely,

frames formed by taking sub-rectangles of Haar-distributed orthogonal matrices. This was formally proved by Edelman [39] and Farrell [44]. In the same paper, Farrell showed that Wachter’s distribution arises also as the limiting empirical spectral distribution of subsets taken from random Fourier frames, namely, frames obtained by taking a random subset of rows from the DFT matrix.

The discovery of the ETF-MANOVA relation was inspired by ideas on robust interpolation in the analog coding literature [82]. The work in [64] (described in Chapter 2) observed that if a deterministic frame is generated by selecting rows corresponding to a difference set from the DFT matrix (which is a specific way to construct ETFs - see Section 4.1.2), then the spectra of random subsets exhibit a typical favorable behavior. The work in [66] then revealed a previously unknown and possibly far-reaching random matrix universality phenomenon, that arises in the covariance matrix of randomly selected subsets taken from some tight and equiangular tight frames. We shall next describe the empirical method and findings of [66].

6.1 Distance measures

Let us consider two observables, one based on a measure of distance between empirical spectral distributions, and one based on the difference between specific test functions applied to the empirical spectral distributions. Specifically, let

$$\|\mu_1 - \mu_2\|_{KS} \triangleq \max_x |\mu_1(x) - \mu_2(x)| \quad (6.1)$$

denote the Kolmogorov–Smirnov (KS) distance between two cumulative distribution functions (CDFs). For an $m \times k$ sub-frame F_S with a Gram matrix $G_S = F_S^\dagger F_S$, taken from an $m \times n$ frame F , define

$$\Delta_{KS}(G_S) \triangleq \left\| \mu_{G_S}(x) - \mu^{\text{MANOVA}}(x) \right\|_{KS} \quad (6.2)$$

where μ_{G_S} is the ESD (5.1) of G_S , and $\mu^{\text{MANOVA}}(x)$ is the MANOVA distribution with a density $f_{\beta,\gamma}(x)$ (5.5), where $\gamma = m/n$ and $\beta = k/m$.

This is one of many possible ways to measure the distance between the empirical spectral distribution of a given frame-subset covariance matrix G_S and the limiting empirical spectral law. Second, for a functional Ψ that can be applied to an ESD, i.e., to the vector of eigenvalues of a Gram matrix, we let

$$\Delta_{\Psi}(G_S) \triangleq \left| \Psi(\mu_{G_S}) - \Psi(\mu^{\text{MANOVA}}) \right| \quad (6.3)$$

where the functional of a general distribution μ is defined in a similar way, i.e., $\Psi(\mu) = \int \Psi(x) d\mu(x)$; e.g., for the MSE goodness (3.6) it is $\Psi_{\text{MSE}}(\mu) = \int x^{-1} d\mu(x)$, and for the (high-SNR) Shannon transform (3.7b) it is $\Psi_{\text{Shannon}}(\mu) = \int \log(x) d\mu(x)$. (Note that $\int d\mu(x) = 1$.) See Chapter 3 for various functionals Ψ under study. Unlike the KS distance, which measures total distance between entire spectral distributions, the value Δ_{Ψ} measures the difference as seen through the specific prism of Ψ .

6.2 Frames under study

Table 6.1 shows the frames studied in [66]. They include several frames of both random and deterministic design. All frames studied were tight; some were tight but not equiangular, while some were ETFs. Both real and complex frames were studied.

6.3 Empirical observation method

For a specific frame family with a fixed aspect ratio $\gamma = m/n$, and a fixed sub-frame aspect ratio $\beta = k/m$, and for each frame size n under study, we have generated an $m \times n$ frame matrix of a given size and sampled frame subsets uniformly at random over $S \subset [n]$, $|S| = k$. We then computed the values Δ_{KS} , as well as Δ_{Ψ} for all functionals Ψ under study. This was repeated for increasing frame sizes available in the frame family. Separately, for each triplet (n, m, k) , we have performed independent draws from the $\text{MANOVA}(n, m, k)$ ensembles

Table 6.1: Frames under study

Label	Name	\mathbb{R} or \mathbb{C}	Natural γ	Tight frame	Equiangular	References
Deterministic frames						
DSS	Difference-set spectrum	\mathbb{C}		Yes	Yes	[133]
GF	Grassmannian frame	\mathbb{C}	1/2	Yes	Yes	[115, Corollary 2.6b]
RealPF	Real Paley's construction	\mathbb{R}	1/2	Yes	Yes	[115, Corollary 2.6a]
ComplexPF	Complex Paley's construction	\mathbb{C}	1/2	Yes	Yes	[100]
Alltop	Quadratic Phase	\mathbb{C}	1/L	Yes	No	[93, eq. S4]
SS	Chirp Spikes and Sines	\mathbb{C}	1/2	Yes	No	[40]
SH	Spikes and Hadamard	\mathbb{R}	1/2	Yes	No	[40]
Random frames						
HAAR	Unitary Haar frame	\mathbb{C}		Yes	No	[39], [44]
RealHAAR	Orthogonal Haar frame	\mathbb{R}		Yes	No	[39]
RandDFT	Random Fourier transform	\mathbb{C}		Yes	No	[44]
RandDCT	Random Cosine transform	\mathbb{R}		Yes	No	

(5.4) and calculated the analogous quantities. To inspect the possibility of convergence to a limit of these quantities as the frame size grows, and the convergence rate, we have plotted the value of Δ_{KS} , as well as Δ_{Ψ} over the frame size. To observe an exponential decrease of the form Cn^{-b} for some exponent b , simple linear regression of $\log(\Delta)$ against $\log(n)$ (with an intercept term) was performed to extract the value b and its standard error. To observe an exponential decrease of the form $Cn^{-b} \log^{-a}(n)$ for some exponents a and b , simple linear regression of $\log(\Delta)$ against $\log(n)$ and $\log(\log(n))$ (with an intercept) was performed to extract the values a and b and their standard errors.

6.4 Findings

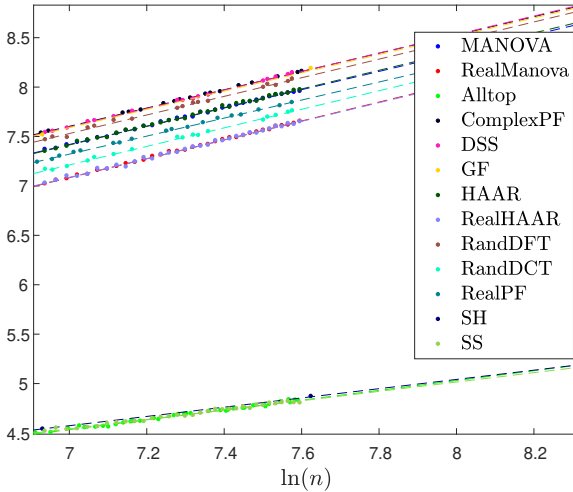


Figure 6.1: KS-distance (6.2) for $\gamma = 0.5$ and $\beta = 0.8$. Plot shows $-\frac{1}{2} \ln \text{Var}_K(\Delta_{KS}(G_S^{(n)}))$ over $\ln(n)$.

Figures 6.1 and 6.2, taken from [66], show examples of these tests for both distance measures. The results demonstrate clearly that Δ_{KS} and Δ_{Ψ} decrease to zero. The fluctuations, namely the rate of convergence, show an excellent fit to the exponential rates. Moreover, for ETFs, we observe that the exponent b measured in ETFs is statistically indistin-

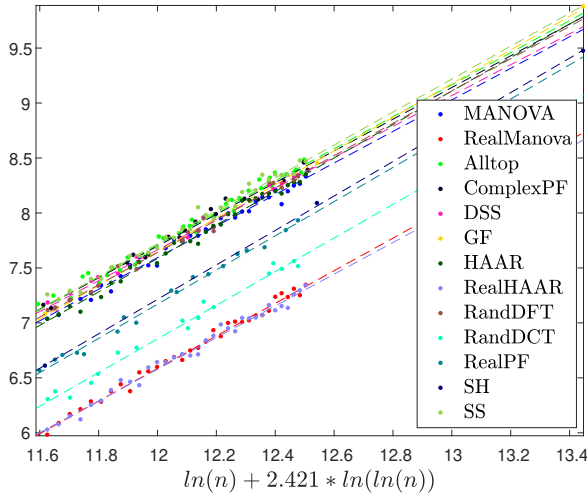


Figure 6.2: Functional distance (6.3) for Ψ_{MSE} , $\gamma = 0.5$ and $\beta = 0.8$. Plot shows $-\ln \mathbb{E}_K(\Delta_\Psi(G_S^{(n)})^2)$.

guishable from the exponent measured for the MANOVA distribution, in the sense that the null hypothesis that they are identical cannot be rejected. For the deterministic near-ETF cases (SS, SH and Alltop), the slope in Figure 6.1 (KS distance) is slightly smaller, while the slope in Figure 6.2 (functional distance) is statistically indistinguishable from that of the MANOVA ensemble. We may conclude that the convergence rate to the MANOVA limit appears to be universal within the ETF family, and almost universal in the larger class of near ETFs.

7

Moments of an ETF subset

The empirical ETF-MANOVA relation of Chapter 6 puts up many challenges for a theoretical explanation. In this chapter we take off the “statistician hat” and put on an “information theorist hat”. This leads us to focus our attention on the *typical asymptotic* behavior of an ETF subset. We demonstrate how the classical moments method of random matrix theory, [1], [45], described in Chapter 5, can be used to prove analytically the convergence of the empirical spectral distribution (5.1) of a randomly-selected subset of an ETF to Wachter’s asymptotic MANOVA distribution (5.5).¹ Similar tools were used in [4] to establish convergence of the spectra of subsets of binary code-based frames to the Marchenko-Pastur distribution. The results in this chapter were originally reported in [63], [67], [80].

For any $m \times n$ (deterministic) unit-norm frame F , consider the $m \times m$ random matrix

$$FPF^\dagger, \tag{7.1}$$

¹The proof is complete for $\gamma = 1/2$, but still partial for a general $0 < \gamma < 1$.

where the randomness comes from the “selection matrix” P . That is,

$$P = \text{diag}[P_1, \dots, P_n] \quad (7.2)$$

is a diagonal matrix with $\{0, 1\}$ elements on its diagonal, where $P_i = 1$ if i is in the (random) subset S , and $P_i = 0$ otherwise. Specifically, we shall assume that the P_i 's are generated Bernoulli(p),

$$P_i = \begin{cases} 1, & \text{with probability } p, \\ 0, & \text{with probability } 1 - p; \end{cases} \quad (7.3)$$

in other words, each frame vector is selected independently with probability p . Compared with a combinatorial (n choose k) selection of the subset S (assumed in the empirical results of Chapter 6), Bernoulli selection fits the information-theoretic i.i.d. model of Chapter 2, is easier for analysis, and does not seem to affect the asymptotic results.

Since in (7.1) all columns $i \notin S$ of F are zeroed, we have

$$FPF^\dagger = F_S F_S^\dagger$$

which is the Hessian of the selected sub-frame F_S (1.2). By properties of the trace operator, the trace-power of the Gram matrix is equal to the trace-power of the Hessian:

$$\text{trace} \left((F_S^\dagger F_S)^r \right) = \text{trace} \left((F_S F_S^\dagger)^r \right),$$

for any power $r = 1, 2, \dots$. Hence, in light of the moment method (5.7), we define the expected r th moment of a randomly-selected subset from a frame F , as

$$m_r \triangleq \frac{1}{n} \mathbb{E} \left[\text{trace} \left((FPF^\dagger)^r \right) \right] \quad (7.4)$$

where the expectation $\mathbb{E}[\cdot]$ is over the diagonal (Bernoulli p) elements of P .²

²For mathematical convenience, we normalize by the frame size n , rather than the frame dimension $m = \gamma n$, or the sub-frame (expected) size $k = |S| = pn$.

7.1 Low-order moments: exact analysis

For a small moment order r , we can compute the exact (non-asymptotic) mean (7.4) and variance of the sub-frame r th moment, for any ETF, as a function of m and n (for which an $m \times n$ ETF indeed exists). Furthermore, we can compare the mean to the r th moment of Wachter's MANOVA distribution [37, table 4]:³

$$m_r^{\text{MANOVA}}(\gamma, p) = p(x+1)^{r-1} - (1-p)^2 \sum_{j=0}^{r-2} (1-p)^j (x+1)^{r-2-j} N_{j+1} \left(x \frac{p}{1-p} \right) \quad (7.5)$$

for $0 \leq \gamma, p \leq 1$, and $r = 1, 2, \dots$, where $N_j(q) = \sum_{i=1}^j N(j, i) q^i$ is the Narayana polynomial, $N(j, i) = \frac{1}{j} \binom{j}{i} \binom{j}{i-1}$ is the Narayana number, and

$$x \triangleq \frac{n}{m} - 1 = \frac{1}{\gamma} - 1 \quad (7.6)$$

is the ‘‘net redundancy’’. For $r = 1, \dots, 4$, the MANOVA moments (7.5) become

$$m_1^{\text{MANOVA}}(\gamma, p) = p \quad (7.7a)$$

$$m_2^{\text{MANOVA}}(\gamma, p) = p + p^2 x \quad (7.7b)$$

$$m_3^{\text{MANOVA}}(\gamma, p) = p + p^2 3x + p^3 (x^2 - x) \quad (7.7c)$$

$$m_4^{\text{MANOVA}}(\gamma, p) = p + p^2 6x + p^3 (6x^2 - 4x) + p^4 (x^3 - 3x^2 + x). \quad (7.7d)$$

Let us define:

$$\Delta(\gamma, p, r, n) \triangleq \begin{cases} 0, & r = 2, 3 \\ p^2 (1-p)^2 \frac{x^2}{n-1}, & r = 4. \end{cases} \quad (7.8)$$

³In [37] the normalization outside the moment (7.4) is pn instead of n , while the x -axis is normalized by γ , so overall their moment is γ^r/p times the moment in (7.5).

Theorem 7.1 (Expected moments [63], [67]). If F is any m -by- n unit-norm (real or complex) ETF (4.2), then the expected sub-frame r th moment (7.4) is given by

$$m_r^{\text{ETF}} = m_r^{\text{MANOVA}}(\gamma, p) + \Delta(\gamma, p, r, n) \quad (7.9)$$

for $r = 1, 2, 3$ and 4.

Note that the second term in (7.9) is either zero or it vanishes asymptotically as n goes to infinity. Therefore, the asymptotic r th moment of an ETF sequence with aspect ratio γ is equal to $m_r^{\text{MANOVA}}(\gamma, p)$, for $r = 1, 2, 3$ and 4, in line with the empirical results of [66] (Chapter 6).

Proof. For any frame F , the trace-power in (7.4) can be written as trace $\left((PF^\dagger F)^r \right)$, where P is given in (7.2), and $F^\dagger F$ is the Gram matrix of the frame. Now, recall from linear algebra that the trace of a matrix product is given by sums of cyclic chains of products of elements. In particular, if $A^{(1)}, \dots, A^{(r)}$ are $n \times n$ matrices with elements $a_{ij}^{(k)}$, then

$$\text{trace} \left(A^{(1)} \cdots A^{(r)} \right) = \sum_{i_1=1}^n \cdots \sum_{i_r=1}^n a_{i_1 i_2}^{(1)} a_{i_2 i_3}^{(2)} \cdots a_{i_r i_1}^{(r)}. \quad (7.10)$$

Thus, the mean r th moment (7.4) involves sums of length- r chains of products of cross correlations $\langle \mathbf{f}_i, \mathbf{f}_j \rangle$, and powers of p depending on how many distinct pairs $i \neq j$ appear in the chain.

In the case where F is an ETF, the Gram matrix can be written in the form

$$F^\dagger F = \{ \langle \mathbf{f}_i, \mathbf{f}_j \rangle \} = I_n + \mu(F)S \quad (7.11)$$

as in (4.4), where S is either the Seidel adjacency matrix (4.5) in the real ETF case (with ± 1 on the off diagonal elements), or a “generalized adjacency matrix” (with phase values on the off diagonal elements) in the complex ETF case. The first moment ($r = 1$) is thus given by

$$m_1^{\text{ETF}} = \frac{1}{n} \mathbb{E} \left[\sum_{i=1}^n \langle \mathbf{f}_i, \mathbf{f}_i \rangle P_i \right] = \frac{1}{n} \mathbb{E} \left[\sum_{i=1}^n P_i \right] = \frac{1}{n} \sum_{i=1}^n p = p \quad (7.12)$$

where we used the unit-norm condition $\langle \mathbf{f}_i, \mathbf{f}_i \rangle = 1$, and $E[P_i] = p$. The second moment ($r = 2$) is given by

$$m_2^{\text{ETF}} = \frac{1}{n} E \left[\sum_{i,j=1}^n |\langle \mathbf{f}_i, \mathbf{f}_j \rangle|^2 P_i P_j \right] \quad (7.13a)$$

$$= p + p^2 \frac{1}{n} \sum_{i \neq j} |\langle \mathbf{f}_i, \mathbf{f}_j \rangle|^2 \quad (7.13b)$$

$$= p + p^2 x \quad (7.13c)$$

where in (7.13b) we used the unit-norm condition for $i = j$, and $E[P_i P_j] = p^2$ for $i \neq j$; and in (7.13c) we used the fact that the (mean-squared) Welch bound (3.1) amounts to

$$\frac{1}{n} \sum_{i \neq j} |\langle \mathbf{f}_i, \mathbf{f}_j \rangle|^2 \geq \frac{1}{\gamma} - 1 = x \quad (7.14)$$

with equality for a tight frame. The full computation in [63], [67] shows that tightness is sufficient also for the third moment m_3 in (7.9), while the ETF condition (4.2) is *necessary* for the fourth moment m_4 in (7.9). See Chapter 10. \square

The *empirical spectral variance* (ESV) is defined as the variance of the ESD, given by the second moment of the ESD minus the squared first moment of the ESD. This should not be confused with the *variance of the moment* as a random variable, which is considered in the next theorem.

Theorem 7.2 (Moment variance). The variance of the r th moment

$$V_r \triangleq \text{Var} \left[\frac{1}{n} \text{trace} \left((FPF^\dagger)^r \right) \right] \quad (7.15)$$

is given for an ETF for $r = 1$ and 2 by

$$V_1^{\text{ETF}} = \frac{p - p^2}{n} \quad (7.16)$$

$$V_2^{\text{ETF}} = \frac{1}{n} \left[p + t_2 p^2 + t_3 p^3 + t_4 p^4 \right] \quad (7.17)$$

where $t_2 = -1 + 4x + 2x^2/(n-1)$, $t_3 = 4x[-1 + x(n-2)/(n-1)]$, and $t_4 = x^2(6-4n)/(n-1)$, and where x is the net redundancy (7.6). Equality (7.16) holds for any unit-norm frame F , while (7.17) holds only if F is an ETF.

Proof. See Appendix C. □

Note that both variances in Theorem 7.2 vanish as $O(1/n)$; and that they are equal if $\gamma = 1$ ($x = 0$), in which case the sub-frame spectrum is supported only on 0 and 1. Returning to the empirical spectral variance mentioned before the theorem, since both m_1 and m_2 are asymptotically deterministic, it follows that the ESV of an ETF is given asymptotically by $m_2 - m_1^2 = p + p^2x - p^2$. See Chapter 10.

7.2 General moments: asymptotic analysis

The exact expression for the expected r th moment (7.4) of an ETF subset becomes complicated for $r > 4$, and it contains more terms (beyond (7.8)) that vanish as the frame size n goes to infinity. These vanishing terms might depend also on the specific ETF construction, and not only on n and the ratios γ and p . We next focus our attention on the non-vanishing terms, in order to apply the asymptotic moment method (5.8)-(5.9) of RMT.

Since an $m \times n$ ETF does not exist for every m, n pair, we look on a subsequence of dimensions n_1, n_2, \dots , and a corresponding sequence of m_i 's for which (i) an $m_i \times n_i$ ETF exists, and (ii) the aspect ratios m_i/n_i converge to some fixed $0 < \gamma < 1$. For such a sequence F_1, F_2, \dots of ETFs, the selection probability $0 \leq p \leq 1$ induces a corresponding sequence of expected r th moment $m_r^{(n_1)}, m_r^{(n_2)}, \dots$ according to (7.4). Let us define the asymptotic r th moment

$$m_r^{(\infty)}(\text{ETF}, \gamma, p) \triangleq \lim_{i \rightarrow \infty} m_r^{(n_i)} \quad (7.18)$$

provided that this limit exists and is unique (independent of the specific ETF sequence).

7.2.1 Recursive computation of moments

We next define a recursive procedure for computing $m_r^{(\infty)}(\text{ETF}, \gamma, p)$, for $r = 1, 2, \dots$. We start by defining a real-valued sequence A_1, A_2, A_3, \dots , by its two initial values

$$A_1 = \frac{2 - \gamma^{-1}}{2\sqrt{\gamma^{-1} - 1}}, \quad A_2 = 1, \quad (7.19)$$

and the recursive relation:

$$A_{s+1} = \sum_{i=1}^s A_i A_{s+1-i}, \quad s = 2, 3, \dots, \quad (7.20)$$

for $0 < \gamma < 1$. Note that for $\gamma = 0.5$ all the odd elements (including A_1) are zero.

Second, given a moment order r , define $\Pi(r, t)$ as the set of partitions of $[r]$ into t sets, for $1 \leq t \leq r$.⁴ Note that the size of $\Pi(r, t)$ is exponential in r , for $1 < t < r$. The extreme cases $\Pi(r, 1)$ and $\Pi(r, r)$ contain only one partition: the whole set $(1, 2, \dots, r)$, and singletons $(1, 2, \dots, r)$, respectively. As examples for the general case, $\Pi(4, 2)$ contains seven partitions (four with one singleton and one triplet, and three with two doubles): $(1, 234)$, $(2, 134)$, $(3, 124)$, $(4, 123)$, $(12, 34)$, $(13, 24)$, $(14, 23)$; while $\Pi(5, 3)$ contains twenty five partitions (ten with two singletons and one triplet, fifteen with two doubles and one singleton). A partition is called a ‘‘crossing partition’’ if for some two sets \mathcal{A} and \mathcal{B} in π , and four elements $a_1, a_2 \in \mathcal{A}$ and $b_1, b_2 \in \mathcal{B}$, we have $a_1 < b_1 < a_2 < b_2$. In the first example above $(13, 24)$ is a crossing partition, while in the second example above $(13, 24, 5)$, $(13, 25, 4)$, $(14, 25, 3)$, $(14, 2, 35)$, $(24, 1, 35)$ are crossing partitions [96].

For each non-crossing partition $\pi \in \Pi(r, t)$, define an associated graph $G(\pi)$ with r edges and t vertices, where each pair of consecutive elements in $[r]$ are connected with an edge in a cyclic manner, i.e., $1 \rightarrow 2, 2 \rightarrow 3, \dots, r \rightarrow 1$, and each subset of π is a vertex. For example,

⁴In view of the trace-product formula (7.10), $\Pi(r, t)$ amounts to all cases with t distinct indices in the expression for the r th moment (7.4).

the graph of $\pi = (12, 34)$ has two vertices (12) and (34), with two edges going between them, and two loops = an edge from each vertex to itself. The non-crossing property implies that the graph $G(\pi)$ has the shape of a “cactus”, [80], hence it can be decomposed into cycles, and we denote by $\text{cyc}(\pi) = \{s\}$ the set of lengths s of cycles in $G(\pi)$. Note that the sum of $s \in \text{cyc}(\pi)$ is equal to the number of edges r . Figure 7.1 shows the graph of the (non-crossing) partition $\pi = (12, 35, 4)$ in $\Pi(5, 3)$, which contains two cycles of length 2 and one cycle of length 1 (loop), hence $2 + 2 + 1 = 5 = r$.

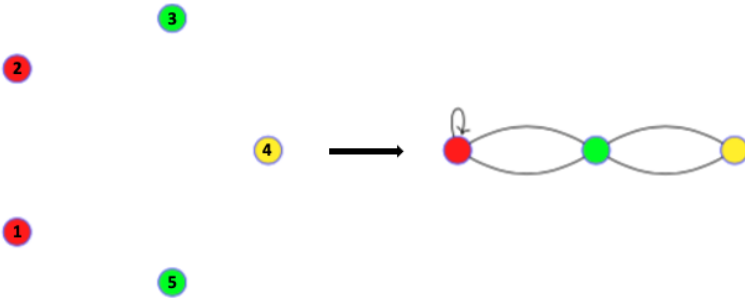


Figure 7.1: $G(\pi)$ of the partition $\pi = (12, 35, 4)$

Now, given both $0 < \gamma < 1$ and r , the “value” of a cycle of length s is defined as A_s (7.20). The “value” of a non-crossing partition π is defined as the product of the values of its cycles, while the “value” of a crossing partition is defined as zero:

$$V^*(\pi, \gamma) = \begin{cases} \prod_{s \in \text{cyc}(\pi)} A_s, & \pi = \text{non-crossing}, \\ 0, & \pi = \text{crossing}, \end{cases} \quad (7.21)$$

where \prod denotes product. For example, the value of the partition in Figure 7.1 is $V^*((12, 35, 4), \gamma) = A_1 A_2^2$. In the extreme case of $t = 1$, there is a unique $\pi = (12 \dots r)$, and $G(\pi)$ contains one vertex with r loops, so $V^*(\pi, \gamma) = A_1^r$. In the other extreme of $t = r$, there is a unique $\pi = (1, 2, \dots, r)$, and $G(\pi)$ contains one cycle between r vertices, so $V^*(\pi, \gamma) = A_r$.

Finally, for a given probability $0 < p < 1$, we use the formula (7.21) for the value of partitions to define the centralized quantity:

$$m_r^{\text{central}}(\gamma, p) = \sum_{t=1}^r \left(\sum_{\pi \in \Pi(r,t)} V^*(\pi, \gamma) \right) p^t, \quad (7.22)$$

from which we compute the decentralized quantity:

$$m_r^*(\gamma, p) = \left(\frac{\gamma^{-1}}{2} \right)^r \cdot p + \sum_{j=1}^r \binom{r}{j} \cdot K_{r,j} \quad (7.23)$$

where

$$K_{r,j} = (\gamma^{-1} - 1)^{j/2} \cdot \left(\frac{\gamma^{-1}}{2} \right)^{r-j} \cdot m_j^{\text{central}}(\gamma, p). \quad (7.24)$$

The relation between the decentralized quantity (7.23), which is the output of the recursive computation procedure above, and the r th moment of a random subset of an ETF, is stated in the next theorem.

Theorem 7.3 (Recursive formula for moments [65], [80]). Let $m_r^{(n_i)} = (1/n_i)E \left[\text{trace} \left((F_i P_i F_i^\dagger)^r \right) \right]$ denote the r th moment (7.4) of a random subset of the frame F_i , where F_i , $i = 1, 2, \dots$ is any sequence of $m_i \times n_i$ ETFs of increasing dimensions with a limiting aspect ratio $m_i/n_i \rightarrow \gamma$ as $i \rightarrow \infty$. Then, the sequence $m_r^{(n_1)}, m_r^{(n_2)}, \dots$ has a limit $m_r^{(\infty)}(\text{ETF}, \gamma, p)$ (see (7.18)), and this limit is equal to the output (7.23) of the recursive computation procedure above:

$$m_r^{(\infty)}(\text{ETF}, \gamma, p) = m_r^*(\gamma, p). \quad (7.25)$$

The proof of Theorem 7.3 for real-valued redundancy-2 ($\gamma = 1/2$) ETFs appears in [80]. The extension to general ($0 < \gamma < 1$, complex) ETFs was established during the writing of this survey paper, and it appears in [65].

7.2.2 The redundancy-2 case

The work in [80] established a closed-form expression for $m_r^*(1/2, p)$, the $\gamma = 1/2$ case in the right hand side of (7.25), using special properties that

hold in this case: (i) the relation $n_i = 2m_i$ holds *exactly* for each i for an infinite sequence of Paley ETFs; (ii) the Gram-Seidel adjacency matrix relation (4.4), (7.11) is particularly simple; (iii) the MANOVA(1/2, β) distribution is symmetric around its mean; (iv) its centralized version is equal to the Kesten-McKay distribution [37]; and (v) the A_s 's in (7.20) for odd s are zero, and for even s become

$$A_s = C_{s/2-1}$$

where $C_i = \frac{1}{i+1} \binom{2i}{i}$, $i = 1, 2, \dots$ are the Catalan numbers. Luckily, the inner sum in (7.22) (sum of products of Catalan numbers over all partitions in $\Pi(r, t)$), has an explicit closed form. Moreover, after the outer summation, (7.22) coincides with the Kesten-McKay moments [88]. This result is summarized in the following theorem.

Theorem 7.4. (Paley-Kesten-McKay relation [80]) For $\gamma = 1/2$ we have

$$m_r^{\text{central}}(1/2, p) = m_r^{\text{KM}}(p) \quad (7.26a)$$

and therefore

$$m_r^*(1/2, p) = m_r^{\text{MANOVA}}(1/2, p) \quad (7.26b)$$

where $m_r^{\text{central}}(\gamma, p)$ and $m_r^*(\gamma, p)$ are the centralized and non-centralized quantities in (7.22) and (7.23), respectively, and where $m_r^{\text{KM}}(p)$ and $m_r^{\text{MANOVA}}(\gamma, p)$ are the r th moments of the Kesten-McKay distribution [88], [37, table 4] and the MANOVA distribution (7.5), respectively.

Theorems 7.3 and 7.4 imply that for a sequence of redundancy-2 ($\gamma = 1/2$) ETFs of growing dimensions, the mean r th moment converges to the r th MANOVA moment:

$$m_r^{(\infty)}(\text{ETF}, 1/2, p) = m_r^*(1/2, p) = m_r^{\text{MANOVA}}(1/2, p). \quad (7.27)$$

The status of the analysis for a general $0 < \gamma < 1$ is somewhat subtle. While the recursive formula (7.25) for the asymptotic mean r th moment

is already fully proved, we are still missing a closed-form expression for $m_r^*(\gamma, p)$ (the right hand side of (7.25)). Thus, the identity

$$m_r^*(\gamma, p) \stackrel{?}{=} m_r^{\text{MANOVA}}(\gamma, p) \quad (7.28)$$

remains as a conjecture, which, together with the identity (7.25), would imply the desired result:

$$m_r^{(\infty)}(\text{ETF}, \gamma, p) \stackrel{?}{=} m_r^{\text{MANOVA}}(\gamma, p). \quad (7.29)$$

We used a symbolic computer program to verify that (7.28) indeed holds (for all $0 < \gamma < 1$) for a finite sequence of moments $r = 1, 2, \dots, r_m$.⁵

7.3 Concentration

The moment method (see Section 5.1) requires to establish two facts in order to conclude the desired convergence of the ESD to the limiting MANOVA law: (i) that the *mean* moments converge to the corresponding moments of the MANOVA law (5.8); and (ii) *concentration* of the moments (5.9). As discussed in Section 7.2.2, the first fact is partially established (the proof is complete for $\gamma = 1/2$, and “almost” complete for a general $0 < \gamma < 1$). As for the second fact, the analysis of Paley (redundancy-2) ETFs in [80, Thm. 1] can be extended to show the following result for a general sequence of unit-norm tight frames, whose mean centralized moments converge.

Theorem 7.5 (ESD concentration). Fix a bounded probability distribution μ on the real line, parameters $\gamma, p \in (0, \frac{1}{2})$, a lacunary sequence $L \subset \mathbb{N}$, and a sequence $\{F^{(n)}\}_{n \in L}$ of $[\gamma n] \times n$ unit norm tight frames. Suppose that when drawing random subsets $S_n \subseteq [n]$ with Bernoulli(p) elements, the random subensembles $H_n := F_{S_n}^{(n)}$ exhibit convergence in expectation of the centralized r th moments:

$$\mathbb{E}\left[\frac{1}{pn} \text{tr}\left[\left(\frac{1}{p}(H_n^\dagger H_n - I)\right)^r\right]\right] \rightarrow \int_{\mathbb{R}} x^r d\mu(x)$$

⁵The computation complexity is high due to the exponential growth of the set $\Pi(r, t)$ with r . So far we were able to verify (7.28) for $r = 1, \dots, 10$, and we intend to extend it further using parallel (“cloud”) computation.

for each $r \in \mathbb{N}$. Then, the empirical spectral distribution of $\frac{1}{p}(H_n^\dagger H_n - I)$ converges almost surely to μ .

The concentration result of Theorem 7.5, together with a confirmation of the currently open conjecture (7.29), would establish an analytic proof for the asymptotic behavior predicted by the empirical observations of Chapter 6. Namely, a typical subset from a general ETF has asymptotically a MANOVA spectrum:

$$\mu_{G_S}^{(n)} \rightarrow \mu_{\gamma, \beta}^{\text{MANOVA}} \quad (7.30)$$

as n goes to infinity, where $G_S = F_S F_S^\dagger$ is the Gram matrix of a sub-frame F_S selected with probability p (7.3); $\mu_{G_S}^{(n)}$ is the sub-frame ESD (5.1); γ and β are the asymptotic aspect ratios (2.12) of the sequence of frames $F^{(n)}$ and sub-frames $F_{S_n}^{(n)}$, respectively; and $\mu_{\gamma, \beta}^{\text{MANOVA}}$ is the MANOVA distribution whose density is given in (5.5).

8

Sub-frame inequalities

In the applications discussed in Sections 1 and 2, the frame dimension m is a design parameter that has an optimal value. On the one hand, the more *rectangular* is the subset ($m > k$ in source coding with erasures, $m < k$ in vector Gaussian channels), the more compact is its typical eigenvalue spread. On the other hand, the deviation from a *square* subset corresponds to wasting degrees of freedom: more DFT coefficients need to be quantized in source coding with erasures, less information symbols can be transmitted over a MIMO channel with “0/1 fading”, or less users can be active in non-orthogonal multiple access.

In this section we focus on the former effect, i.e., on the advantage of a more rectangular subset. Specifically, we show a monotonic improvement of the sub-frame performance measures defined in Chapter 3, $L_{Shannon}^*(n, m, k)$, $L_{MSE}^*(n, m, k)$, $L_{Shannon}^*(\gamma, \beta)$ and $L_{MSE}^*(\gamma, \beta)$, as the subset aspect ratio $\beta = k/m$ deviates from 1. Our analysis builds upon *information theoretic “subset” inequalities* for entropy and Fisher Information, and their implications to determinants and inverse-traces of positive semi-definite matrices [30], [33], [71].

The monotonic behavior (in k/m) of the optimum performance over

all frames (3.9) and (3.3) follows from a similar behavior that holds for any *fixed* frame. For some $m \times n$ frame F , recall the average subset log-determinant (Shannon transform) defined in (3.8) for $m \leq k \leq n$:

$$L_{\text{Shannon}}(F, k) \triangleq \frac{1}{\binom{n}{k}} \sum_{S:|S|=k} \frac{1}{m} \cdot \log \left(\det \left(\frac{m}{k} \cdot F_S \cdot F_S^\dagger \right) \right), \quad (8.1)$$

and recall the average subset trace-inverse (MSE goodness) defined in (3.2) for $1 \leq k \leq m$:

$$L_{\text{MSE}}(F, k) \triangleq \frac{1}{\binom{n}{k}} \sum_{S:|S|=k} \log \left(\frac{1}{k} \cdot \text{trace} \left((F_S^\dagger \cdot F_S)^{-1} \right) \right). \quad (8.2)$$

Theorem 8.1. For any $m \times n$ unit-norm frame F , the average subset Shannon transform (3.8) is monotonically non-decreasing with the subset size k :

$$L_{\text{Shannon}}(F, k) \leq \dots \leq L_{\text{Shannon}}(F, n) \leq 0 \quad (8.3)$$

for $m \leq k \leq n$.

Proof: This is a variation on the subset determinant inequality for increasing subsets in [33]. Unlike in [33], the size of the (positive definite) sub-matrices $F_S F_S^\dagger$, for $|S| = m, m+1, \dots, n$, is constant ($m \times m$), and only the *inner* dimension k is increasing. See the details of the proof in Appendix B. \square

Theorem 8.2. For any $m \times n$ unit-norm frame F , the average logarithmic noise amplification (3.2) is monotonically non-decreasing with the subset size k :

$$0 \leq L_{\text{MSE}}(F, k) \leq \dots \leq L_{\text{MSE}}(F, m) \quad (8.4)$$

for $1 \leq k \leq m$.

Proof: The proof is based on a trace-inverse inequality for increasing subsets of a general covariance matrix, [71]. See the details in Appendix B. \square

Theorems 8.1 and 8.2 immediately imply the same monotonic behavior for the best attainable performance over all $m \times n$ frames in (3.9) and (3.3), because for each k we can select a *different* frame to further improve the goodness.¹

Corollary 1. The optimum (n, m, k) Shannon transform goodness (3.9) is monotonically non-decreasing with the subset size k :

$$L_{\text{Shannon}}^*(n, m, k) \leq \dots \leq L_{\text{Shannon}}^*(n, m, n) \leq 0 \quad (8.5)$$

for $m \leq k \leq n$, and the optimum (n, m, k) logarithmic noise amplification (3.3) is monotonically non-decreasing with the subset size k :

$$0 \leq L_{\text{MSE}}^*(n, m, k) \leq \dots \leq L_{\text{MSE}}^*(n, m, m) \quad (8.6)$$

for $1 \leq k \leq m$. A similar monotonic behavior as a function of β (for a fixed γ) holds for the asymptotic measures $L_{\text{Shannon}}^*(\gamma, \beta)$ and $L_{\text{MSE}}^*(\gamma, \beta)$.

Remarks:

1. The negativity and positivity of L_{Shannon} and L_{MSE} , respectively, follows because the arguments of the logarithms in their definition can be written as geometric-to-arithmetic and arithmetic-to-harmonic means ratios for eigenvalues, (3.6) and (3.7b).
2. The case $k = m$ is worst for both goodness criteria, and they both improve (L_{Shannon} increases / L_{MSE} decreases) as k moves away from m , i.e., the sub-matrix F_S becomes more rectangular.
3. Without the normalization by k in (8.2) the MSE sub-frame inequality becomes trivial, because for every two nested subsets $S_1 \subset S_2 \subset [n]$, we have $\text{trace} \left((F_{S_1}^\dagger \cdot F_{S_1})^{-1} \right) \leq \text{trace} \left((F_{S_2}^\dagger \cdot F_{S_2})^{-1} \right)$.

¹For example, if F_k^* is the $m \times n$ frame achieving $L_{\text{Shannon}}^*(n, m, k)$, then $L_{\text{Shannon}}^*(n, m, k) = L_{\text{Shannon}}(F_k^*, k) \leq L_{\text{Shannon}}(F_k^*, k+1) \leq L_{\text{Shannon}}^*(n, m, k+1)$.

4. The right-hand side of (8.3) is reminiscent of the “determinant criterion”, $\det(F \cdot F^\dagger)$, for space-time coding over a Rayleigh fading channel [117], [121] (viewing the full frame F as the difference between two codewords in the space-time code). See Section 9.3.
5. In Corollary 1 above the frame dimensions n and m are held fixed while the subset size k varies. To fully justify the role of the design parameter m (or β) in the applications, we need to study the behavior when k and n are held fixed while m varies. This means that the frame F must vary with the subset aspect ratio β while keeping $k/n = p = \gamma\beta$ fixed. Empirically, for a fixed frame family, the dependence of the goodness measures on β is much stronger than their dependence on the frame aspect ratio γ . Hence a similar behavior should be expected for $L_{Shannon}^*(\gamma = p/\beta, \beta)$ and $L_{MSE}^*(\gamma = p/\beta, \beta)$, for a fixed p , as β deviates from 1. See, e.g., Figure 9.1. A more delicate analysis of this dependence is left for further study.

9

Applications

In this section we elaborate on some of the applications of analog frame codes in digital communication and signal processing, as specified in Table 1.1 in the Introduction section: non-orthogonal code-division multiple access (NOMA/CDMA), discrete-Fourier transform (DFT) codes, space-time codes (STC), analog to digital (A/D) conversion, multiple-description (MD) source coding, the new application of *coded computing*, training of deep neural networks (DNN), and phase transition in compressed sensing (CS). We provide numerical examples that clearly demonstrate that ETFs outperform other common frame codes.

9.1 NOMA/CDMA

Consider the multiple-access channel with partially active users: m channel resources are allocated in a fixed (non-orthogonal) manner between $n \geq m$ users, where at any given time only $k = pn$ out of the n users are active [102], [114], [126], [136], [137]. Here m can be thought of as the time-bandwidth product of the channel, and $\beta = k/m$ is the effective “loading factor” of the system. The resource allocation is done

via CDMA, i.e.,

$$\mathbf{y} = \sum_{i=1}^n x_i \mathbf{f}_i + \mathbf{z} = F\mathbf{x} + \mathbf{z}, \quad (9.1)$$

if all the users are active, and

$$\mathbf{y} = \sum_{i \in S} x_i \mathbf{f}_i + \mathbf{z} = F_S \mathbf{x}_S + \mathbf{z}, \quad (9.2)$$

if only a k -subset $S \subset [n]$ of the users is active, where $\mathbf{x} = (x_1, \dots, x_n)^\dagger$ represents the information symbols of the n users, \mathbf{f}_i is the length- m spreading sequence of user i , $\mathbf{z} = (z_1, \dots, z_m)^\dagger$ is additive white Gaussian noise (AWGN), and $\mathbf{y} = (y_1, \dots, y_m)^\dagger$ is the input to the (joint) receiver. The $m \times n$ frame $F = [\mathbf{f}_1 | \dots | \mathbf{f}_n]$, (1.1), defines the mapping from user symbols to channel signals, and the $m \times k$ subframe F_S and the subvector \mathbf{x}_S correspond to the k active users.

The relevant fidelity criterion depends on the type of the front-end receiver: matched-filter (MF), minimum mean-squared error (MMSE), or maximum likelihood (ML) [126], [136]. The simplest one, the matched-filter receiver, gives rise to the total interference power (average squared cross-correlation) criterion, which is independent of the activity number k , and *tightness* is sufficient for frame optimization; see the Welch bound (3.1) and [108]. The other two receivers give rise to k -subset criteria: MMSE (3.2) and log-determinant (Shannon transform) (3.8), which call for much stronger “ (n, m, k) ” frame symmetry conditions.

Let us focus on the (optimal) maximum-likelihood receiver. For a fixed F_S , the multiple access (MAC) sum capacity C_S (assuming a white Gaussian input [30]) is given by $\log(\det[I_m + \text{SNR} \cdot F_S F_S^\dagger])$ bits, where SNR is the signal-to-noise ratio per user. Since in a practical system the loading factor $\beta = k/m$ is smaller than or equal to one, it is preferable to rewrite C_S with respect to the smaller dimension k , i.e., as $\log(\det[I_k + \text{SNR} \cdot F_S^\dagger F_S])$ (the two expressions are equal since the nonzero eigenvalues of $F_S F_S^\dagger$ and $F_S^\dagger F_S$ are the same). The average capacity per resource (i.e., normalized by m) with respect to a uniform

selection of the subset S is thus given by

$$C = \frac{1}{\binom{n}{k}} \sum_{S:|S|=k} \frac{1}{m} \log(\det[I_k + \text{SNR} \cdot F_S^\dagger F_S]) \quad (9.3)$$

bits per resource. Note that for fixed n and k (equivalently fixed activity level $p = k/n$), one may wish to optimize the number of resources m , for $n \geq m \geq k$ (equivalently the loading factor $k/n \leq \beta \leq 1$) that maximizes the capacity per resource. Figure 9.1, taken from [111], shows the average capacity C as a function of β for several frame families. ETF clearly outperforms all other frames at its optimal β operation point. Figure 9.1-B shows the “practical capacity” (a quantity related to the concept of “lattice decoding” [125], [140]), which is equal to (9.3) without the “ I_k ” term inside the logarithm. This quantity - similar to the Shannon-transform performance measure in (3.8) - is more sensitive to eigenvalues of $F_S^\dagger F_S$ near zero; it thus demonstrates more clearly the gaps between the different frames and the optimal β operation point for each frame [111].

A similar behavior was observed in “irregular pulse-shape” optimization for faster-than-Nyquist TDMA signaling with FFE-DFE equalization [31].

9.2 DFT codes

Linear transformation can also be used to introduce redundancy against fading (or erasures or impulses) plus noise. Say, m information symbols $\mathbf{x} = (x_1, \dots, x_m)^\dagger$ are transformed into a larger n -vector signal $F^\dagger \mathbf{x}$, and the receiver gets a random k subset S corrupted with noise:

$$\mathbf{y} = F_S^\dagger \mathbf{x} + \mathbf{z} \quad (9.4)$$

where $\mathbf{y} = (y_1, \dots, y_k)^\dagger$ is the erased receiver input, and F^\dagger plays the role of the “coding” transformation. Note that in contrast to the partially-active multiple access channel (9.2), here F^\dagger expands the dimension $m : n$, and the interesting regime where the channel can be inverted is

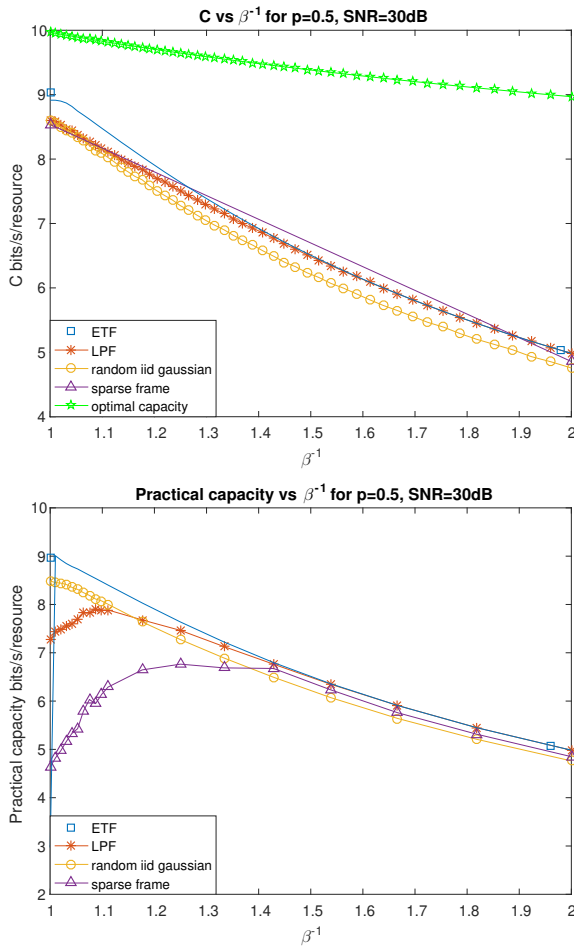


Figure 9.1: Average capacities per resource of a NOMA/CDMA system for a fixed activity level $p = \gamma\beta = k/n = 0.5$, as a function of the loading factor $\beta = k/m$, for several frames: random (5.3), LPF (2.7), Steiner ETF [50], and sparse [137]. All frame dimensions vary around 100×200 . A. regular capacity (9.3). B. practical capacity.

$n \geq k \geq m$. Wolf [131] proposed the concept of *DFT codes*, where F is a LPF frame, as a means to mitigate the effect of impulse noise which acts similarly to the erasures in (9.4). The redundancy introduced by the frame F allows the receiver to estimate the information symbols \mathbf{x} after the $n - k$ impulses were detected and removed (erased). A later work by Marshall [82] hinted to the fact that irregular selection of DFT frequencies leads to better estimation performance. See also [122], [123], [141].

9.3 Space-time codes (STC)

A space-time code can be viewed as a two-dimensional - space/time - analog modulation scheme, tailored to a vector-input block-fading channel, that introduces diversity against random fading in the spatial dimension. Codes for fading Gaussian channels need to preserve a sufficient Hamming distance after the coordinates were randomly attenuated by fading [121]. Rayleigh fading gives rise to the “product measure” [121, sec. 3.2.2], which becomes the “determinant criterion” for STC [117]. More specifically, STC transforms a message A into an $m \times n$ codeword F_A of m channel uses in time over n channel uses in space (n transmit antennas). The pairwise error between two such codewords A and B in the presence of Rayleigh fading is bounded by some (SNR-dependent) constant divided by the determinant $\det[(F_A - F_B) \cdot (F_A - F_B)^\dagger]$, [117], [121, sec. 3.3.2]. If we take B to be the zero codeword, then the goodness of the codeword A is inverse proportional to $\det[F_A \cdot F_A^\dagger]$. In the presence of 0/1 spatial fading, the equivalent codeword is $(F_A)_S$, where $S \subset [n]$ is the set of surviving spatial coordinates. If a random set of k coordinates survive, where $k \geq m$, then we get that the error probability in the presence of a combination of 0/1 and Rayleigh fading is bounded by

$$P_e(A \rightarrow 0) \leq \frac{1}{\binom{n}{k}} \sum_{S:|S|=k} \frac{SNR^{-m}}{\det[(F_A)_S (F_A)_S^\dagger]}. \quad (9.5)$$

The RHS of (9.5) can be seen as a k -dependent criterion for STC design, which reduces to the usual “determinant criterion” for $k = n$ ($p = 1$). Figure 9.2 illustrates this measure as a function of $p = k/n$ for several “frames” F_A . The clear advantage of ETFs for moderate p gives rise to the question: can we choose multiple space-time codewords, such that all pairwise differences will be “near ETF”?

9.4 Over-sampling and Δ - Σ modulation

Sampling of a band-limited signal beyond its Nyquist rate allows to trade off quantization resolution (distortion) for time resolution (rate) [139]. The distortion enhancement follows since the desired signal has a low-pass spectrum in the over-sampled domain, while the quantization noise is approximately white and can be filtered out at the reconstruction. Δ - Σ modulation enhances this effect using a “noise shaping” feedback filter around the quantizer, that creates a high-pass quantization noise spectrum, hence lower reconstruction distortion for the same quantization resolution [23], [97]. Interestingly, it was recognized that the mapping between the original (Nyquist-sampled) signal to the Δ - Σ modulated signal can be viewed as a frame expansion [8]. This opens the door to more general Δ - Σ modulation schemes, that are robust against various forms of interference and erasures [15], [41], [59], [115].

9.5 Multiple-description (MD) source coding

When a source is transmitted over a lossy packet network, where ACK/NAK feedback cannot be assumed, one may wish for graceful degradation as a function of the number of erased/received packets. [54], [58]. In MD coding, the source is split into n “descriptions”, where a priori unknown subset of the descriptions arrive to the receiver; it is convenient to assume that the receiver gets either a subset of size k , or all the n descriptions [103].

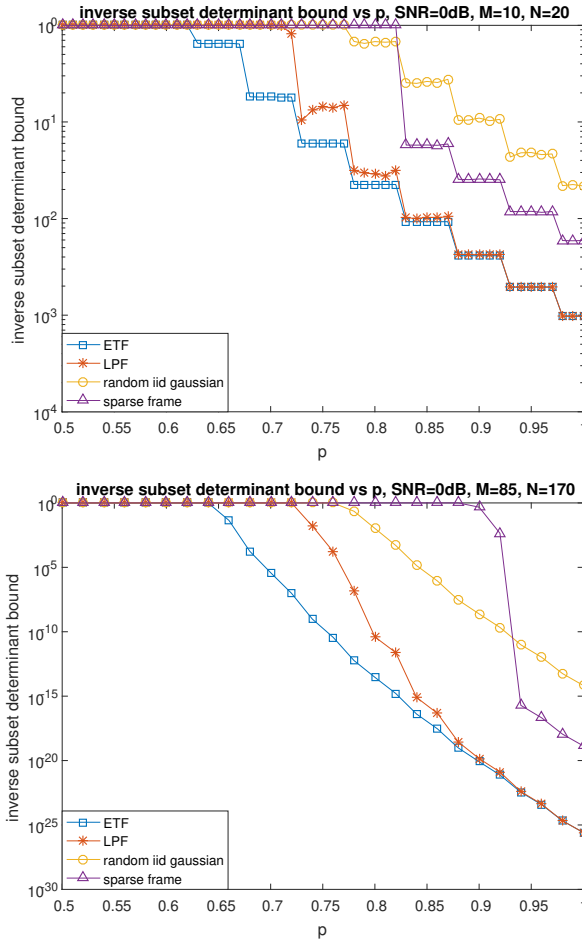


Figure 9.2: The “inverse subset determinant” bound (9.5) of space-time codes, for a fixed $\gamma = 0.5$ as a function of the not-erased probability $p = k/n$, for several frames: random (5.3), LPF (2.7), Paley ETF [50], and sparse [137]. Frame dimensions $m \times n =$: (A) 10×20 . (B) 85×170 .

A simple solution based on Δ - Σ modulation for the case ($n = 2$, $k = 1$) was proposed in [98]. The Δ - Σ -two-description coding scheme uses 1:2 oversampling ratio, where the two descriptions are created by splitting into even and odd samples, and where the noise shaping loop controls the distortion ratio between the $k = 1$ case (even or odd samples) and the $k = 2$ case (all samples). It is shown in [98] that this solution achieves the optimal MD rate-distortion region for a Gaussian source under quadratic distortion if we use an optimal dithered (lattice) quantizer [99]. Naturally, one may wish to extend this solution to a general (n, k) pair using $m : n$ oversampling ratio, for some $m \leq k$, with periodic allocation of the samples to the n descriptions. This extension suffers, however, from *noise amplification* whenever the received descriptions do not form a uniform sampling pattern [84], [85], which is exactly the same as the *signal amplification* problem in band-limited interpolation for “source coding with erasures” (Chapter 2).

The fact that ETFs - which are highly robust against random erasures - correspond to “irregular spectrum” (see the difference-set DFT construction in Section 4.1.2), inspired the idea to modify the interpolation filter in the MD Δ - Σ modulation scheme to be an “irregular interpolator” [56]. Figure 9.3, taken from [56], demonstrates this idea in MD image (JPEG-based) coding. See also [101].

9.6 Coded distributed computation (CDC)

Analog MDS (Reed-Solomon) codes were recently proposed to protect against straggling worker nodes in distributed computation of a linear function; e.g., of the gradient in training a deep neural network [76], [107]. Specifically, to obtain the matrix multiplication XA with K ideal workers, the master node breaks A into K pieces $[A_1, \dots, A_K]$, and distribute the partial multiplications XA_1, \dots, XA_K . If there are more workers but some are stragglers, say, only K out of N compute their task in time, the master worker can use the generator matrix of a $K : N$

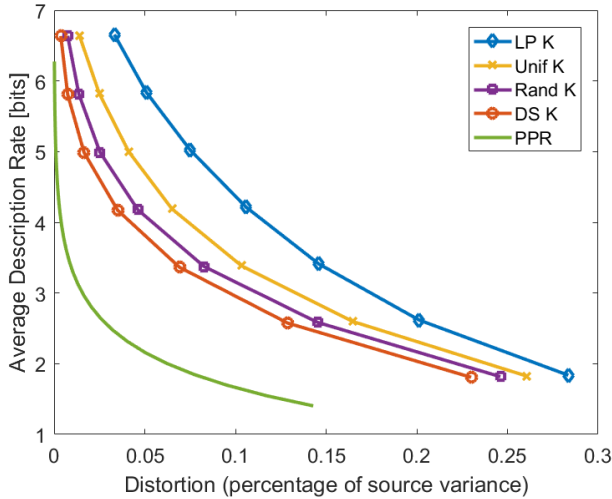


Figure 9.3: Rate-distortion performance of Δ - Σ MD coding with over-sampling ratio $n : m = 31 : 6$, where $k = 6$ descriptions are received out of $n = 31$ transmitted descriptions, for several interpolation filters: low pass (LP), difference-set (DS), uniform (Unif), and random (rand) spectrum interpolation filter, compared to the “PPR bound” [103].

“analog erasure-correction code” to expand A_1, \dots, A_K into $\tilde{A}_1, \dots, \tilde{A}_N$, so XA can be computed from any K subset of XA_1, \dots, XA_N . For example, for $K = 2, N = 3$ the code is simply $\tilde{A}_1 = A_1, \tilde{A}_2 = A_2$ and $\tilde{A}_3 = A_1 + A_2$, and analog versions of BCH and Reed Solomon codes provide simple encoding and decoding schemes for more general (K, N) pairs [76], [78], [107]. It is insightful to think of the expansion as multiplying A by a frame F with an aspect ratio N/K , i.e., $\tilde{A} = AF$, where F is composed of $K \times N$ square blocks, each being a scaled identity matrix $g_{i,j}I$, for $i \in [K], j \in [N]$. For example, in the 2:3 example above all the g ’s are 0/1, and

$$F = \begin{bmatrix} I & 0 & I \\ 0 & I & I \end{bmatrix}.$$

Now suppose that beyond the stragglers problem, we also face noise due to finite word-length computation. That is, the master node needs

to reconstruct XA from

$$Y_S = (XAF)_S + Z$$

where S denotes the subset of non straggling workers and Z denotes the computation noise. Our goal is to find coding frames F which are resilient to noise, i.e., numerically stable [43], [105]. The challenge though is to keep the simplicity of encoding and decoding of analog codes inspired from digital erasure correction codes [4], [20], [107], yet enjoy the better robustness to analog noise of ETFs.

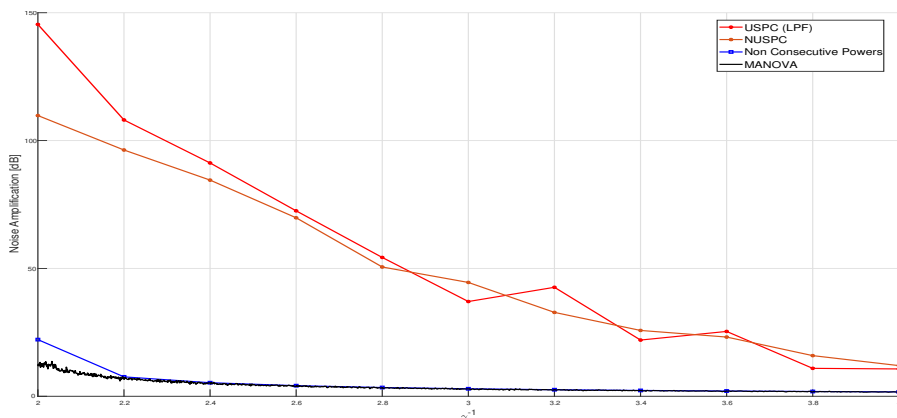


Figure 9.4: Comparison of noise amplification Vs. the frame redundancy γ^{-1} for several polynomial codes: uniform sampled unit circle (USPC), non-uniform sampled unit circle (NUSPC), and non-consecutive (difference-set) powers, compared to the MANOVA curve. Figure is taken from [135].

9.7 Neural networks

The robustness of ETF subsets, revealed in [64], [66], inspired the work of Bank and Girayes [6], [7] on training of deep neural networks with Dropout. Their scheme regularizes the training of the parameters in each iteration, so that they form a set of vectors with a low coherence, just like a subset from an ETF.

9.8 Frames in compressed sensing: phase transition

Pose the compressed sensing measurement as $x \mapsto Ax = y$. We observe y and wish to recover x for A known. Denote our chosen signal reconstruction scheme by $\mathcal{R} : t \mapsto x$. For example, \mathcal{R} can be $\mathcal{R} : y \mapsto \operatorname{argmin}_{y=Ax} \|x\|_1$. The basic question in (noiseless) compressed sensing is - for which *(matrix, signal)* pair (A, x) do we have $\mathcal{R}(y) = x$? When the underlying model includes randomness in the pair (A, x) , one can ask this question either in the worst-case sense (asking to characterize those cases (A, x) when $\mathcal{R}(y) = x$ w.p 1) or average-case sense (asking to characterize those cases (A, x) when $\mathcal{R}(y) = x$ with high probability).

The Restricted Isometry Property became popular as it appeared in sufficient conditions for worst-case recovery in compressed sensing problems. However, these sufficient conditions are known to be far from tight, and indeed explain only a fraction of the cases (A, x) in which recovery (using ℓ_1 minimization, say) is known to hold.

The situation is different when one considers average-case recovery. Donoho and Tanner [35] developed a theory that places cases (A, x) on a sparsity-undersampling phase plane. Using large-scale experiments they have identified - empirically at first - an asymptotic phase transition phenomenon, which holds approximately for finite (A, x) and exactly in the large-system limit. An exact formula for the asymptotic phase transition was later identified for Gaussian i.i.d sensing matrices A and a variety of signal models x . In a definite sense, then, the average-case analysis is satisfying and complete.

In [93] the authors reported a curious phenomenon: the same empirical apparatus that had been previously used to establish the existence of the Donoho-Tanner phase transition for the case of Gaussian sensing matrices, has been applied to deterministic sensing matrices based on known frame constructions including ETFs. The authors reported overwhelming empirical evidence, based on a very large parallel computation, that most of the deterministic frames under study, when used as the

sensing matrix A in a recovery problem and when using a variety of reconstruction algorithms, exhibit a phase transition that agrees with that of Gaussian matrices.

This observed universality, in which many different frame constructions exhibit a single, universal compressed sensing phase transition has not, to the best of our knowledge, proved rigorously. However in contrast with theory based on Restricted Isometry Property it provides a complete characterization, within a specified framework, of the success and failure of recovery of sparse vectors using ℓ_1 minimization and related algorithms. The connection between this universal phenomenon and the new ETF-MANOVA relation is yet to be found.

10

ETF optimality conjecture

The examples of Chapter 9 (see also Figure 1.1) showed that ETFs are superior to all other frame families that were investigated: LPF, random and code-based, in terms of their performance as analog codes. We are tempted to conjecture that ETFs outperform all other frames, and achieve the optimal frame performance characteristics (3.3), (3.9) and (3.11) defined in Chapter 3. In this chapter we provide some analytic support for the “ETF superiority” conjecture. We show that the Welch lower bound (3.1) naturally extends to random frame subsets and to higher-order moments (3rd and 4th moments in (7.4)), and that the extended bound is achieved by (and sometimes only by) ETFs.

10.1 Erasure Welch bound

Theorem 10.1 (Erasure Welch Bound (EWB) of order $r = 2, 3, 4$ [63], [67]). For any m -by- n unit-norm frame F , selection probability p , and moment orders $r = 2, 3, 4$, the expected sub-frame r th moment (7.4) is lower bounded by

$$m_r \geq m_r^{\text{ETF}} \tag{10.1}$$

where m_r^{ETF} is the corresponding value for an ETF given by Theorem 7.1 (using (7.7)-(7.8) even if an ETF does not exist for the pair (m, n)). Equality holds for $r = 2, 3$ if and only if F is a tight frame, and for $r = 4$ if and only if F is an ETF.

The case $(r = 2, p = 1)$ in Theorem 10.1 is equivalent to the (mean-squared) Welch bound (3.1). Thus, the EWB generalizes the Welch bound in two senses. First, it is a bound on random k -subsets of F rather than on the entire set of its pairwise moments. Second, it is a bound on higher order ($r = 3, 4$) moments.¹

Proof. For the case $r = 2$, the equivalent form (7.14) of the mean-squared Welch bound (3.1), and the expression (7.13b) for m_2 , imply

$$m_2 \geq p + p^2 x = m^{\text{MANOVA}}(\gamma, p, 2) = m_2^{\text{ETF}}, \quad (10.2)$$

where the last two equations follow from (7.7b) and Theorem 7.1. The Welch bound equality condition implies that (10.2) holds with equality for any tight frame. The proof for $r = 3, 4$ is based on Jensen's inequality, and it appears in [63], [67]. \square

10.2 Minimum empirical variance and kurtosis

The EWB has an interesting implication on ETF having the most compact spectral distribution of a randomly selected sub-frame. By (7.12) and Theorem 10.1, all unit-norm frames share the same expected sub-frame 1st moment $m_1 = p$; thus minimizing the expected sub-frame 2nd moment m_2 amounts to minimizing the *empirical spectral variance*

$$\text{ESV} = m_2 - m_1^2 \quad (10.3)$$

of a *typical* sub-frame (typical in the sense that its moment matches the ensemble average), among all unit-norm frames. Moreover, all unit-norm *tight* frames share the same expected sub-frame 2nd moment $m_2 =$

¹Our definition is different than the generalized Welch bound on the average r th power of the absolute cross-correlation [130].

$p + p^2x$, and 3rd moment $m_3 = p + 3xp^2 + (x^2 - x)p^3$; thus minimizing the expected sub-frame 4th moment m_4 amounts to minimizing the *empirical spectral kurtosis*

$$\text{ESK} = \frac{m_4 - 4m_3m_1 + 6m_2m_1^2 - 3m_1^4}{(m_2 - m_1^2)^2} \quad (10.4)$$

of a typical sub-frame, among all unit-norm *tight* frames. We can thus use the MANOVA 1st-to-4th moments to lower bound the variance and kurtosis of the limiting sub-frame ESD of any sequence of unit-norm (*tight*) frames.

Theorem 10.2 (Minimum sub-frame ESV and ESK). Consider any sequence of unit-norm frames with increasing dimensions, whose aspect ratio converges to γ , and whose (Bernoulli- p selected) sub-frame ESD $\mu_{G_S}^{(n)}$ converges to some limiting law μ (see (7.30)). The asymptotic sub-frame ESV (10.3) is lower bounded by that of a *tight* frame:

$$\text{ESV} \geq p + (x - 1)p^2 \quad (10.5)$$

where $x = 1/\gamma - 1$. Moreover, if the sequence of frames is *tight*, then the asymptotic sub-frame ESK (10.4) is lower bounded by that of an ETF:

$$\text{ESK} \geq \frac{p + p^2(6x - 4) + p^3(6x^2 - 16x + 6) + p^4(x^3 - 7x^2 + 11x - 3)}{p^2(x^4 + 2x^2 + 1) - p^3(2x^2 + 2) + p^4}. \quad (10.6)$$

Recalling that the variance and kurtosis are measures for the spread of a distribution about its mean, Theorem 10.2 indicates that ETFs have the *most compact typical sub-frame ESD* among all unit-norm frames.

Figure 10.1 shows a comparison of the sub-frame moments, and the corresponding variance and kurtosis, for several *tight* frames, as well as for a random (i.i.d.) frame.

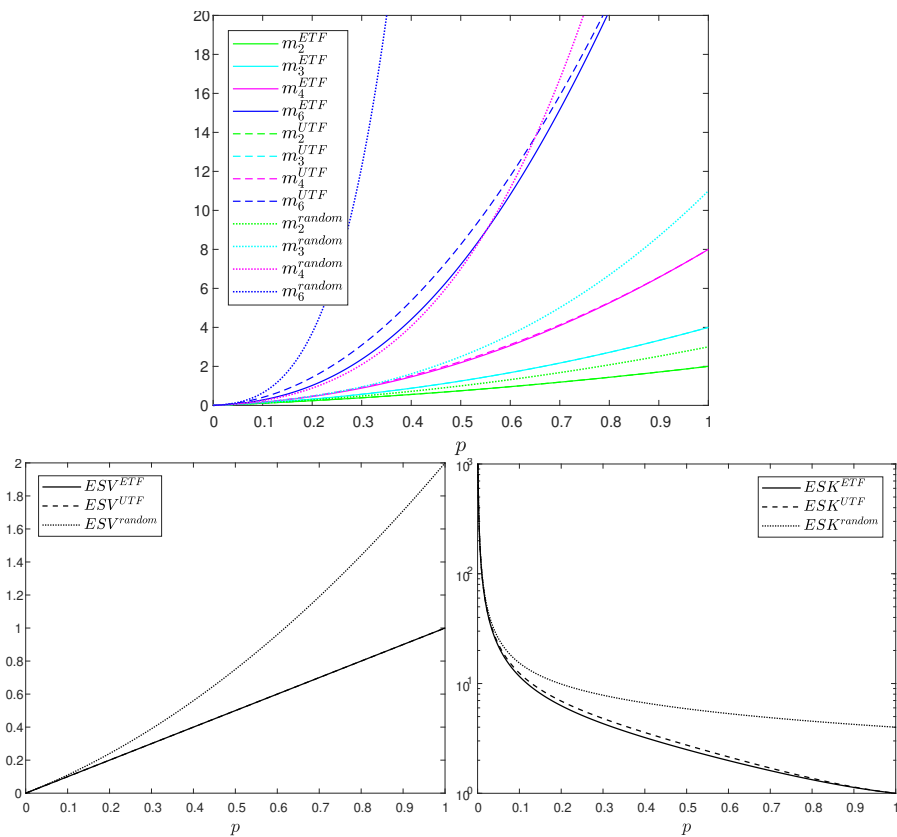


Figure 10.1: Comparison between a repetition (unit-norm tight) frame (UTF); random (i.i.d.) frame; and ETF, where all frames are with aspect ratio $\gamma = 1/2$. The x -axis shows the sub-frame selection probability p . The y -axis shows the sub-frame moments 1-6 (top), the empirical spectral variance (bottom-left), and the empirical spectral kurtosis (bottom-right).

11

Conclusion and discussion

This survey paper sheds light on the great potential of incorporating ideas from information theory and random matrix theory into frame theory. While our original motivation was practical: design of robust analog codes, the new point of view suggests new insights about the intersection between frame theory and random matrix theory.

In all the applications we considered, exact mean-case performance is given by an expression of the form

$$\mathbf{E}_S[\Psi(\lambda(G_S))]$$

where Ψ is a functional of the empirical spectrum, which depends on the example. Here, S denotes a “typical” (randomly selected) subframe of the frame F under consideration, $G_S = F_S^\dagger F_S$ is the Gram matrix, $\lambda(G_S)$ is the spectrum of G_S , and \mathbf{E}_S the expectation with respect to random selection of sub-frame S . (Note that $\lambda(G_S)$ is equivalent to the empirical spectral distribution μ_{G_S} in (5.1).)

A common property of the three functionals Ψ mentioned in Chapter 3 is that a frame, whose typical sub-frame exhibits a spectrum that is narrower and more removed from zero gives better performance.

From this perspective, “good” frames have the property that typical subframes have a compact and zero-removed support.

Questions. Generalizing from the examples we have seen, we arrive at fundamental new questions which span frame theory and random matrix theory:

1. How does one calculate quantities of the form $\mathbf{E}_S[\Psi(\lambda(G_S))]$ for various functionals Ψ ?
2. How can we design “good frames” - namely frames whose typical subframe has a spectrum with support as small and as zero-removed as possible?
3. Does there exist a “best frame”, namely, a frame with “best” spectrum (with respect to one of the performance measures, or all of them)? If it exists, can we characterize it?

Answers. In this survey we review recent results which attempt to answer the questions above:

1. For a large variety of well known frames (Table 6.1), and a large variety of functionals Ψ (Chapter 3), the quantity $\mathbf{E}_S[\Psi(\lambda(G_S))]$ can be calculated to good and known precision (Chapter 6). Specifically,

$$\mathbf{E}_S [\Psi (\lambda(G_S))] \approx \Psi (f_{\beta,\gamma})$$

where $f_{\beta,\gamma}$ is a known cumulative distribution function that depends on the aspect ratios of the frame in question.

2. Certain tight frames - of both deterministic and random design - are “good frames” in the sense that the spectrum of their typical subframe converges to a universal limiting spectral distribution $f_{\beta,\gamma}$ (Chapter 5). In fact, this universal limiting distribution function is the famous Wachter (Jacobi) asymptotic distribution familiar from random matrix theory, whose support is indeed compact and zero-removed.

3. There is empirical and theoretic evidence that suggest that equian-gular tight frames in fact achieve the best performance, asymptotically as the frame size grows (Chapter 10).

More generally, this survey suggests that the spectrum of a typical subframe, taken from a frame with certain design properties, is a fascinating object - both from a theoretical perspective and a practical perspective. Here, “typical” is taken to mean a subframe selected uniformly at random from the set of all subframes. Our results revolve around a fascinating universality property, whereby the spectrum of (the Gramian of) a typical subframe is indistinguishable from that of a matrix from the MANOVA (Jacobi) random matrix ensemble, both in finite- n and asymptotically. We summarize formal mathematical results and ample empirical evidence supporting this universality property, discuss it from a mathematical point of view, and present its many practical repercussions (Sections 6 and 9).

Interestingly, this universality property holds for a certain kind of *deterministic* frames, just as it holds for certain random frames. This means that, curiously, a famous random matrix theory law arises in a deterministic and highly symmetric geometrical object. While one can find hints in the literature that this random-matrix phenomena can be suspected to arise asymptotically in these highly symmetric deterministic frames, the fact that universality holds for finite- n as well is striking in our opinion. We highlight the many open questions and open problems that arise in this fascinating study of spectra of random sub-frames.

11.1 Summary of asymptotic results for ETF subsets

The ETF-MANOVA relation of Sections 6 and 7 implies:

$$L_{\text{MSE}}(\text{ETF}, \gamma, p) = \log \left(\int_{\lambda_-}^{\lambda_+} \frac{1}{x} \cdot f_{\gamma, p}(x) dx \right), \quad (11.1)$$

$$L_{\text{Shannon}}(\text{ETF}, \gamma, p) = \int_{\lambda_-}^{\lambda_+} \log(x) \cdot f_{\gamma,p}(x) dx, \quad (11.2)$$

and (by the convergence of the extreme eigenvalues¹)

$$L_{\text{StRIP}}(\text{ETF}, \gamma, p, \delta) = \begin{cases} 1, & \text{if } \delta < \min\{1 - \lambda_-, \lambda_+ - 1\} \\ 0, & \text{otherwise,} \end{cases} \quad (11.3)$$

for the three performance measures (3.2), (3.7b) and (3.11), where $f_{\gamma,p}(x)$ and its support edges (λ_-, λ_+) are given in (5.5) (with $p = \beta\gamma$). The ETF superiority conjecture implies that the *optimal* measures (3.4), (3.9) and (3.11) are given by:

$$L_{\text{MSE}}^*(\gamma, p) = L_{\text{MSE}}(\text{ETF}, \gamma, p), \quad (11.4)$$

$$L_{\text{Shannon}}^*(\gamma, p) = L_{\text{Shannon}}(\text{ETF}, \gamma, p), \quad (11.5)$$

and

$$L_{\text{StRIP}}^*(\gamma, p, \delta) = L_{\text{StRIP}}(\text{ETF}, \gamma, p, \delta). \quad (11.6)$$

The central conjecture of our work and main open question is whether ETF are indeed the best possible frames under random subset selection.

11.2 Open questions and conjectures

We are left with many thoughts and directions for future research. Let us mention a few.

1. Asymptotic ETF-MANOVA theorem: find a closed-form expression for the r th moment recursion formula (7.23), in order to prove the conjectured identity (7.28).

¹ While the asymptotic results in Chapter 7 are only concerned with the bulk spectrum, our empirical results (Chapter 6, [66]) demonstrate a “Tracy-Widom” kind of result ([1], [45]) regarding the high-probability convergence of the extreme eigenvalues to λ_{\pm} of the MANOVA law.

2. Beyond ESD: find other RMT-like properties of a typical ETF sub-frame; e.g., isotropic behavior of eigen-vectors; convergence of the extreme eigenvalues (see footnote 1); diagonal of the Gram matrix, etc.
3. MANOVA ensemble: what makes a typical ETF sub-frame similar to the ratio of i.i.d. matrices (5.4) in the MANOVA definition?
4. Sub-frame selection: Bernoulli(p) (i.i.d.) versus combinatorial (n choose k). Confirm the asymptotic equivalence. Is (and how much) the *non*-asymptotic behavior different?
5. Is the *non*-asymptotic behavior *universal* for all ETFs, or dependent on the specific ETF construction? See beginning of Section 7.2.
6. Symmetries of ETF: In the course of analyzing the r th-moment (7.4), we identified some invariant properties of small chains of products, which seem to hold for various ETF constructions, that may be useful to characterize the *non*-asymptotic behavior of the moments [63].
7. Method of proof: can we find alternative proofs for the ETF-MANOVA relation via transform or free-probability methods? See [45] and the result of [104].
8. Near ETF: how far can we relax the equi-angular and tightness conditions, without changing the asymptotic MANOVA behavior?
9. Spherical codes: find similarities and distinction between maximal distance spherical codes and ETFs.
10. Low-pass frames: do randomly-selected sub-frames of LPF have a limiting ESD?
11. RMT-like behavior of frames: are there other families of deterministic frames that exhibit a (possibly different) limiting sub-frame

- ESD? What is the set of attainable distributions for fixed γ and β ? Is this set convex (closed under mixtures of frame families)?
12. Erasure Welch bound: how does the EWB (10.1) connect to Welch's generalized bound for higher-order moments of the cross-correlations [130]; can we derive one from the other?
 13. ETF superiority: find a sharper definition (beyond variance, kurtosis and functional (" Ψ ") measures).
 14. Coded distributed computing (CDC): modify the noise amplification performance measure (3.2) to the case where one needs to recover only the input sum (or one projection or subspace), rather than full inversion [135].
 15. Source with erasures: can we obtain the full MMSE gain, and eliminate the "+1" penalty term in (2.11) for a general β ?
 16. Sub-frame rectangularity: do the performance inequalities in Chapter 8 continue to hold if we fix p and let both β and γ vary accordingly?
 17. Analog versus digital: are analog codes inherently inferior to digital codes? do ETF minimize the gap to Shannon's theoretical optimum performance?

Acknowledgements

Matan Gavish was partially supported by the Israel Science Foundation, grant 1523/16.

Dustin G. Mixon was partially supported by AFOSR FA9550-18-1-0107 and NSF DMS 1829955.

Ram Zamir was partially supported by the Israel Science Foundation, grants 676/15 and 2623/20.

We thank Ofer Zeitouni for suggesting the moment approach to prove the ETF-MANOVA theorem.

Appendices

A

Entropy-coded dithered quantization

To assess the rate-distortion performance (2.11) of the analog coding scheme, we shall adopt the additive-noise “test channel” of entropy-coded (subtractive) dithered quantization (ECDQ) [138]. In this model, $Q^{(\text{dither})}(\tilde{\mathbf{x}}) = \tilde{\mathbf{x}} + \mathbf{Z}$, where \mathbf{Z} is an independent uniform or Gaussian noise, and the quantizer entropy is given by the mutual information $H(Q^{(\text{dither})}(\tilde{\mathbf{X}})) = I(\tilde{\mathbf{X}}; \tilde{\mathbf{X}} + \mathbf{Z})$.¹ The equivalent error in the important samples, $\mathbf{E}_s = \hat{\mathbf{X}}_s - \mathbf{X}_s$ is thus, by (2.8), given by $\mathbf{E}_s = F_S^\dagger \cdot (\tilde{\mathbf{X}} + \mathbf{Z}) - \mathbf{X}_s = F_S^\dagger \cdot \mathbf{Z}$, implying that the mean-squared distortion per important sample (2.2) is

$$D = \frac{1}{k} E \left\{ \|\mathbf{E}_s\|^2 \right\} = \frac{\sigma_z^2}{k} \cdot \text{trace}\{F_S^\dagger F_S\} = \sigma_z^2, \quad (\text{A.1})$$

where σ_z^2 is the quantizer mean-squared error, and the last equation follows since F_S has k unit-norm columns.² Since the decoder is blind

¹To be more precise, the quantizer operation is given by $Q(\tilde{\mathbf{x}} + \text{dither}) - \text{dither}$, where dither is uniform over the fundamental quantizer cell. For good high-dimensional lattice quantizers, this uniform dither distribution tends to be white Gaussian. See [140].

²Further improvement can be obtained using minimum mean-squared error “Wiener” estimation, [64], but this is negligible when $\sigma_x^2 \gg D$.

to the location of important samples (that affect the correlation of the vector $\tilde{\mathbf{X}}$), the coding rate is equal to that of a *white* Gaussian vector $\tilde{\mathbf{W}}$ with the same power as $\tilde{\mathbf{X}}$, [75]. Assuming the LS estimator (2.9), we have $E\|\tilde{\mathbf{X}}\|^2 = \sigma_x^2 \cdot \text{trace}\{(F_S^\dagger F_S)^{-1}\}$, so the ECDQ mutual information formula (with a Gaussian dither) becomes:

$$R_{\text{analog}} = \frac{1}{n} I(\tilde{\mathbf{W}}; \tilde{\mathbf{W}} + \mathbf{Z}) \quad (\text{A.2})$$

$$= \frac{m}{2n} \cdot \log \left(1 + \frac{\frac{1}{m} E\|\tilde{\mathbf{X}}\|^2}{\sigma_z^2} \right) \quad (\text{A.3})$$

$$= \beta \cdot \frac{p}{2} \cdot \log \left(1 + \frac{\sigma_x^2}{D} \cdot \frac{\text{trace}\{(F_S^\dagger F_S)^{-1}\}}{m} \right) \quad (\text{A.4})$$

where $\beta \triangleq k/m$, and we used (2.2) with $k = pn$.

B

Information theoretic proofs for sub-frame inequalities

In proving Theorems 8.1 and 8.2 we use the following two lemmas.

Lemma B.1. For any $m \times n$ frame F , and $k < n$,

$$\frac{1}{\binom{n}{k}} \sum_{S:|S|=k} F_S \cdot F_S^\dagger = \frac{k}{n} \cdot F \cdot F^\dagger, \quad (\text{B.1})$$

where the average in the left hand side is over all k -subsets of $\{1, \dots, n\}$ as in (3.8)-(3.2).

Remark: For Bernoulli(p) selection, i.e., when each index in $\{1, \dots, n\}$ belongs to S with probability p independently of the other indices, the lemma becomes $E_S\{F_S \cdot F_S^\dagger\} = p \cdot F \cdot F^\dagger$, where $E_S\{\cdot\}$ denotes expectation with respect to the selection of S .

Proof: The case $k = 1$ of (B.1) is the standard expansion $\sum_{i=1}^n \mathbf{f}_i \cdot \mathbf{f}_i^\dagger = F \cdot F^\dagger$ (multiplied by $1/n$), where the \mathbf{f}_i 's are the columns of F . For a general k , let P denote a random diagonal matrix, whose $\{0, 1\}$ diagonal elements correspond to the selection of the subset S . That is, $F_S \cdot F_S^\dagger = F \cdot P \cdot F^\dagger$, where the diagonal of P is uniform over all n choose k binary vectors with k ones and $n - k$ zeroes. Thus

$E_S\{F_S \cdot F_S^\dagger\} = E_S\{F \cdot P \cdot F^\dagger\} = F \cdot E_S\{P\} \cdot F^\dagger = F \cdot (k/n \cdot I_n) \cdot F^\dagger$, which is the right-hand side of (B.1). \square

Lemma B.2. For $k_1 < k_2 < n$, if S_2 is uniformly drawn from all k_2 subsets of $\{1, \dots, n\}$, and S_1 is uniformly drawn from all k_1 subsets of S_2 , then S_1 is uniform on all k_1 subsets of $[n]$.

Proof: Since the distribution of S_1 is invariant under the action of the symmetric group of $[n]$, it is necessarily uniform. \square

Proof of Theorem 8.1: We first prove the inequality with respect to the “edge”: $L(F, k) \leq L(F, n)$, and then extend to any $k_1 < k_2$. The Ky Fan inequality [30], says that if K_1 and K_2 are $m \times m$ PSD matrices, then

$$\det[a \cdot K_1 + (1 - a) \cdot K_2] \geq \det[K_1]^a \cdot \det[K_2]^{1-a} \quad (\text{B.2})$$

for any $0 < a < 1$, which by taking logarithm implies that $\log \det[K]$ is concave [30]. Thus, starting from (3.8),

$$L_{\text{Shannon}}(F, k) = E_S\{\log[\sqrt[m]{\det(F_S \cdot F_S^\dagger)/(k/m)}]\} \quad (\text{B.3})$$

$$\leq \log[\sqrt[m]{\det(E_S\{F_S \cdot F_S^\dagger\})/(k/m)}] \quad (\text{B.4})$$

$$= \log[\sqrt[m]{\det(k/n \cdot F \cdot F^\dagger)/(k/m)}] \quad (\text{B.5})$$

$$= \log[\sqrt[m]{\det(F \cdot F^\dagger)/(n/m)}] \quad (\text{B.6})$$

$$= L_{\text{Shannon}}(F, n) \quad (\text{B.7})$$

where the second line is by Jensen’s inequality and the log concavity of the determinant (B.2), and the third line is by the identity in Lemma B.1. Turning to the general case, for $k_1 < k_2 < n$, let $S_1 \subset S_2$ denote a k_1 -subset of a k_2 -subset S_2 of $\{1, \dots, n\}$. By the definition of the average

subset Shannon transform of a frame (3.8), we have

$$L_{\text{Shannon}}(F, k_1) = E_{S_1} \{ \Psi_{\text{Shannon}}(F_{S_1}) \} \quad (\text{B.8})$$

$$= E_{S_2} \{ E_{S_1|S_2} \{ \Psi_{\text{Shannon}}(F_{S_1}) \} \} \quad (\text{B.9})$$

$$= E_{S_2} \{ L_{\text{Shannon}}(F_{S_2}, k_1) \} \quad (\text{B.10})$$

$$\leq E_{S_2} \{ L_{\text{Shannon}}(F_{S_2}, k_2) \} \quad (\text{B.11})$$

$$= E_{S_2} \{ \Psi_{\text{Shannon}}(F_{S_2}) \} \quad (\text{B.12})$$

$$= L_{\text{Shannon}}(F, k_2) \quad (\text{B.13})$$

where $E_{S_1|S_2} \{ \cdot \}$ denotes expectation over a uniform distribution on all k_1 -subsets of a given S_2 , and $E_{S_2} \{ \cdot \}$ denotes expectation over a uniform distribution on all k_2 -subsets of $\{1, \dots, n\}$. The second line follows from Lemma B.2 by iterated expectation; the third line follows by viewing F_{S_2} as the full frame in the inner expectation; the inequality follows from the first part of the proof (B.3)-(B.7) setting $k = k_1$ and $n = k_2$; and the last two lines are again by the definition (3.8). \square

Proof of Theorem 8.2: For an $n \times n$ covariance matrix K (i.e., K is a non-negative matrix), and a k -subset $S \subset \{1, \dots, n\}$, let K_S denote the corresponding $k \times k$ sub-matrix of K . Define the *subset trace-inverse* of the covariance K as the average of $\text{trace}(K_S^{-1})/k$ over all k -subsets:

$$M_k^{(n)} = \frac{1}{\binom{n}{k}} \sum_{S:|S|=k} \frac{1}{k} \text{trace}(K_S^{-1}), \quad (\text{B.14})$$

for $k = 1, \dots, n$. For example, the two extremes are $M_1^{(n)} = 1/n \sum_{i=1}^n (K_{ii})^{-1}$, and $M_n^{(n)} = 1/n \sum_{i=1}^n (K^{-1})_{ii}$. It is shown in [71] that the sequence of subset trace inverses is monotonically non decreasing, i.e.,

$$M_1^{(n)} \leq M_2^{(n)} \leq \dots \leq M_n^{(n)} \quad (\text{B.15})$$

with equality if and only if the covariance matrix K is proportional to identity.¹ This inequality can be thought of as the ‘‘MSE counterpart’’ of

¹If the matrix K is Toeplitz (corresponding to stationary vector), then the

the subset determinant inequality in [30] and [33]. Using similar tools as in [30], we can show the same inequality also for *subset log trace-inverse*. Namely, letting

$$L_k^{(n)} = \frac{1}{\binom{n}{k}} \sum_{S:|S|=k} \log \left(\frac{1}{k} \text{trace} \left(K_S^{-1} \right) \right), \quad (\text{B.16})$$

we have

$$L_1^{(n)} \leq L_2^{(n)} \leq \dots \leq L_n^{(n)}. \quad (\text{B.17})$$

Proof: Starting with the right edge, noting that $\binom{n}{n} = 1$ and $\binom{n}{n-1} = n$, we have

$$\begin{aligned} L_n^{(n)} &= \log \left(\frac{1}{n} \text{trace} \left(K^{-1} \right) \right) \\ &= \log \left(M_n^{(n)} \right) \\ &\geq \log \left(M_{n-1}^{(n)} \right) \\ &= \log \left(\frac{1}{n} \sum_{S:|S|=n-1} \frac{1}{n-1} \text{trace} \left(K_S^{-1} \right) \right) \\ &\geq \frac{1}{n} \sum_{S:|S|=n-1} \log \left(\frac{1}{n-1} \text{trace} \left(K_S^{-1} \right) \right) \\ &= L_{n-1}^{(n)}, \end{aligned} \quad (\text{B.18})$$

where the equality lines are by definition; the first inequality follows from (B.15); and the second inequality follows by Jensen. We then continue similarly to the second part of the proof of Theorem 8.1 to prove that $L_k^{(n)} \leq L_{k+1}^{(n)}$ for any k . Specifically, by Lemma B.2, when computing $L_k^{(n)}$ we first condition on a specific $(k+1)$ -subset S_2 and average over all its k -subsets, and then average over all $(k+1)$ -subsets

inequality between the two edges, $M_1^{(n)} \leq M_n^{(n)}$, follows from the arithmetic-to-harmonic means inequality applied to the eigenvalues $\lambda_1, \dots, \lambda_n$ of K , and equality holds if and only if the eigenvalues are constant, i.e., $K = \lambda I$. (This is because by the Toeplitz property $K_{ii} = \sigma^2$ for all i , and therefore $M_1^{(n)} = 1/\sigma^2$; furthermore, $\sigma^2 = \text{trace}(K)/n = (\lambda_1 + \dots + \lambda_n)/n$, while the eigenvalues of K^{-1} are the reciprocals of the eigenvalues of K , so $M_n^{(n)} = (1/\lambda_1 + \dots + 1/\lambda_n)/n$.)

S_2 of $\{1, \dots, n\}$. By (B.18), the inner average is upper bounded by the log trace-inverse of K_{S_2} , which becomes $L_{k+1}^{(n)}$ after taking the outer average. \square

Theorem 8.2 now follows from (B.17) by viewing the $F^\dagger \cdot F$ as the covariance matrix K , so $L_{MSE}(F.k) = L_k^{(n)}$. (Note that for $k > m$ the matrix $F_S^\dagger F_S$ is singular, so $L_k^{(n)}$ is infinite.)

C

Variance of 1st and 2nd moments (proof of Theorem 7.2)

Using the moment-variance formula (7.15),

$$\begin{aligned} V_r &\triangleq \text{Var} \left[\frac{1}{n} \text{trace} \left((FPF^\dagger)^r \right) \right] \\ &= E \left[\left(\frac{1}{n} \text{trace} \left((FPF^\dagger)^r \right) \right)^2 \right] - m_r^2 \end{aligned}$$

we obtain for $r = 1$,

$$\begin{aligned}
V_1^{\text{ETF}} &= \mathbb{E} \left[\left(\frac{1}{n} \text{trace} (FPF^\dagger) \right)^2 \right] - \mathbb{E} \left[\frac{1}{n} \text{trace} (FPF^\dagger) \right]^2 \\
&= \mathbb{E} \left[\left(\frac{1}{n} \text{trace} (FPF^\dagger) \right)^2 \right] - m_1^2 \\
&= \frac{1}{n^2} \mathbb{E} \left[\left(\sum_{i=1}^n \langle \mathbf{f}_i, \mathbf{f}_i \rangle P_i \right) \left(\sum_{j=1}^n \langle \mathbf{f}_j, \mathbf{f}_j \rangle P_j \right) \right] - p^2 \\
&= \frac{1}{n^2} \mathbb{E} \left[\left(\sum_{i=1}^n P_i \right) \left(\sum_{j=1}^n P_j \right) \right] - p^2 \\
&= \frac{1}{n^2} [np + n(n-1)p^2] - p^2 \\
&= \frac{1}{n} [p - p^2]. \tag{C.1}
\end{aligned}$$

For $r = 2$, we obtain

$$\begin{aligned}
V_2^{\text{ETF}} &= \mathbb{E} \left[\left(\frac{1}{n} \text{trace} ((FPF^\dagger)^2) \right)^2 \right] - \mathbb{E} \left[\frac{1}{n} \text{trace} ((FPF^\dagger)^2) \right]^2 \\
&= \mathbb{E} \left[\left(\frac{1}{n} \text{trace} ((FPF^\dagger)^2) \right)^2 \right] - m_2^2 \\
&= \frac{1}{n^2} \mathbb{E} \left[\left(\sum_{i,j=1}^n |\langle \mathbf{f}_i, \mathbf{f}_j \rangle|^2 P_i P_j \right) \left(\sum_{k,m=1}^n |\langle \mathbf{f}_k, \mathbf{f}_m \rangle|^2 P_k P_m \right) \right] - (p + p^2 x)^2. \tag{C.2}
\end{aligned}$$

If F is an ETF, then according to the Welch bound $|\langle \mathbf{f}_i, \mathbf{f}_j \rangle|^2 = \frac{x}{n-1}$ for $i \neq j$. Similarly to the computation of the moments, we split to cases by number of distinct values of $\{i, j, k, m\}$.

$$\begin{aligned}
& \mathbb{E} \left[\left(\sum_{i,j=1}^n |\langle \mathbf{f}_i, \mathbf{f}_j \rangle|^2 P_i P_j \right) \left(\sum_{k,m=1}^n |\langle \mathbf{f}_k, \mathbf{f}_m \rangle|^2 P_k P_m \right) \right] = np \\
& + \left[n(n-1) + 4n(n-1) \frac{x}{n-1} + 2n(n-1) \frac{x^2}{(n-1)^2} \right] p^2 \\
& + \left[2n(n-1)(n-2) \frac{x}{n-1} + 4n(n-1)(n-2) \frac{x^2}{(n-1)^2} \right] p^3 \\
& + n(n-1)(n-2)(n-3) \frac{x^2}{(n-1)^2} p^4. \tag{C.3}
\end{aligned}$$

It follows that

$$\begin{aligned}
V_2 = \frac{1}{n} & \left[p + \left(-1 + 4x + \frac{2x^2}{n-1} \right) p^2 + \left(-4x + \frac{4(n-2)x^2}{n-1} \right) p^3 \right. \\
& \left. + \left(\frac{(6-4n)x^2}{n-1} \right) p^4 \right]. \tag{C.4}
\end{aligned}$$

References

- [1] G. Anderson, A. Guionnet, and O. Zeitouni, *An Introduction to Random Matrices*. Cambridge University Press, 2009.
- [2] G. W. Anderson and B. Farrell, “Asymptotically liberating sequences of random unitary matrices,” pp. 381–413, *Advances in Mathematics*, vol. 255, 2014.
- [3] M. Appleby, T.-Y. Chien, S. Flammia, and S. Waldron, “Constructing exact symmetric informationally complete measurements from numerical solutions,” p. 165–302, *Journal of Physics A: Mathematical and Theoretical*, vol. 51, no. 16, 2018.
- [4] B. Babadi and V. Tarokh, “Spectral distribution of random matrices from binary linear block codes,” pp. 3955–3962, *IEEE Transactions on Information Theory*, vol. 57, no. 6, 2011.
- [5] A. S. Bandeira, D. G. Mixon, and J. Moreira, “A conditional construction of restricted isometries,” pp. 372–381, *International Mathematics Research Notices*, vol. 2017, no. 2, 2017.
- [6] D. Bank and R. Giryes, “On the relationship between dropout and equiangular tight frames,” *arXiv preprint arXiv:1810.06049*, 2018.
- [7] D. Bank and R. Giryes, “An ETF view of dropout regularization,” *British Machine Vision Virtual Conference, 2020*, 2020.

- [8] J. J. Benedetto, O. Yilmaz, and A. M. Powell, "Sigma-delta quantization and finite frames," in *2004 IEEE International Conference on Acoustics, Speech, and Signal Processing*, vol. 3, pp. iii–937, 2004.
- [9] J. J. Benedetto and J. D. Kolesar, "Geometric properties of Grassmannian frames for \mathbb{R}^2 and \mathbb{R}^3 ," pp. 1–17, *EURASIP Journal on Advances in Signal Processing*, 2006.
- [10] T. Berger, "Rate distortion theory: A mathematical basis for data compression," 1971.
- [11] R. E. Blahut, "Algebraic fields, signal processing, and error control," pp. 874–893, *Proceedings of the IEEE*, vol. 73, no. 5, 1985.
- [12] R. E. Blahut, *Digital transmission of information*. Addison-Wesley, 1990, pp. 457–483.
- [13] B. G. Bodmann and J. Haas, "Achieving the orthoplex bound and constructing weighted complex projective 2-designs with Singer sets," pp. 54–71, *Linear Algebra and its Applications*, vol. 511, 2016.
- [14] H. Bolcskei, F. Hlawatsch, and H. G. Feichtinger, "Frame-theoretic analysis of oversampled filter banks," pp. 3256–3268, *IEEE Transactions on signal processing*, vol. 46, no. 12, 1998.
- [15] P. Boufounos, A. V. Oppenheim, and V. K. Goyal, "Causal compensation for erasures in frame representations," pp. 1071–1082, *IEEE Transactions on Signal Processing*, vol. 56, no. 3, 2008.
- [16] J. Bourgain, S. Dilworth, K. Ford, S. Konyagin, D. Kutzarova, *et al.*, "Explicit constructions of RIP matrices and related problems," pp. 145–185, *Duke Mathematical Journal*, vol. 159, no. 1, 2011.

- [17] J. Bourgain, S. J. Dilworth, K. Ford, S. V. Konyagin, and D. Kutzarova, “Breaking the k_2 barrier for explicit RIP matrices,” in *Proceedings of the forty-third annual ACM symposium on Theory of computing*, pp. 637–644, 2011.
- [18] B. Bukh and C. Cox, “Nearly orthogonal vectors and small antipodal spherical codes,” pp. 359–388, *Israel Journal of Mathematics*, vol. 238, 2020.
- [19] T. T. Cai and A. Zhang, “Sharp rip bound for sparse signal and low-rank matrix recovery,” pp. 74–93, *Applied and Computational Harmonic Analysis*, vol. 35, no. 1, 2013.
- [20] R. Calderbank, S. Howard, and S. Jafarpour, “Construction of a large class of deterministic sensing matrices that satisfy a statistical isometry property,” pp. 358–374, *IEEE journal of selected topics in signal processing*, vol. 4, no. 2, 2010.
- [21] E. J. Candes, “The restricted isometry property and its implications for compressed sensing,” pp. 589–592, *Comptes Rendus Mathematique*, vol. 346, no. 9-10, 2008.
- [22] E. J. Candes and T. Tao, “Near-optimal signal recovery from random projections: Universal encoding strategies?” Pp. 5406–5425, *IEEE transactions on information theory*, vol. 52, no. 12, 2006.
- [23] J. Candy, *Oversampling delta-sigma data converters: theory, design, and simulation*. University of Texas Press, 1992.
- [24] P. G. Casazza and G. Kutyniok, *Finite frames: Theory and applications*. Springer, 2012.
- [25] E. Chou, C. S. Güntürk, F. Krahmer, R. Saab, and Ö. Yılmaz, “Noise-shaping quantization methods for frame-based and compressive sampling systems,” in *Sampling theory, a renaissance*, Springer, 2015, pp. 157–184.
- [26] H. Cohn and A. Kumar, “Universally optimal distribution of points on spheres,” pp. 99–148, *Journal of the American Mathematical Society*, vol. 20, no. 1, 2007.

- [27] C. J. Colbourn and J. H. Dinitz, *Handbook of combinatorial designs*. CRC press, 2006.
- [28] J. H. Conway, R. H. Hardin, and N. J. Sloane, “Packing lines, planes, etc.: Packings in Grassmannian spaces,” pp. 139–159, *Experimental mathematics*, vol. 5, no. 2, 1996.
- [29] T. M. Cover and M. Chiang, “Duality between channel capacity and rate distortion with two-sided state information,” pp. 1629–1638, *IEEE Transactions on Information Theory*, vol. 48, no. 6, 2002.
- [30] T. Cover and J. Thomas, *Elements of Information Theory*. Wiley, 1991.
- [31] Y. Dadush, *The advantage of irregular pulse shape for NOMA*. Project, Tel Aviv University, 2018.
- [32] I. Daubechies, A. Grossmann, and Y. Meyer, “Painless nonorthogonal expansions,” in *Fundamental Papers in Wavelet Theory*, Princeton University Press, 2009, pp. 372–384.
- [33] A. Dembo, T. M. Cover, and J. A. Thomas, “Information theoretic inequalities,” pp. 1501–1518, *IEEE Transactions on Information Theory*, vol. 37, no. 6, 1991.
- [34] C. Ding and T. Feng, “A generic construction of complex codebooks meeting the Welch bound,” pp. 4245–4250, *IEEE transactions on information theory*, vol. 53, no. 11, 2007.
- [35] D. Donoho and J. Tanner, “Observed universality of phase transitions in high-dimensional geometry, with implications for modern data analysis and signal processing,” pp. 4273–4293, *Philosophical Transactions of the Royal Society A: Mathematical, Physical and Engineering Sciences*, vol. 367, no. 1906, 2009.
- [36] D. L. Donoho, M. Elad, and V. N. Temlyakov, “Stable recovery of sparse overcomplete representations in the presence of noise,” pp. 6–18, *IEEE Transactions on information theory*, vol. 52, no. 1, 2006.

- [37] A. Dubbs and A. Edelman, “Infinite random matrix theory, tridiagonal bordered Toeplitz matrices, and the moment problem,” pp. 188–201, *Linear Algebra and its Applications*, vol. 467, 2015.
- [38] R. J. Duffin and A. C. Schaeffer, “A class of nonharmonic Fourier series,” pp. 341–366, *Transactions of the American Mathematical Society*, vol. 72, no. 2, 1952.
- [39] A. Edelman and B. D. Sutton, “The beta-Jacobi matrix model, the CS decomposition, and generalized singular value problems,” pp. 259–285, *Foundations of Computational Mathematics*, vol. 8, no. 2, 2008.
- [40] M. Elad, “Sparse and redundant representations: From theory to applications in signal and image processing,” 2010.
- [41] Y. C. Eldar and H. Bolcskei, “Geometrically uniform frames,” pp. 993–1006, *IEEE Transactions on Information Theory*, vol. 49, no. 4, 2003.
- [42] L. Erdős and B. Farrell, “Local eigenvalue density for general MANOVA matrices,” pp. 1003–1032, *Journal of Statistical Physics*, vol. 152, no. 6, 2013.
- [43] M. Fahim and V. R. Cadambe, “Numerically stable polynomially coded computing,” in *2019 IEEE International Symposium on Information Theory (ISIT)*, pp. 3017–3021, 2019. DOI: [10.1109/ISIT.2019.8849468](https://doi.org/10.1109/ISIT.2019.8849468).
- [44] B. Farrell, “Limiting empirical singular value distribution of restrictions of discrete Fourier transform matrices,” pp. 733–753, *Journal of Fourier Analysis and Applications*, vol. 17, no. 4, 2011.
- [45] A. R. Feier, “Methods of proof in random matrix theory,” Ph.D. dissertation, Harvard University, 2012.
- [46] M. Fickus, J. Jasper, and D. G. Mixon, “Packings in real projective spaces,” pp. 377–409, *SIAM Journal on Applied Algebra and Geometry*, vol. 2, no. 3, 2018.

- [47] M. Fickus, J. Jasper, D. G. Mixon, and J. Peterson, “Group-theoretic constructions of erasure-robust frames,” pp. 131–154, *Linear Algebra and its Applications*, vol. 479, 2015.
- [48] M. Fickus and D. G. Mixon, “Tables of the existence of equiangular tight frames,” *arXiv preprint arXiv:1504.00253*, 2015.
- [49] M. Fickus, D. G. Mixon, and J. C. Tremain, “Constructing a large family of equiangular tight frames,” *Proc. Sampl. Theory Appl*, 2011.
- [50] M. Fickus, D. G. Mixon, and J. C. Tremain, “Steiner equiangular tight frames,” pp. 1014–1027, *Linear algebra and its applications*, vol. 436, no. 5, 2012.
- [51] S. Foucart and M.-J. Lai, “Sparsest solutions of underdetermined linear systems via lq-minimization for $0 < q < 1$,” pp. 395–407, *Applied and Computational Harmonic Analysis*, vol. 26, no. 3, 2009.
- [52] S. Foucart and H. Rauhut, “A mathematical introduction to compressive sensing,”
- [53] C. A. Fuchs, M. C. Hoang, and B. C. Stacey, “The SIC question: History and state of play,” p. 21, *Axioms*, vol. 6, no. 3, 2017.
- [54] A. E. Gamal and T. Cover, “Achievable rates for multiple descriptions,” pp. 851–857, *IEEE Transactions on Information Theory*, vol. 28, no. 6, 1982.
- [55] A. Gersho and R. M. Gray, *Vector quantization and signal compression*, vol. 159. Springer Science & Business Media, 2012.
- [56] M. Goren and R. Zamir, “Diversity image coding using irregular interpolation,” *IEEE Transactions on Image Processing*, 2021.
- [57] V. K. Goyal, M. Vetterli, and N. T. Thao, “Quantized overcomplete expansions in \mathbb{R}^N : Analysis, synthesis, and algorithms,” pp. 16–31, *IEEE Transactions on Information Theory*, vol. 44, no. 1, 1998.

- [58] V. K. Goyal, “Multiple description coding: Compression meets the network,” pp. 74–93, *IEEE Signal processing magazine*, vol. 18, no. 5, 2001.
- [59] V. K. Goyal, J. Kovačević, and J. A. Kelner, “Quantized frame expansions with erasures,” pp. 203–233, *Applied and Computational Harmonic Analysis*, vol. 10, no. 3, 2001.
- [60] V. K. Goyal, M. Vetterli, and J. Kovacevic, “Multiple description transform coding: Robustness to erasures using tight frame expansions,” in *Information Theory, 1998. Proceedings. 1998 IEEE International Symposium on*, IEEE, p. 408, 1998.
- [61] S. Gurevich and R. Hadani, “The statistical restricted isometry property and the Wigner semicircle distribution of incoherent dictionaries,” *arXiv preprint arXiv:0812.2602*, 2008.
- [62] J. I. Haas IV, N. Hammen, and D. G. Mixon, “The Levenstein bound for packings in projective spaces,” in *Wavelets and Sparsity XVII*, International Society for Optics and Photonics, vol. 10394, p. 103940V, 2017.
- [63] M. Haikin, *An analog coding frame-work*. MSc thesis, Tel Aviv University (also on arXiv preprint arXiv:1809.07315), 2018.
- [64] M. Haikin and R. Zamir, “Analog coding of a source with erasures,” in *IEEE International Symposium on Information Theory (ISIT)*, IEEE, pp. 2074–2078, 2016.
- [65] M. Haikin and R. Zamir, “Moments of subsets of general equian-gular tight frames,” *arXiv preprint arXiv:2107.00888*, 2021.
- [66] M. Haikin, R. Zamir, and M. Gavish, “Random subsets of struc-tured deterministic frames have MANOVA spectra,” E5024–E5033, *Proceedings of the National Academy of Sciences*, vol. 114, no. 26, 2017.
- [67] M. Haikin, R. Zamir, and M. Gavish, “Frame moments and Welch bound with erasures,” in *2018 IEEE International Symposium on Information Theory (ISIT)*, IEEE, pp. 2057–2061, 2018.

- [68] I. Haviv and O. Regev, “The restricted isometry property of subsampled Fourier matrices,” in *Geometric aspects of functional analysis*, Springer, 2017, pp. 163–179.
- [69] R. B. Holmes and V. I. Paulsen, “Optimal frames for erasures,” pp. 31–51, *Linear Algebra and its Applications*, vol. 377, 2004.
- [70] J. Jasper, E. J. King, and D. G. Mixon, “Game of Sloanes: Best known packings in complex projective space,” in *Wavelets and Sparsity XVIII*, International Society for Optics and Photonics, vol. 11138, 111381E, 2019.
- [71] A. Khina, A. Yeredor, and R. Zamir, “Monotonicity of the trace-inverse of covariance submatrices and “two-sided prediction”,” *IEEE Transactions on Information Theory*, submitted September 2020.
- [72] G. S. Kopp, “SIC-POVMs and the Stark conjectures,” *International Mathematics Research Notices*, 2019.
- [73] J. Kovacevic and A. Chebira, *An introduction to frames*. Now Publishers Inc, 2008.
- [74] F. Kraemer, S. Mendelson, and H. Rauhut, “Suprema of chaos processes and the restricted isometry property,” pp. 1877–1904, *Communications on Pure and Applied Mathematics*, vol. 67, no. 11, 2014.
- [75] A. Lapidot, “On the role of mismatch in rate distortion theory,” pp. 38–47, *IEEE Transactions on Information Theory*, vol. 43, no. 1, 1997.
- [76] K. Lee, M. Lam, R. Pedarsani, D. Papailiopoulos, and K. Ramchandran, “Speeding up distributed machine learning using codes,” pp. 1514–1529, *IEEE Transactions on Information Theory*, vol. 64, no. 3, 2018.
- [77] V. Levenshtein, “Bounds on the maximal cardinality of a code with bounded modulus of the inner product,” in *Soviet Math. Dokl.*, vol. 25, pp. 526–531, 1982.

- [78] S. Li and S. Avestimehr, “Coded computing: Mitigating fundamental bottlenecks in large-scale distributed computing and machine learning,” pp. 1–148, *Foundations and Trends® in Communications and Information Theory*, vol. 17, no. 1, 2020. DOI: [10.1561/0100000103](https://doi.org/10.1561/0100000103). [Online]. Available: <http://dx.doi.org/10.1561/0100000103>.
- [79] D. J. Love, R. W. Heath, and T. Strohmer, “Grassmannian beamforming for multiple-input multiple-output wireless systems,” pp. 2735–2747, *IEEE transactions on information theory*, vol. 49, no. 10, 2003.
- [80] M. Magsino, D. G. Mixon, and H. Parshall, “Kesten–McKay law for random subensembles of Paley equiangular tight frames,” pp. 1–22, *Constructive Approximation*, 2020.
- [81] V. A. Marčenko and L. A. Pastur, “Distribution of eigenvalues for some sets of random matrices,” p. 457, *Mathematics of the USSR-Sbornik*, vol. 1, no. 4, 1967.
- [82] T. Marshall, “Coding of real-number sequences for error correction: A digital signal processing problem,” pp. 381–392, *IEEE Journal on selected areas in communications*, vol. sac-2, no. 2, 1984.
- [83] E. Martinian, G. W. Wornell, and R. Zamir, “Source coding with distortion side information,” pp. 4638–4665, *IEEE Transactions on Information Theory*, vol. 54, no. 10, 2008.
- [84] A. Mashiach, J. Ostergaard, and R. Zamir, “Sampling versus random binning for multiple descriptions of a bandlimited source,” in *IEEE Information Theory Workshop (ITW)*, IEEE, pp. 1–5, Seville, 2013.
- [85] A. Mashiach, J. Østergaard, and R. Zamir, “Multiple description delta-sigma quantization with individual and central receivers,” in *Electrical and Electronics Engineers in Israel (IEEEI), 2010 IEEE 26th Convention of*, IEEE, pp. 000 942–000 946, 2010.

- [86] A. Mashiach and R. Zamir, “Noise-shaped quantization for nonuniform sampling,” in *Information Theory Proceedings (ISIT), 2013 IEEE International Symposium on*, IEEE, pp. 1187–1191, 2013.
- [87] J. L. Massey and T. Mittelholzer, “Welch’s bound and sequence sets for code-division multiple-access systems,” in *Sequences II*, Springer, 1993, pp. 63–78.
- [88] B. D. McKay, “The expected eigenvalue distribution of a large regular graph,” pp. 203–216, *Linear Algebra and its Applications*, vol. 40, 1981.
- [89] G. Mikhail, “Infinite families of optimal systems of biangular lines related to representations of $sl(2, \mathbb{F}_q)$,” *arXiv preprint arXiv:2012.02718*, 2020.
- [90] D. G. Mixon, “Explicit matrices with the restricted isometry property: Breaking the square-root bottleneck,” in *Compressed sensing and its applications*, Springer, 2015, pp. 389–417.
- [91] D. G. Mixon and H. Parshall, “The optimal packing of eight points in the real projective plane,” pp. 1–12, *Experimental Mathematics*, 2019.
- [92] D. G. Mixon and H. Parshall, “Globally optimizing small codes in real projective spaces,” pp. 234–249, *SIAM Journal on Discrete Mathematics*, vol. 35, no. 1, 2021.
- [93] H. Monajemi, S. Jafarpour, M. Gavish, D. L. Donoho, S. 3. 3. Collaboration, *et al.*, “Deterministic matrices matching the compressed sensing phase transitions of gaussian random matrices,” pp. 1181–1186, *Proceedings of the National Academy of Sciences*, vol. 110, no. 4, 2013.
- [94] R. J. Muirhead, *Aspects of multivariate statistical theory*, vol. 197. John Wiley & Sons, 2009.
- [95] O. R. Musin and A. S. Tarasov, “The Tammes problem for $N = 14$,” pp. 460–468, *Experimental Mathematics*, vol. 24, no. 4, 2015.

- [96] A. Nica and R. Speicher, *Lectures on the combinatorics of free probability*, vol. 13. Cambridge University Press, 2006.
- [97] O. Ordentlich and U. Erez, “Performance analysis and optimal filter design for sigma-delta modulation via duality with dpcm,” pp. 1153–1164, *IEEE Transactions on Information Theory*, vol. 65, no. 2, 2019.
- [98] J. Østergaard and R. Zamir, “Multiple-description coding by dithered Delta-Sigma quantization,” pp. 4661–4675, *IEEE Transactions on Information Theory*, vol. 55, no. 10, 2009.
- [99] L. Ozarow, “On a source-coding problem with two channels and three receivers,” pp. 1909–1921, *The Bell System Technical Journal*, vol. 59, no. 10, 1980.
- [100] R. E. Paley, “On orthogonal matrices,” pp. 311–320, *Studies in Applied Mathematics*, vol. 12, no. 1-4, 1933.
- [101] M. Palgy, J. Østergaard, and R. Zamir, “Multiple description image/video compression using oversampling and noise shaping in the dct-domain,” in *Electrical and Electronics Engineers in Israel (IEEEI), 2010 IEEE 26th Convention of*, IEEE, pp. 000 965–000 969, 2010.
- [102] Y. Polyanskiy, “A perspective on massive random-access,” in *2017 IEEE International Symposium on Information Theory (ISIT)*, IEEE, pp. 2523–2527, 2017.
- [103] S. S. Pradhan, R. Puri, and K. Ramchandran, “N-channel symmetric multiple descriptions-part I: (n, k) source-channel erasure codes,” pp. 47–61, *IEEE Transactions on Information Theory*, vol. 50, no. 1, 2004.
- [104] R. Raich and J. Kim, “On the eigenvalue distribution of column sub-sampled semi-unitary matrices,” in *Statistical Signal Processing Workshop (SSP), 2016 IEEE*, IEEE, pp. 1–5, 2016.
- [105] A. Ramamoorthy and L. Tang, “Numerically stable coded matrix computations via circulant and rotation matrix embeddings,” *arXiv preprint arXiv:1910.06515*, 2019.

- [106] G. Rath and C. Guillemot, “Frame-theoretic analysis of DFT codes with erasures,” pp. 447–460, *IEEE Transactions on Signal Processing*, vol. 52, no. 2, 2004.
- [107] N. Raviv, I. Tamo, R. Tandon, and A. G. Dimakis, “Gradient coding from cyclic mds codes and expander graphs,” pp. 7475–7489, *IEEE Transactions on Information Theory*, vol. 66, no. 12, 2020.
- [108] M. Rupp and J. L. Massey, “Optimum sequence multisets for synchronous code-division multiple-access channels,” pp. 1261–1266, *IEEE Transactions on Information Theory*, vol. 40, no. 4, 1994.
- [109] J. J. Seidel, *Geometry and combinatorics*. Academic Press, 2014.
- [110] D. Seidner and M. Feder, “Noise amplification of periodic nonuniform sampling,” pp. 275–277, *IEEE Transactions on Signal Processing*, vol. 48, no. 1, 2000.
- [111] M. Slamovich and R. Zamir, “Frame based codes for partially active NOMA,” *arXiv preprint arXiv:2102.03604*, 2021.
- [112] D. Slepian and J. Wolf, “Noiseless coding of correlated information sources,” pp. 471–480, *IEEE Transactions on Information Theory*, vol. 19, no. 4, 1973.
- [113] P. Steinhagen and H. W. Lenstra, “Chebotarëv and his density theorem,” pp. 26–37, *The Mathematical Intelligencer*, vol. 18, no. 2, 1996.
- [114] R.-A. Stoica, G. T. F. De Abreu, T. Hara, and K. Ishibashi, “Massively concurrent non-orthogonal multiple access for 5G networks and beyond,” pp. 82 080–82 100, *IEEE Access*, vol. 7, 2019.
- [115] T. Strohmer and R. W. Heath Jr, “Grassmannian frames with applications to coding and communication,” pp. 257–275, *Applied and computational harmonic analysis*, vol. 14, no. 3, 2003.
- [116] T. Tao, *Topics in random matrix theory*, vol. 132. American Mathematical Soc., 2012.

- [117] V. Tarokh, N. Seshadri, and A. R. Calderbank, "Space-time codes for high data rate wireless communication: Performance criterion and code construction," pp. 744–765, *IEEE Transactions on Information Theory*, vol. 44, no. 2, 1998.
- [118] M. Thill and B. Hassibi, "Low-coherence frames from group fourier matrices," pp. 3386–3404, *IEEE Transactions on Information Theory*, vol. 63, no. 6, 2017.
- [119] M. Tomlinson, C. J. Tjhai, M. A. Ambroze, M. Ahmed, and M. Jibril, "Analogue BCH codes and direct reduced echelon parity check matrix construction," in *Error-Correction Coding and Decoding*, Springer, 2017, pp. 299–314.
- [120] J. A. Tropp, "On the conditioning of random subdictionaries," pp. 1–24, *Applied and Computational Harmonic Analysis*, vol. 25, no. 1, 2008.
- [121] D. Tse and P. Viswanath, *Fundamentals of wireless communication*. Cambridge university press, 2005.
- [122] A. Tulino, S. Verdú, G. Caire, and S. Shamai, "The Gaussian erasure channel," in *Information Theory, 2007. ISIT 2007. IEEE International Symposium on*, IEEE, pp. 1721–1725, 2007.
- [123] A. M. Tulino, G. Caire, S. Shamai, and S. Verdú, "Capacity of channels with frequency-selective and time-selective fading," pp. 1187–1215, *IEEE Transactions on Information Theory*, vol. 56, no. 3, 2010.
- [124] A. M. Tulino and S. Verdú, "Random matrix theory and wireless communications," pp. 1–182, *Foundations and Trends® in Communications and Information Theory*, vol. 1, no. 1, 2004.
- [125] R. Urbanke and B. Rimoldi, "Lattice codes can achieve capacity on the awgn channel," pp. 273–278, *IEEE transactions on Information Theory*, vol. 44, no. 1, 1998.
- [126] S. Verdu and S. Shamai, "Spectral efficiency of CDMA with random spreading," pp. 622–640, *IEEE Transactions on Information Theory*, vol. 45, no. 2, 1999.

- [127] K. W. Wachter, “The limiting empirical measure of multiple discriminant ratios,” pp. 937–957, *The Annals of Statistics*, 1980.
- [128] S. Waldron, “On the construction of equiangular frames from graphs,” pp. 2228–2242, *Linear Algebra and its applications*, vol. 431, no. 11, 2009.
- [129] S. F. Waldron, *An introduction to finite tight frames*. Springer, 2018.
- [130] L. Welch, “Lower bounds on the maximum cross correlation of signals (corresp.),” pp. 397–399, *IEEE Transactions on Information theory*, vol. 20, no. 3, 1974.
- [131] J. Wolf, “Redundancy, the discrete Fourier transform, and impulse noise cancellation,” pp. 458–461, *IEEE Transactions on Communications*, vol. 31, no. 3, 1983.
- [132] W. K. Wootters and B. D. Fields, “Optimal state-determination by mutually unbiased measurements,” pp. 363–381, *Annals of Physics*, vol. 191, no. 2, 1989.
- [133] P. Xia, S. Zhou, and G. B. Giannakis, “Achieving the Welch bound with difference sets,” pp. 1900–1907, *IEEE Transactions on Information Theory*, vol. 51, no. 5, 2005.
- [134] L. P. Yaroslavsky, “Can compressed sensing beat the nyquist sampling rate?” P. 079 701, *Optical Engineering*, vol. 54, no. 7, 2015.
- [135] R. Yosibash and R. Zamir, “Frame codes for distributed coded computation,” in *The 11th International Symposium on Topics in Coding, Montreal*, IEEE, to appear, 2021.
- [136] B. M. Zaidel, S. Shamai, and S. Verdú, “Multicell uplink spectral efficiency of coded DS-CDMA with random signatures,” pp. 1556–1569, *IEEE Journal on Selected Areas in Communications*, vol. 19, no. 8, 2001.

- [137] B. M. Zaidel, O. Shental, and S. S. Shitz, “Sparse NOMA: A closed-form characterization,” in *2018 IEEE International Symposium on Information Theory (ISIT)*, IEEE, pp. 1106–1110, 2018.
- [138] R. Zamir and M. Feder, “On universal quantization by randomized uniform/lattice quantizers,” pp. 428–436, *IEEE Transactions on Information Theory*, vol. 38, no. 2, 1992.
- [139] R. Zamir and M. Feder, “Rate-distortion performance in coding bandlimited sources by sampling and dithered quantization,” pp. 141–154, *IEEE Transactions on Information Theory*, vol. 41, no. 1, 1995. DOI: [10.1109/18.370112](https://doi.org/10.1109/18.370112).
- [140] R. Zamir, *Lattice Coding for Signals and Networks: A Structured Coding Approach to Quantization, Modulation, and Multiuser Information Theory*. Cambridge University Press, 2014.
- [141] A. Zanko, A. Leshem, and E. Zehavi, “Iterative decoding of robust analog product codes,” in *2014 IEEE 28th Convention of Electrical & Electronics Engineers in Israel*, IEEE, 2014.
- [142] G. Zauner, “Quantum designs: Foundations of a noncommutative design theory,” pp. 445–507, *International Journal of Quantum Information*, vol. 9, no. 01, 2011.